Wideband Mixer EVM Characterization through a VNA Setup at Sub-THz Frequencies

Zerui Gao

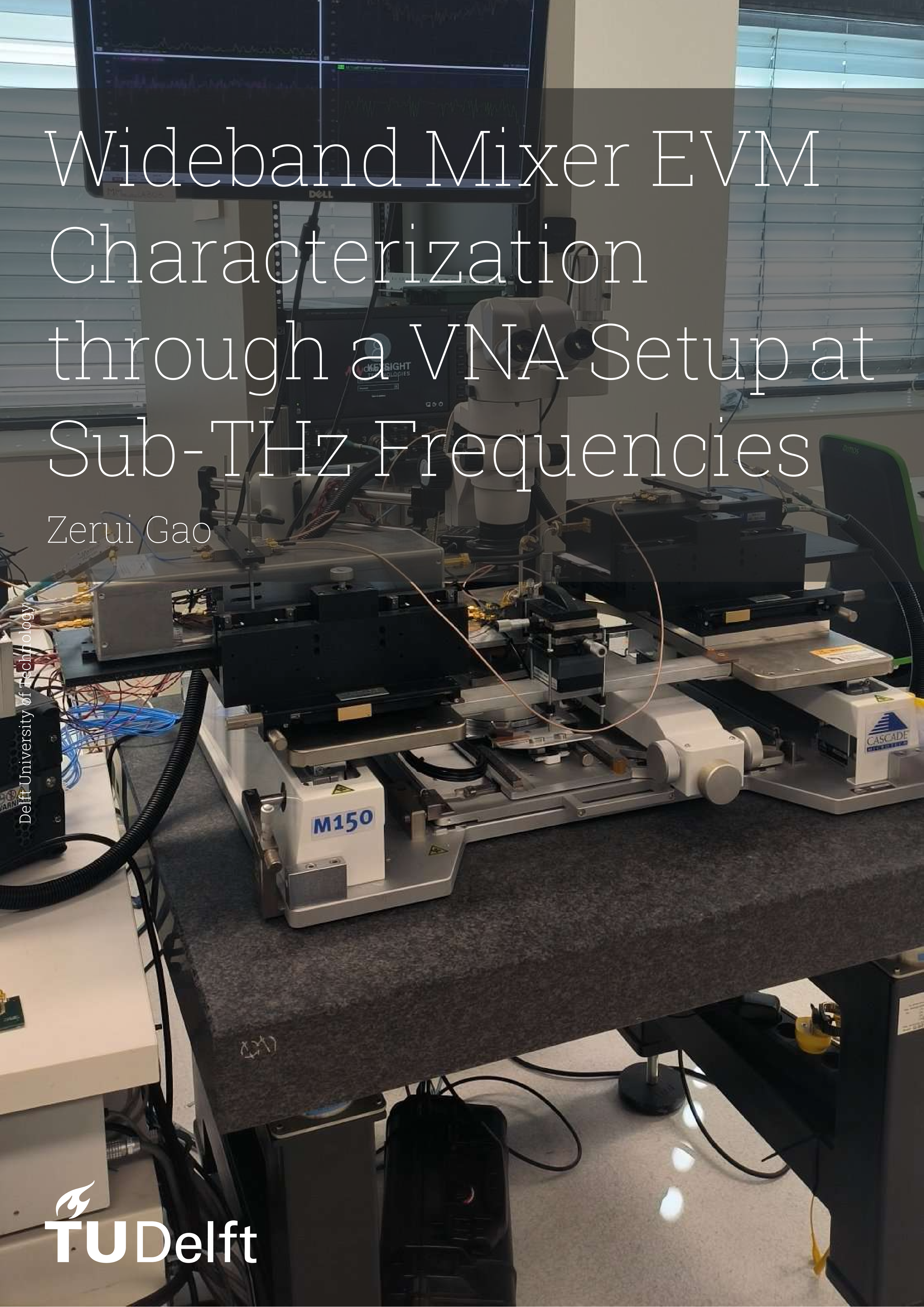

Delft University of Technology

TU Delft

Wideband Mixer EVM Characterization through a VNA Setup at Sub-THz Frequencies

by

Zerui Gao

Student Name	Student Number
Zerui	5710421

Project Duration: October, 2023 - August, 2024

Thesis Committee: N. Llombart, M. Alonso-delPino, M. Spirito, F. Fioraneli

TU Delft

Abstract

This work aims to build a measurement test bench for wideband mixer EVM characterization at sub-terahertz frequencies. A VNA based setups with two frequency extenders are implemented. While one of the VNA sources can be used as the LO input, the other source will be swept over a frequency grid so that the RF output of the mixer under test will be down converted and read out tone by tone. Then the modulated signals is expected be reconstructed from the frequency domain measurement result, which will be demodulated for EVM characterization. A two-tier calibration method is used to extract the absolute power from the target RF channel. The key performance of the mixer under test, such as conversion loss, image rejection ratio and linearity is measured over a IF bandwidth up to 4GHz. Nevertheless, the major challenge for VNA based EVM measurements are the unhandled phase between the two sources of VNA, preventing the system to reconstruct a stable time domain signals. To solve this problem, an auxiliary phase channel setup is proposed, which is able to carry the unhandled phase information from one of the VNA source, thus providing a stable phase measurements for EVM measurements. To validate the proposed setups, the adjusted phase is derived from measurement results of the MUT channel and the results from the auxiliary channel. A phase stability of ± 5 degrees can be achieved with the proposed setups. Finally, EVM characterization is performed base on the proposed setup. A EVM floor of -30dB is achieved with a 300MHz QPSK signal, the error due to thermal noise is reduced due to the narrow band receiver of the VNA.

Acknowledgements

This section is dedicated to expressing my gratitude to those who have helped me with the difficulties encountered during my thesis.

First of all, I would like to express my appreciation to dr. M. Alonso-delPino, dr. M.Spirito and N. van Rooijen for being my daily supervisors. Their knowledge and guidance have supported me during the project and allowed me to push the thesis to a higher level.

Furthermore, I would like to thank every one in the THz Sensing group. Every week I was able to learn from others' presentations and get insights from their works.

Finally, I would like to thank to those who worked in the lab for always being open and trying to help each other out. You effort have saved me a lot of time on the instrument setups.

Zerui Gao
Delft, August 2024

Contents

Abstract i

Acknowledgements ii

1 Introduction 1
1.1 Communications at Sub-THz Frequencies . . . 1
1.2 I/Q Mixer for Communication Systems . . . 1
1.2.1 Figures of merits of the mixer . . . 2
1.3 Measurement Challenges for EVM Characterization . . . 4
1.3.1 EVM definition . . . 4
1.3.2 EVM measurement methods . . . 5
1.4 State of the art – Characterization Techniques at Sub-Terahertz . . . 6
1.5 Goal of the Thesis . . . 7

2 Measurement Setup and Calibration 8
2.1 Mixer Under Test with Evaluation Board . . . 8
2.2 Proposed Measurement Setup . . . 9
2.3 Operation of the Proposed Setup . . . 11
2.4 System Calibration . . . 13
2.4.1 First tier calibration . . . 13
2.4.2 Second tier calibration . . . 14
2.4.3 IF power calibration . . . 15
2.4.4 IF port characterization . . . 15

3 Mixer Power Spectrum Characterization and Optimization 17
3.1 Mixer Power Spectrum Analysis . . . 17
3.2 Image Rejection Ratio . . . 18
3.3 Conversion Loss . . . 19
3.4 Mixer Linearity . . . 20

4 Reference Phase Channel Implementation for a Frequency Extender Based Setup 22
4.1 Introduction . . . 22
4.2 Proposed Reference Channel Setup . . . 23
4.3 Validation of the Reference Channel Operation . . . 24
4.3.1 Simulation verification in ADS . . . 24
4.3.2 Measurement verification using a fundamental mixer at WR10 . . . 27
4.4 Implementation of the Reference Channel . . . 30
4.4.1 Auxiliary AWG channel . . . 30
4.4.2 Sample Marker Out from AWG . . . 31
4.4.3 Phase stability measurement of the AWG outputs . . . 32

4.5 Phase Stability Measurements of the Proposed Measurement Setup 33
4.5.1 Single-tone signal measurements 35
4.5.2 Modulated signal measurements 36

5 EVM Measurement 41
5.1 EVM Floor Measurements at Baseband 41
5.2 EVM Measurements without Reference Phase Channel 42
5.2.1 Narrowband EVM measurements 42
5.2.2 Wideband EVM measurements 44
5.3 EVM Measurements with Oscilloscope 50
5.4 EVM Measurements with Reference Phase Channel 52
5.4.1 EVM measurement with 2MHz grid 55
5.5 Discussion 56

6 Conclusion and Future Work 57
6.1 Conclusion 57
6.2 Future Work 58

References 59

A Signal Modulation and Demodulation Process 61
A.1 Schematic layout of modulation process 61
A.2 Pulse shaping filter 62
A.3 Demodulation of the signal 62

B Phase Stability of measurement with Agilent N5242A VNA 64

C Reference Phase Channel Implementation with WR10 66

1

Introduction

1.1. Communications at Sub-THz Frequencies

Until the last decade, the sub-Terahertz (THz) spectrum was not explored due to the lack of low-cos integrated technologies with the advances of electronics and specifically integrated technologies . This part of the spectrum is progressively more attractive and communication application with such bandwidth are becoming a reality.

Advanced Integrated Circuits (IC) technologies have being developed at such high frequencies to realize high performance transceivers. Different use-cases have been presented which require RF front-ends composed of I/Q mixers above 120GHz, to achieve bandwidths larger than 5GHz. However, these high carrier frequencies components also increase the complexity of the measurement setups for the circuits at such high frequencies. Specially, on-wafer calibration using both vector and absolute power measurements remain challenging [6] [8]. This work is focused on the on wafer amplitude and phase measurements of a mixer at sub-THz frequencies, which would allow us to characterize its key performance and perform wideband modulated signals measurements.

1.2. I/Q Mixer for Communication Systems

Modern communication systems rely on the digital modulation techniques, such as QPSK and 16QAM. In digital modulation, a binary sequence is subdivide in to pairs of two consecutive bits. Furthermore, each pair of bits can be plotted in a 2D vector form which is the symbol transmitted in the communication links. A constellation diagram is created by plotting all the possible transmitted symbols, as illustrated in Fig 1.1. By using appropriate filter, the minimum occupied bandwidth depends only on the symbol rate as $BW = Rs$. In the mean time, higher order of modulation schemes use more bits to represent one symbol, providing higher data rates. However, this will also leads to a denser constellation diagram, increasing the modulation complexity. Fig. 1.1 shows the constellation diagram of QPSK and 16QAM modulation and the represented bits.

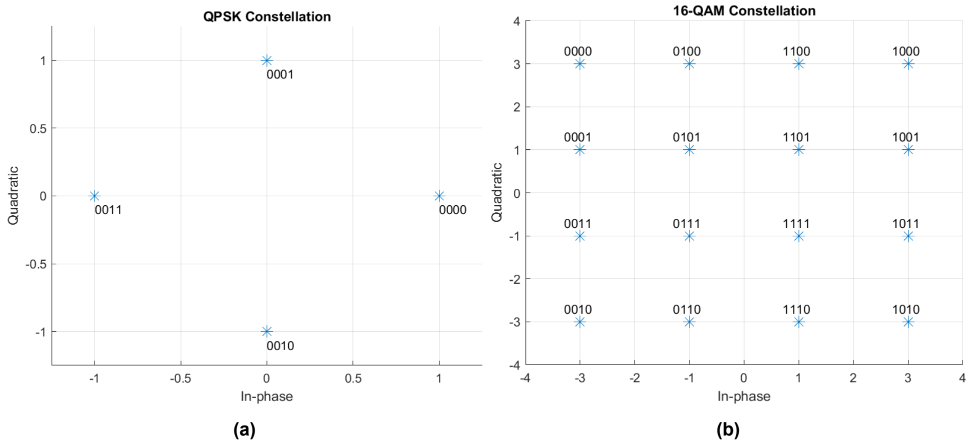

Figure 1.1: Constellation diagram

The generated symbols will be used to form 2 separate baseband waveforms, which are then unconverted by two orthogonal carrier signals to IF band. The use of In-phase (I) and Quadratic (Q) carriers halves the occupied bandwidth, since the two pair of waveforms uses the same bandwidth in an orthogonal method. They can be added together and easily separated at receiver side by demodulation techniques. Figure shows the 2 step transmitter structure provided in [9].

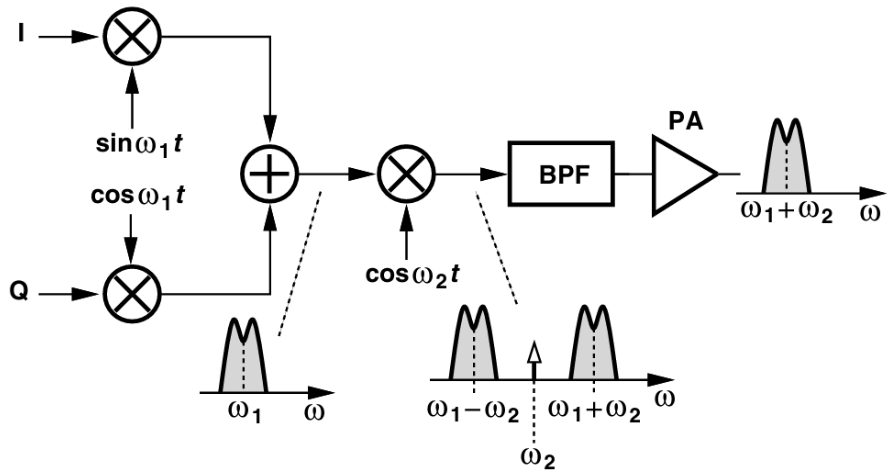

Figure 1.2: Two-step TX

1.2.1. Figures of merits of the mixer

As illustrated in Fig. 1.2,a second step mixer is used to unconverted the modulated signals to RF channel. Therefore, the mixer becomes one of the essential component since it directly link the power at baseband at the power available at RF band. Apart from the working bandwidth, the mixer has some important factors, Conversion Loss (CL) and linearity. In addition, for I/Q mixers which can be optimized for single side band (SSB) conversion and reducing the occupied bandwidth, the Image Rejection Ratio is also an importance factor .

Conversion loss

The CL provides the information of the losses to convert the signal from base band to RF band. For single tone up converted signals, the CL can be calculated as :

$$CL(dB) = P_{IF}(f_{IF}) - P_{RF}(f_{SSB}) \tag{1.1}$$

Where the $P_{IF}(f_{IF})$ is the power of the transmitted tone , and $P_{RF}(f_{SSB})$ is the SSB converted power at the RF output. Typically f_{SSB} is equal to $f_{LO} \pm f_{IF}$, Depending on which side band is optimized.

Image rejection ratio

The IRR describes the ratio between the target converted band signal and the suppressed band signal for I/Q mixers. Let us consider a mixer that is optimized for upper side band conversion (USB). Ideally, the lower side band (LSB) signal will be fully cancelled, resulting a infinite high IRR saving half of the occupied bandwidth. However, due to the imperfection of the components, the unbalance of phase and amplitude between IQ ports will reduce the IRR, resulting an interference to the adjacent channel. The effect of errors in amplitude and phase between I and Q can be expressed analytically by [9] :

$$IRR(dB) = 10 \log 10 \frac{(1+\epsilon)^2 + 2(1+\epsilon)\cos\Delta\phi_{IQ} + 1}{(1+\epsilon)^2 - 2(1+\epsilon)\cos\Delta\phi_{IQ} + 1} \tag{1.2}$$

Where ϵ is the relative gain error between I and Q, and $\Delta\phi_{IQ}$ is the phase error between the two signals. However, the unbalances can be counteracted by applying a correction on the IF input signals. Fig. 1.3 illustrates the how the IRR will be effected by these two factors. As for measurement, the IRR for USB I/Q mixers can be calculated as :

$$IRR(dB) = P_{RF}(f_{USB}) - P_{RF}(f_{LSB}) \tag{1.3}$$

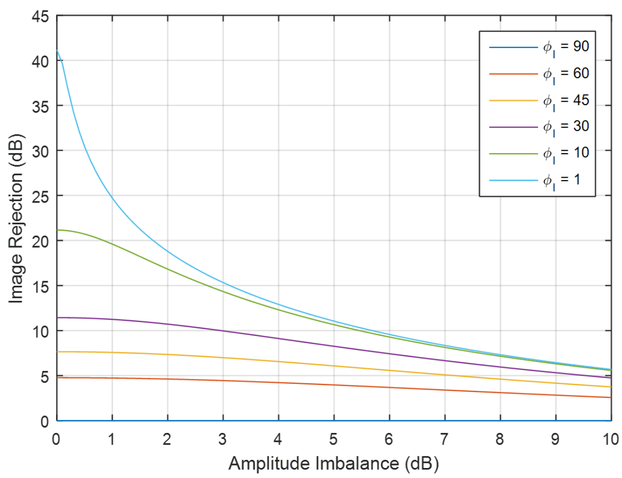

Figure 1.3: IRR with different imbalances

Linearity

Finally, the mixer linearity describe the saturation output power of the mixer, as well as the higher order harmonics that will interfere the in-band and out-of-band signals. As the mixer provides the desired fundamental tones for up-conversion, it will also generate unwanted higher order inter-modulations products, increasing the noise inside the bandwidth or causing interference to adjacent channels. The system linearity is typically determined by output intercept point of second and third order harmonic tons (OIP2, OIP3), which is the output power point at which the extrapolated fundamental- and higher

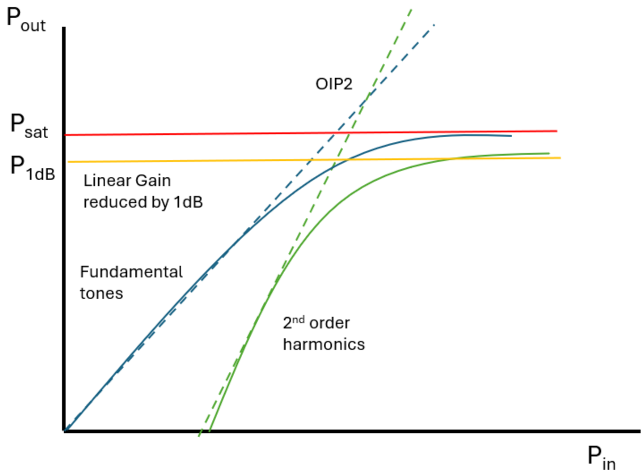

Figure 1.4: Linearity.

order lines intersect on a plot [9]. The linearity of the fundamental tone can also be characterized by P1dB, which is the point that the output power is 1dB less when compared to the ideal linear output, as shown in Fig. 1.4. All these parameters will help us understanding the available power from the mixer and the power of interference or noise that could become the noise for the the communication channels. This is especially useful when analysing the link budge of the communication systems.

1.3. Measurement Challenges for EVM Characterization

While the mixer characterized performance can provide information about the power and noise, they are measured with single tone Continuous Waves (CW) and cannot fully represent the performance when transmitting modulated signals. Error Vector Magnitude (EVM) measurements, is the figure of merits to characterize the performance of the modern digital communication systems.

1.3.1. EVM definition

As discussed in previous section, the randomly bits can be represented by symbols in 2D vector form. For each symbol transmitted, there is an error vector between the ideal reference symbol and the received symbol as illustrated in Fig. 1.5. The Error Vector Magnitude (EVM) determines the performance of communication links by comparing the rms error between the received symbol and reference symbol. Since each symbol can be represented by a two dimension vector, the algorithm for calculating EVM can be written as :

$$EVM = 20log_{10}\left(\sqrt{\frac{\frac{1}{N}\sum_N |y_n - x_n|^2}{\frac{1}{N}\sum_N |x_n|^2}}\right)(dB) \tag{1.4}$$

Where the N is the number symbol transmitted, x is the reference symbol in 2d vector form, and y is the received symbol.

Apparently, EVM directly represent the mismatch between the transmission and receiver side, thus becoming the core parameters to judge the quality of communication links.

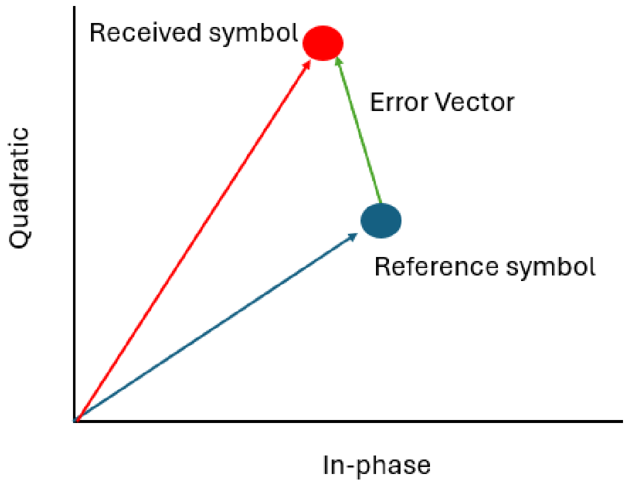

Figure 1.5: Error vector between the reference symbol and received symbol

EVM bathtub curve describes how the EVM changes with different IF input power of the system. As shown in Fig. 1.6, the EVM will increase when the IF power is low, due to the high SNR of the communication system. When the power becomes too high, the system-level non-linearity starts to effect the EVM with intermodulation products. The lowest EVM level (EVM floor) for a system is typically defined by the combination of all the error sources, including the impediments of the device under test and the errors from the used instruments.

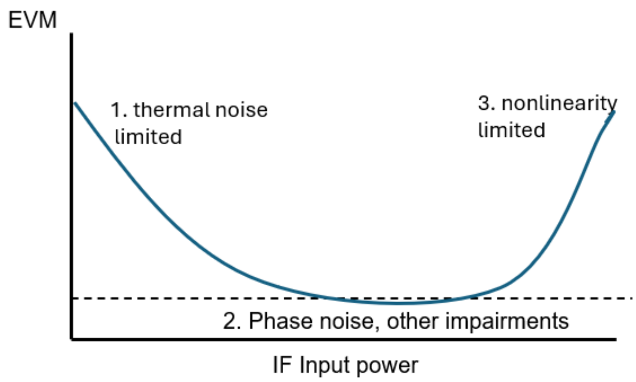

Figure 1.6: EVM bathtub curve example

1.3.2. EVM measurement methods

To measure modulated signals, either a time domain instrument or frequency domain instrument is used. The oscilloscope is the most common time domain instrument when measuring the signals. It uses a Analog-Digital-Converter (ADC) to transfer the received signal voltage level in to digital information, directly obtaining the complete information over the bandwidth until its reaches the Nyquist Sampling rate. However, since the thermal noise is linked to the system bandwidth, the oscilloscope suffers from a limited dynamic range. This is especially critical when measuring signals at sub-terahertz frequencies, since a higher bandwidth leads to a higher noise floor.

Typical frequency domain instruments such vector network analyzer (VNA), provide an alternative narrow band measurement setup. The VNA is a mixer base instrument which down converts the received signal to a certain frequency by the internal LO mixer. Then different internal filters can be applied to achieve a narrow band measurements. The limited bandwidth reduces the thermal noise, resulting a high dynamic range, and providing an accurate power and phase information of modulated signals. The only disadvantage is that to measure the complete BW, the VNA has to sweep its internal LO, which takes longer time than the oscilloscope. Moreover, the internal phase of LO is unhandled in sweeping setups, preventing the system from obtaining a repeatable phase measurements for EVM characterization[14].

1.4. State of the art – Characterization Techniques at Sub-Terahertz

Characterizing mixers or antennas at sub-terahertz frequencies is conducted on-chip using ad hoc measurement setups. These setups employ frequency extenders for generating the LO (local oscillator) signal and detecting the RF (radio frequency) signal, in combination with a VNA. In recent years, modules for extending the frequency range of VNAs have become widely used in network analysis, significantly contributing to advancements in this field .[10]. Yet the measurement setup for wideband modulated signal at sub-THz frequencies is still under investigation.

Table1.1 provides an overview of some state-of-the-art EVM measurement setups for sub-terahertz frequencies.

Table 1.1: Comparison of state-of-the-art EVM measurement

Reference	DUT	symbol rate(baud/s)	RF BW(GHz)	Downconvert Instrument	Receiver Instrument	Modulation	EVM(dB)
[6]	Transmitter	5G	131-137	OML D-band harmonic mixer	Oscilloscope	16QAM	-21.4
[8]	Transmitter	8×1.76G	139-157	D-band down converter	Sampling Scope	16QAM	-19.0
[4]	Power Amplifier	8G	135-145	WR6.5 Down mixer	Oscilloscope	QPSK	-14.6
[3]	Transmitter	30G	120-160	VDI IQ sub-harmonic mixer	Oscilloscope	16QAM	-20.5
[5]	Amplifier	1G	143-145	D-band down converter	VNA	16QAM	-35.8
[2]	Antenna Array	400M	38.75-39.25		VNA	16QAM	-34.0

In [8], a wide band modulated signal is transmitted and received by a D-band antenna. A D-band down-converter is used to convert the signal to the IF band. And the signal is captured by a real-time oscilloscope, which performs demodulation and derives the EVM results. In [6] and [3], oscilloscopes and harmonic mixers are used for down-converting and capturing signals from D-band transmitters. In [4], the EVM is measured for a power amplifier using the similar setups. As listed in the table, an EVM that is greater than -22dB is achieved, possibly due to the limits of the high noise floor from the oscilloscopes.

To overcome these limitations, several setups have been investigated to explore potential EVM measurements with a VNA-based setup. The Vector Network Analyzer operates as a mixer-based receiver, measuring discrete frequency tones instead of real-time domain signals. Classical VNA measurements hinder the reconstruction of time-domain demodulated waveforms because frequency components are measured in separate acquisitions, each involving an unknown and different internal LO phase[1]. Therefore, in [11], [5], [1] and [2], a spectral correlation method has being used to calculate EVM with amplitude information only.Comparing the measurement results, it is clear that VNA-based measurement setups can produce much lower residual EVM due to their high dynamic range. However, the proposed setup in [11] calculates the EVM without the IQ demodulation.

To measure the EVM with demodulation process, in [15] and [14], an auxiliary channel was used to compensate for the random phase shifts of VNA. The time domain signals can be reconstructed from a VNA based-setup and can be used for EVM calculation. Nevertheless, to the best of the author's knowledge, such EVM measurement setups have not been reported that implement frequency extenders to increase the measurement up to the D-band with time do.

1.5. Goal of the Thesis

This work aims to build a test bench for mixer characterization and EVM measurement at sub-terahertz frequency. To obtain measurements results at sub-terahertz frequency, a VNA and frequency extenders are used. To overcome the arbitrary LO phase from the VNA source, an auxiliary channel is used to serve as the LO reference phase of the system. This thesis has been divided into the following segments:

Chapter 2 measurement setup and calibration strategy

Chapter 3 The single tone characterization with the mixer

Chapter 4 Reference phase channel implementation

Chapter 5 EVM measurements and analysis

2

Measurement Setup and Calibration

This chapter describes the measurement setup and the calibration strategy proposed to realize mixer characterization in the 140-170GHz frequency band. Firstly, the mixer under test is presented in Section 2.1. Then the proposed measurement setup is shown in Section 2.2. Section 2.3 explains operation principles of the setup. Finally, the system calibration is described in 2.4.

2.1. Mixer Under Test with Evaluation Board

The Mixer Under Test (MUT) is a passive Gotmix gMDR0036 D-band sub-harmonic IQ mixer [7]. It has an IF bandwidth from DC to 6GHz, and requires a LO frequency of 70-80GHz with 15dBm of input power. The mixer has a differential IQ topology, and as such requires four input ports for the IF. Being a sub-harmonic mixer means that the RF output is 140-170GHz which is the double of the LO input frequency. The commercial MMIC mixer came in a bare die format, and therefore needs to be placed on an evaluation board for robustness and to realize all the interconnections, shown in Fig. 2.1,. While the LO port and RF port will be connected through on-wafer probes to get accurate measurements at D-band, the IF ports and the DC bias feed are realized through SMA ports on the evaluation board, and then connected to the chip by wire-bonding techniques.

Table 2.1 lists some of the typical performance provided by the manufacturer [7]. While the performances such as conversion loss and image rejection ratio are characterized, some important factors relating to the linearity remains unknown.

Table 2.1: Mixer Performance provide by Manufacture

Parameter	Typical Value
RF Bandwidth	140-170GHz
IF Bandwidth	0-6GHz
LO input power	15dBm
Conversion Loss	12dBm
LO-RF isolation	35dB
Image Rejection Ratio	15dB
P1dB	-5dBm
OIP3	TBD
OIP2	TBD

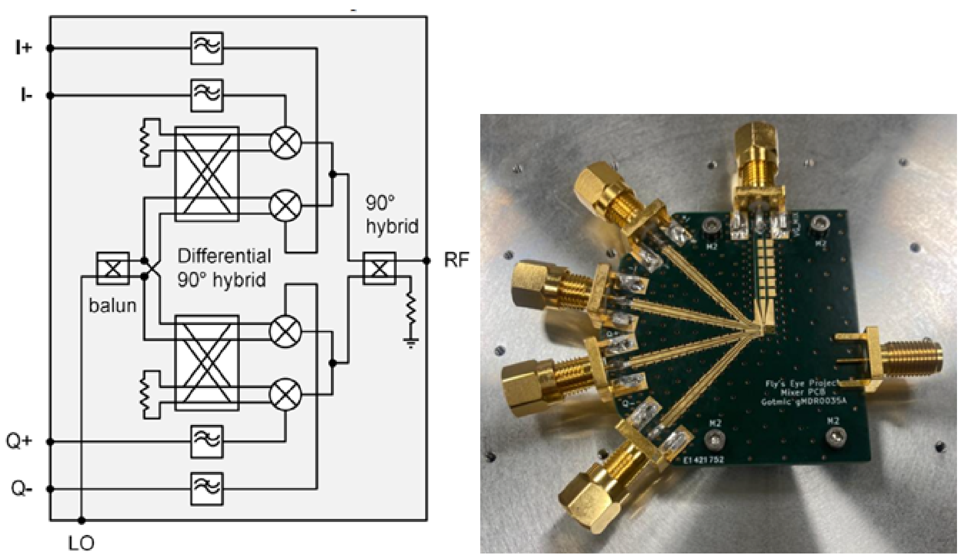

(a) (b)

Figure 2.1: 2.1a Schematic layout of the MUT, 2.1b Mixer on the evaluation Board

2.2. Proposed Measurement Setup

Fig. 2.2 shows the proposed measurement setup, which can be divided into two subsystems. The first one contains the Mixer Under Test (MUT), connected by WR-10 and WR-5 frequency extenders on its LO and RF ports, respectively. The extenders are used to provide LO input and allow for readout of the downconverted input and output signals of the MUT using the VNA receivers. Each wave guide port of the frequency extenders is connected to the RF waveguide probes that land on the RF and LO pads of the mixer under test (MUT). In addition, to accommodate the 90° angle between the RF and LO pads, a 90° flexible waveguide is used to connect the WR-10 extender waveguide and the WR-10 RF probe.

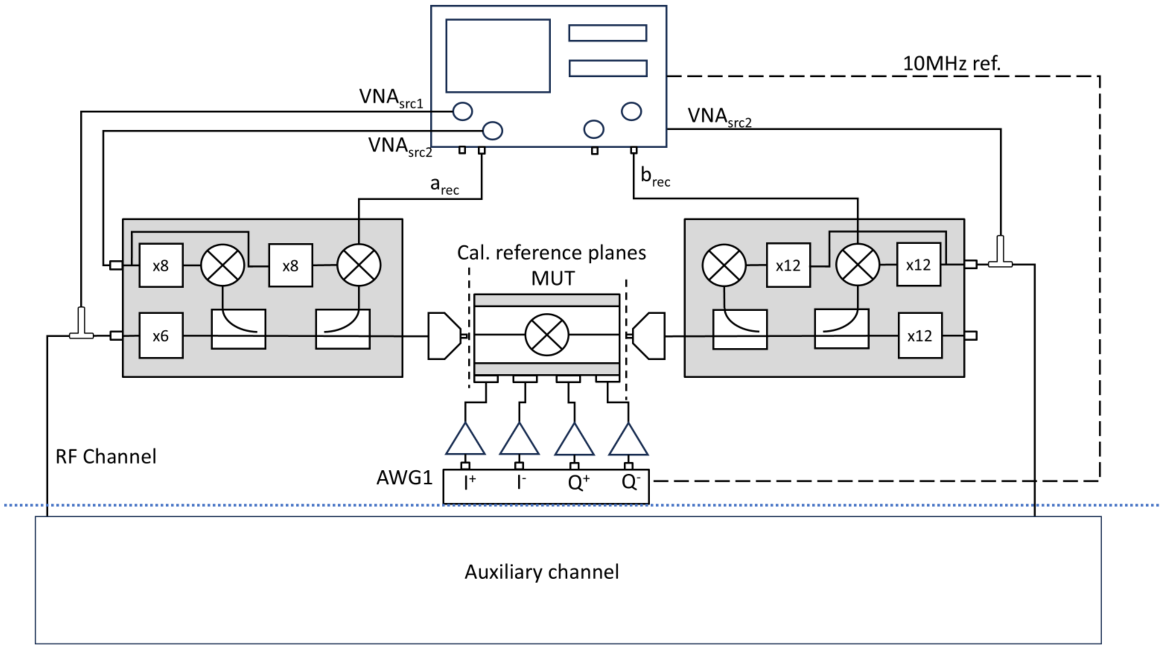

Figure 2.2: Schematic layout of the proposed measurement setup

The LO signal of the mixer covering from 70-80GHz is synthesized using the first source of the VNA VNA_{src1} and multiplied by 6 using the WR-10 extender. To readout the RF signal of the sub-harmonic mixer, the signal is then down converted using the mixer of a WR5 frequency extender, and read out by the one of the VNA receiver b_{rec}. The WR5 mixes the incoming RF signal from the MUT with a signal ($WR5_{LO}$) generated by the second source of the VNA VNA_{src2} that is multiplied by 12. Typically, the down converted IF frequency f_{rec} is set to 279MHz, which gives the minimum conversion loss of the WR5 mixer.

Initially, the differential I/Q signals are generated by two two-channel Agilent N6030A AWG cards, with a sampling frequency up to 1.25GS/s. Therefor it can has a maximum bandwidth until 500MHz, and the data rate can be up to 1Gbps with QPSK modulation. The AWG cards are set to Master/Slave mode for internal clock and trigger synchronization. The 4-channel IF input setups allow to adjust phase and amplitude offset for each port and thereby balance the IF signals to optimize the MUT performance. The AWG cards are synchronized with the VNA by a 10MHz reference clock. Later, the AWG cards are switched to the Keysight M8190A with 12GS/s to characterize the MUT with 4GHz bandwidth. In this case, the data rate of QPSK modulation can go up to 8Gbps.

The MMIC mixer also has a DC bias, which is not shown in the layout. The DC bias is supplied using an Agilent E5270B precision IV analyzer for monitoring voltage and current levels, and subsequent DC power consumption.

The other subsystem is the auxiliary channel used to provide a stable phase reference when performing the EVM measurement. This chapter will focus on the calibration procedure of the RF channel. The detailed implementation and verification of the auxiliary channel will be discussed in Chapter 4.

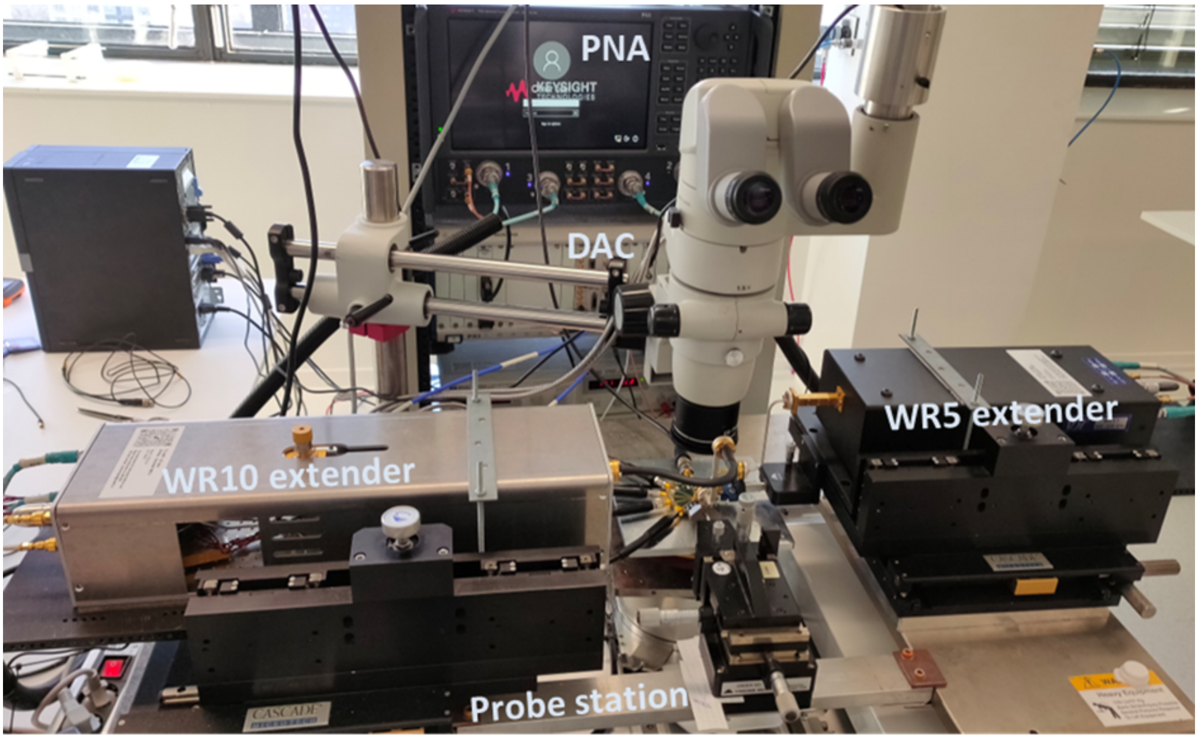

Figure 2.3: The Measurement setup in the lab

2.3. Operation of the Proposed Setup

To generate a upconverted signal at RF output of the MUT. Firstly, the VNA_{src1} will be fixed to CW operation mode to inject the LO signal of the MUT, the LO frequency satisfies $f_{LO} = 6f_{src1}$ and the RF frequency satisfies $f_{RF} = 12f_{src2}$. At the same time, the AWG will inject a wideband modulated signal to the MUT. Since the modulated signal is periodical, its frequency domain spectrum is in discrete form, and the information can be recovered measuring the signal at these specific tones. Therefore, the IF signal can be written as $f_{IF}^{i} = f_{IF}^{0} + k\Delta f$, where the f_{IF}^{0} is the minimum IF frequency, $k = 1 : K$ is a integer and Δf defines the IF frequency grid. The signal occupies a bandwidth of $k\Delta f$. Note that the f_{IF}^{0} can be negative, thus representing both converted LSB and USB band to the RF frequency.

The proposed measurements scheme relies on the frequency sweep of the VNA_{src2} to measure the RF spectrum tone by tone in the target 140-170GHz band. Therefore, the VNA_{src2} will be swept on this frequency grid over the band of interested, and therefore the frequency of VNA_{src2} used for measuring can be written as f_{src2}^{i}. The VNA_{src2} signal will be multiplied by 12 using the internal multiplier of the WR5 mixer, creating a D-band LO $WR5_{LO}$. The $WR5_{LO}$ will downconvert the RF signal at $f_{WR5}^{i} - f_{rec}$ to f_{rec} and be read by one of the VNA receiver b_{rec}. In addition, the received signal at b_{rec} is stored as complex format to record both the amplitude and phase information, as such vector measurements can be performed. This setup must satisfies:

$$12f_{src2}^{i} = 12f_{src1} + f_{IF}^{i} + f_{rec} \tag{2.1}$$

Fig. 2.4a shows how the RF signal is down converted to f_{rec} using the $WR5_{LO}$. However, one it is clear that one problem in this setup is that the extender will also down-convert the image frequency at $12f_{src2} + f_{rec}$ to the readout frequency f_{rec}. As illustrated in Fig. 2.4b and Fig. 2.4c, it is possible that the other IF tone converted to the will become the interference. To avoid the problem additional requirement must satisfy that $2f_{rec} \neq k\Delta$ or $2f_{rec} > K\Delta f$, where $k = 1 : K$ is a integer and Δf defines the IF frequency grid. What's more, to avoid the LO leakage being the interference when measuring the LSB tones, as shown in Fig. 2.4d, the setup is also limited by $k\Delta f + f^0_{IF} \neq 0$

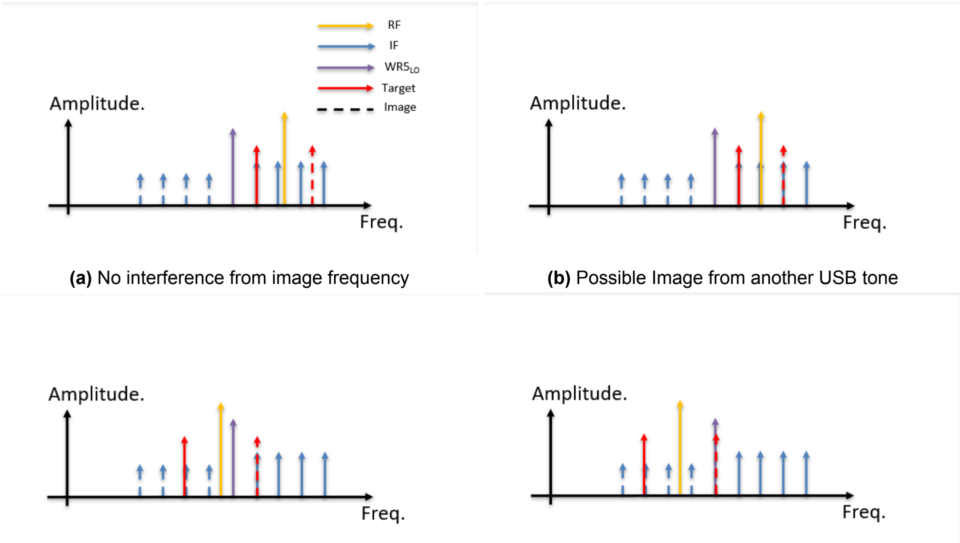

(a) No interference from image frequency

(b) Possible Image from another USB tone

(c) Possible Image from USB when measuring LSB

(d) Possible Image from LO leakage

Figure 2.4: Possible Image frequency examples

To monitor the power fluctuations that incur on the LO, which are significant with the proposed setup, and auxiliary return path of the signal coming from the WR10 extender is read by the VNA using another port a_{rec}. The LO spectrum can be measured using the similar setup, however this path cannot bee read as it is, since the WR10 extender receiver frequency, f'_{rec}, will not coincide with the measurement receiver frequency f_{rec}, due to the hardware difference between the WR10 and WR5 extenders. In order to receive the LO injected power, the VNA_{src2} is swapped to another grid that can down converted the LO spectrum to the 13.33MHz, which is the optimized frequency for WR10. This dual measurement grid operation allows us to calibrate the LO power right after each test procedure of the mixer and accommodate the power fluctuation s due to the temperature or other random drifts.

A table summarizing the frequency sweeping setups are listed in Table 2.2

Table 2.2: Dual measurement grid operation for simultaneous RF spectrum measurements and LO power calibration

RF measurement grid					
LO	IF	RF	b_{rec}	VNA_{src1}	VNA_{src2}
f_{LO}	f_{IF}	f_{RF}	f_{rec}	$f_{LO}/6$	$(f_{RF} + f_{IF} + f_{rec})/12$
LO measurement grid					
LO	IF	RF	a_{rec}	VNA_{src1}	VNA_{src2}
f_{LO}	-	-	f'_{rec}	$f_{LO}/6$	$(f_{LO} + f_{rec})/12$

Fig.2.5 illustrate the example measurement results using the proposed grid setup. In this case, a LO at 85GHz and IF at 200MHz is injected to the MUT. A measurement grid of 5MHz is applied with 2GHz RF bandwidth, resulting in a 201 number of tones measured. The measurement results from receiver a_{rec} contains the input LO at 85GHz and the IF to LO leakage at 85$\pm$0.2GHz. Base on the results from b_{rec}

it is clear to see the up converted IF signals at 170±0.2GHz, LO to RF leakages at 170GHz. Moreover, there are also higher order harmonics at 170±0.4GHz or 170±0.6GHz. Although the system is not calibrated and the amplitude does not reflect the absolute power at each port, it is clear that the USB tone at 170.2GHz dominant the power at RF output, indicating the MUT is working under USB mode.

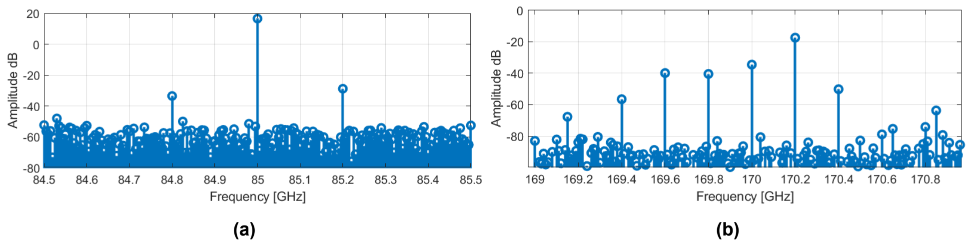

Figure 2.5: Example measurement results from port a_{rec} and b_{rec}

2.4. System Calibration

Having described the PNA vector spectrum analysis measurement setup and the procedure to readout the RF spectrum, this section will discuss the calibration techniques used to derive the relative RF phase and amplitude measured at the probe level, as well as the calibration of the IF input power. A two-tier calibration procedure developed by Vertigo Technologies B.V. is used in this work [13].

2.4.1. First tier calibration

The first-tier calibration aims to link the VNA received signals a_{rec} and b_{rec} to the power at the WR-10 and WR-5 extender waveguide planes, denoted as $T1$ reference plane. Since these two extenders work at different frequencies, Trough, Reflect, Line (TRL) calibration is not possible. Instead, two 1-port Short, Short Offset, Load (SSOL) calibration kits are used to extract the error terms and derive the corrected S-parameters for a_{rec} and b_{rec} signals. The VNA_{src1} is swept to provide a RF frequency from 140GHz to 180GHz for calibration. A frequency grid of 100MHz is created, resulting a total 401 points calibration file. Since the readout at a_{rec} and b_{rec} is fixed at certain frequency, the VNA_{src2} is also fixed for each VNA_{src1} setup. Meanwhile, to link the received signal power to the absolute power at $T1$ reference plane, a VDI PM5 power meter is included in the calibration process. The output power of VNA_{src1} is set as high as possible to reduce the PM5 measuring time, while the VNA_{src2} power is fixed at 15dBm and 10dBm for WR-10 and WR-5 extenders, respectively. This characterizes the extender output powers at saturated levels due to high input VNA_{src2} power.

Then, the PM5 is removed and replaced by matched loads for both extenders. Power leveling is then performed by sweeping the VNA_{src1} in frequency and power whilst obtaining the receiver data a_{rec} and b_{rec}. These data over the whole frequency band at different power levels provides calibrated power at the $T1$ reference plane. A lookup table the relates to the PNA_{RF} power with the WR-10 waveguide output power at different frequency is shown in Fig. 2.6.

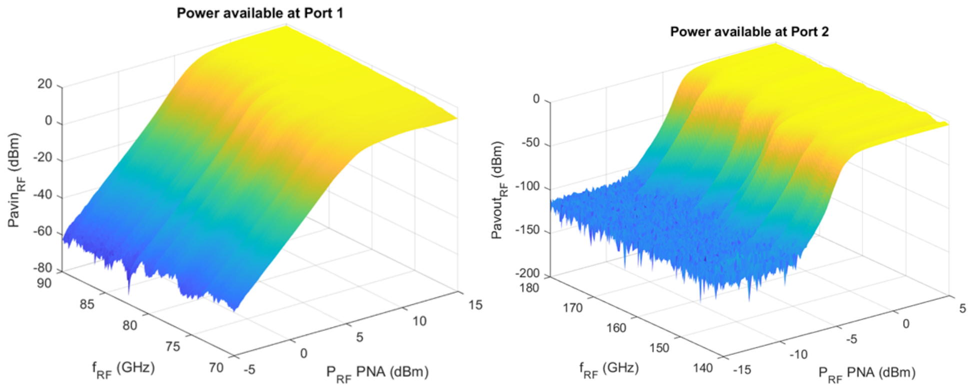

(a) (b)

Figure 2.6: 2.1a available power from a_{rec}, 2.1b available power from b_{rec}

2.4.2. Second tier calibration

The second-tier calibration aims to extract the error terms from the probe and additional waveguides. This calibrates until the probe tips, and therefore directly represents the MMIC once landed on its landing pads. The calibration is on-wafer, and a fused-silica lithographic calibration kit is used to perform 1-port SOL calibration. The procedure is similar to the first-tier calibration, and now the reference plane has been pushed from the extender waveguide to the probe tips. The measured probe and flexible waveguide loss is around 2.7dB for port 1.

An fourth calibration element is then used to verify the calibration process. Fig. 2.7b compares the S-parameters of WR-10 (S_{11}) and WR-5 (S_{22}) probes in amplitude and phase to those of the simulated calibration set. WR-10 shows a small offset of 0.4dB in amplitude and offset of around 20° in phase. WR-5 calibration shows good agreement for frequencies until 160GHz but starts drifting in amplitude afterwards. We note, however, since the simulation results do not contain any losses, also the test calibration kit is an open circuit, where the calibration error will have larger impact on the calibrated results. The MUT will be a matched load, we would expect less impact of the error term inaccuracies. Therefore, we continue the following calibration process.

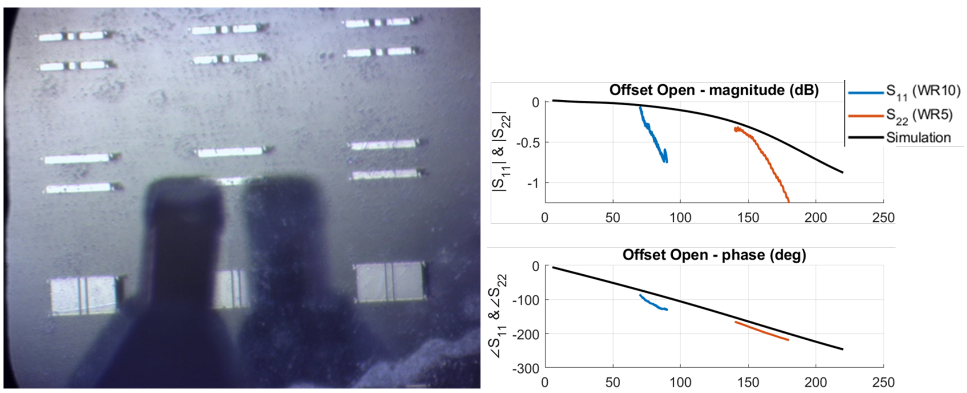

(a) (b)

Figure 2.7: 2.1a on-wafer Cal Kit, 2.1b measured S parameter and Simulation comparisons

2.4.3. IF power calibration

The MUT is a differential IQ mixer and requires 4 IF inputs: $I+$, $I-$, $Q+$, and $Q-$ from the AWG cards. To obtain more IF power than the AWG can provide, each channel is amplified by an LNA which provides sufficient input power, therefore a total of 4 LNAs are used. A spectrum analyzer was used to characterize the output power of each channel. To measure the power, the AWG is configured as sweeping single tone output mode, while the spectrum analyzer measured the corresponding frequency tones with a resolution bandwidth of 500kHz. These measurements will be referred to later when deriving the conversion loss. Fig. 2.8 shows the measure power from the N6030A AWG and M8190A AWG. While the N6030A AWG channels used for different I inputs has a difference less than 0.1dB, the difference between differential Q ports are about 0.8dB. The difference between each port power of M8190A is less than 0.5dB, the power also drops about 10dB as the frequency increases from 100MHz to 4.5GHz. Therefore, pre-distortion is necessary to balance the difference between each channel and the frequency dependent channel response.

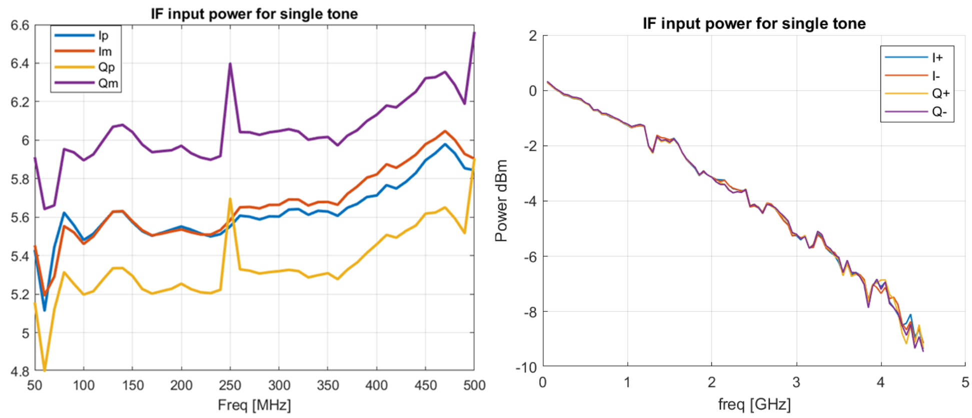

(a) IF power from N6030A

(b) IF power from M8190A

Figure 2.8: Measured IF power from AWG cards

2.4.4. IF port characterization

The IF ports are connected to the MMIC mixer through the evaluation board that has a relatively low transition loss. However, the connections between the board and IF port on the MMIC mixer are realized through wire-bonding techniques, which might have a large influence on the IF bandwidth, therefore, the reflection coefficients of these differential IQ ports also need to be checked to help characterize the mixer. A 2-port VNA is connected to the IF ports for characterization, while other ports are terminated by a 50Ω load. The LO and RF probe need to be landed on MUT, and 15dBm LO power is used to sufficiently drive the MUT to avoid open-ended termination. The test signal is a 100MHz CW tone and the S-parameters are measured at different LO frequencies, and the S_{dc} (differential to common mode) and S_{dd} (differential to differential mode) S parameters are shown in Fig. 2.9.

It can be observed that when the LO frequency is at 70GHz, the S-parameters for both I and Q ports have a poor performance. The S_{dd} and S_{dc} for both IQ ports are less than -10dB for an LO frequency above 75GHz, with a matching until 4GHz. Therefore, the characterization of the MUT will be continued with a LO above 145GHz, with am IF bandwidth until 4GHz.

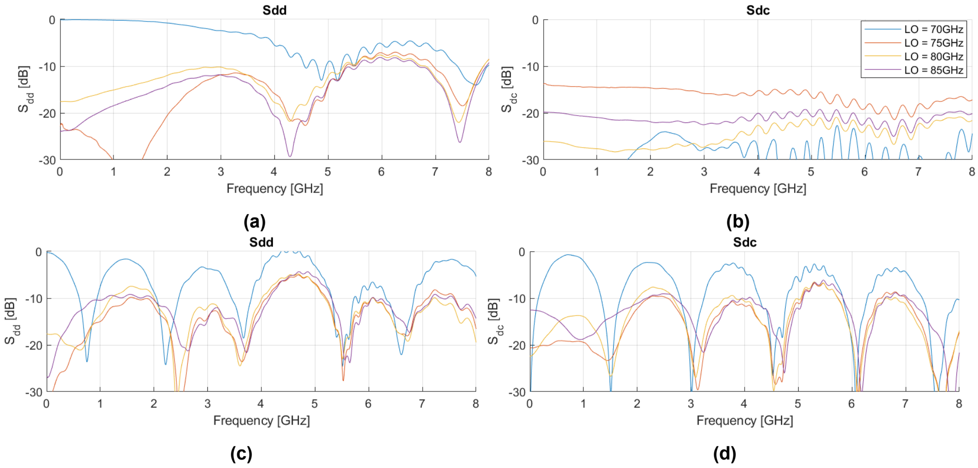

Figure 2.9: Measured Reflection Coefficients for IQ ports

3

Mixer Power Spectrum Characterization and Optimization

After the calibration procedure of Section 2.4, the systematic errors from the proposed setup are de-embedded, allowing the measurement of absolute power at the IF, LO, and RF ports. This helps enables the characterization of the mixer performance at high frequency. Section 3.1 describes how the conversion loss, image rejection ratio and conversion loss is derived from the measured spectrum. Section 3.2 and 3.3 illustrate the measurement results for the CL and IRR of the MUT. Finally, the MUT linearity is discussed in 3.4.

3.1. Mixer Power Spectrum Analysis

Before looking at the optimized performance of the MUT, as a first example we would like to show the calibrated mixer input and output power spectra without optimization. This will help understand the procedure and parameters that are used for optimization.

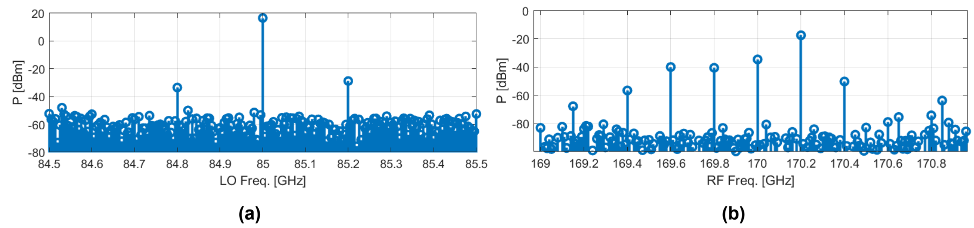

Figure 3.1: Mixer power spectrum for LO input and RF out put, with a 1.1dBm IF input at 200MHz

Fig. 3.1 shows the measured LO input and RF output power spectrum with a 1.1dBm IF input power. The 4 IF ports are excited by a 200MHz CW tone, each with an input power of approximately 5dBm, resulting in a total IF power of 11.6dBm loaded into the mixer. The phase between these four ports follow the differential IQ configuration, without any additional offset. The DC bias is set to -1.4V as the typical value recommended by the manufacturer.

Fig. 3.1a shows the power spectrum at the landing probe tip for the MUT LO input. We can first identify the LO input power around 15dBm at 85GHz. There are also IF to LO leakages at 85.2GHz and 84.8GHz, but they do not significantly impact the mixer performance. Fig. 3.1b shows the RF output power spectrum at the RF landing probe tips. Four major tones can be identified; the Upper Side-Band (USB) power at 170.2GHz, the Lower Side-Band (LSB) power power at 168.8GHz, the higher order harmonic products such as the tones at 170.4GHz and 169.6GHz, and the LO to RF leakage at 150GHz. The USB power is -20dBm, while the LSB power is -40dBm. The Image Rejection Ratio (IRR) can be calculated for each tone as the difference between USB and LSB power, which is 20dB without optimization. The Conversion Loss (CL) can be derived as the difference between IF input power and USB power, which is 31dB. Similarly, the LO to RF leakage is 45dB, derived by the difference between the LO input power and LO leakage.

3.2. Image Rejection Ratio

In this section, the image rejection ratio of the MUT operating at both USB and LSB mode is measured. The RF frequency is 160GHz with an LO input at 15dBm. The IF input power is -5dBm. Different IF frequencies are measured, with the relative IQ phase sweeping over the entire 360 degrees with a 4 degree grid.

Fig. 3.2 shows the measurements results. When the MUT is working on USB mode which has a phase offset close to 0 degree, an IRR of 20dB can be reached with a IQ phase offset of 20 degrees for IF frequencies up until 3GHz. Even in the worst case, where the IF frequency is set to 4GHz, the IRR is still above 15dB, showing a good agreement to the provided data sheet. When the MUT is working under LSB mode, however, a higher IRR can be achieved, up to 35 degrees for 4GHz single tone signals. Meanwhile, the relative phase that provides the highest IRR are not same for different IF frequencies, this indicates the changes of amplitude unbalance of the IQ ports is frequency dependent, due to the different behaviours of the wirebondings and the internal channel response of the MUT.

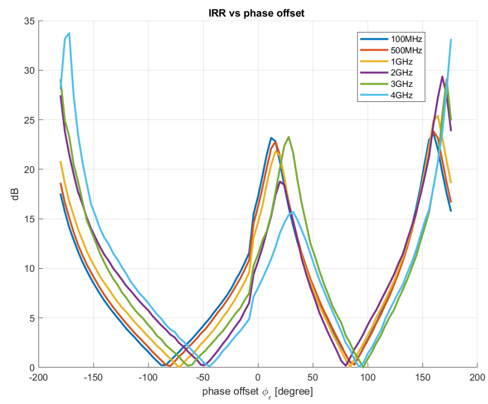

Figure 3.2: IRR versus phase offset at different IF frequencies

Ideally, by carefully tuning the phase and amplitude offset between IQ port, the IRR can be pushed to 50dB, as illustrate in Fig. 3.3. A look up table that contains the optimized phase and gain offset information can be used to optimize the wideband modulated signals.

However, the optmized value may drifts over time. Moreover, due to the limited time for measurements, only a global phase offset of 20degree is applied. Fig. 3.4 shows the measured IRR for different IF

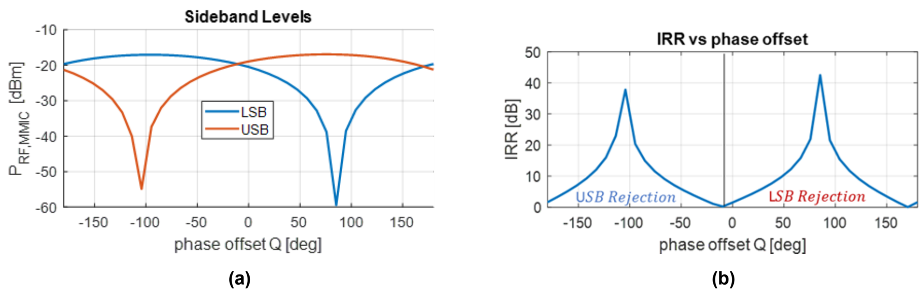

Figure 3.3: Optimized IRR and USB power from previous measurements

frequencies at 160GHz. The LO input power is still 15dBm, and the IF power is -5dBm. The IRR is greater than 19dB when the IF frequency is below 3GHz, then it drops to about 12 when the IF frequency goes up to 4GHz. This value matches to the provided datasheet from Gotmic, where no optimization is performed to the MUT.

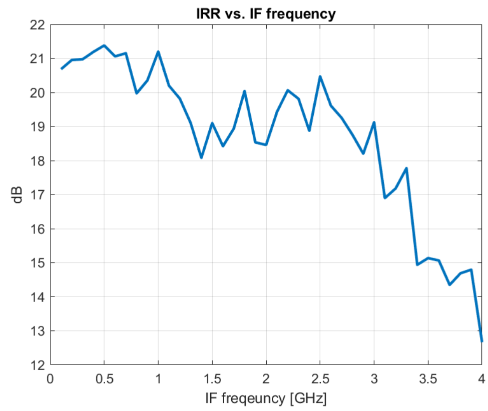

Figure 3.4: IRR vs. IF frequency

3.3. Conversion Loss

With the IRR of the MUT measured, the CL can be easily obtained from the same optimized spectrum results. The mixer operates in a power back-off mode of -30dB, to ensure the mixer works in the linear regime. Fig. 3.5 shows the measurement results. The conversion loss is about 14 to 16dB over the IF frequencies from 100MHz to 4GHz, which are about 2-3dB higher than the given data sheet. The IRR decreases as the IF frequencies increase, which shows similar behaviour compared to the provided data sheet by Gotmic. The mismatch of CL could due to the calibration error, and the wire-bonding losses from IF ports.

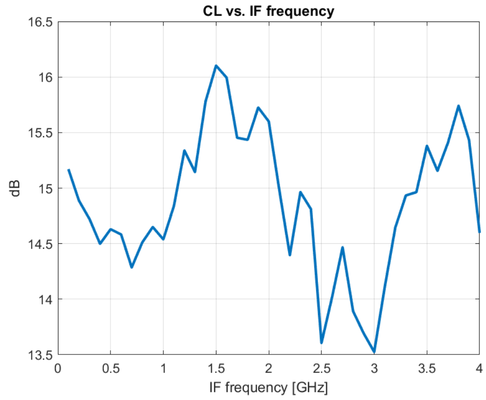

Figure 3.5: CL vs. IF frequency

3.4. Mixer Linearity

To measure the linearity, we start with the same setup used to measure the IRR and CL, keeping the phase offset (20°) while performing an iteration of the AWG output power. For an IF signal of 100MHz, with LO at 80GHz, the USB band signal is at 160.1GHz, and the second and third harmonics appear at 160.2GHz and 160.3GHz. Fig 3.6 shows the relationship between the second and third harmonics, and the fundamental products versus IF input power. The solid lines are measured results, while the dashed lines are extrapolated based on the measurement results to find the OIP2 and OIP3 points.

The P1dB point appears at -10dB when the IF input power reaches around 6dB for all different frequencies. This value is 5dB less compared to the given data-sheet. The difference could be from the difference in conversion loss, where a 3dB higher conversion loss could lead to the difference in P1dB. The OIP2 is around 5dBm, while the OIP3 is around 0dBm. It can be noticed that both 2nd and 3rd harmonics also suffer from saturation when the IF input power is above 5dBm. When the IF is set to 3GHz, however, no intercept points are observed, due to the fact that the high order harmonics are out of the mixer bandwidth.

The P1dB implicates that the maximum power out from the MUT is expected to be around -10dBm. Meanwhile, in this saturation mode, the noise contributed from the higher order harmonics will be about -30dBm, providing a signal interference ratio about 20dB. This will helps to analyse the link budget of the communication system.

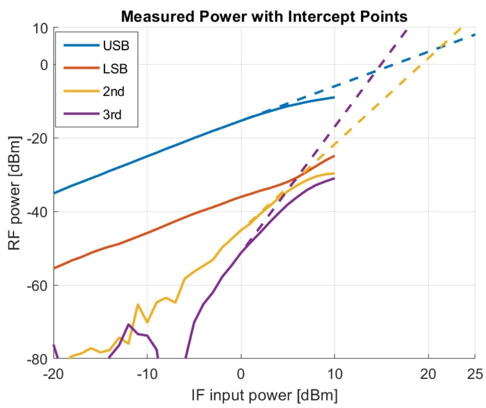

(a) 100MHz

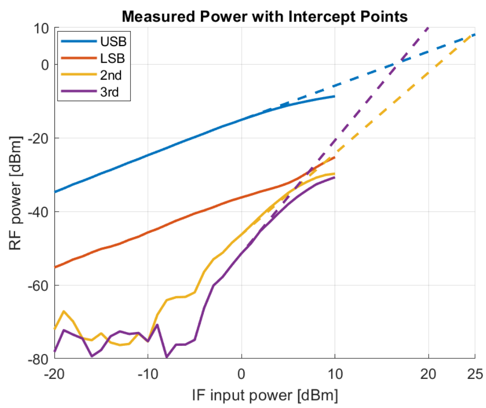

(b) 200MHz

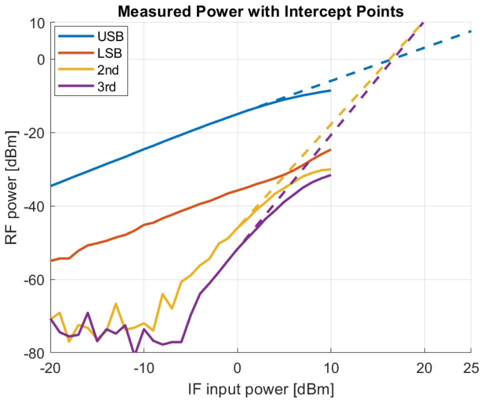

(c) 300MHz

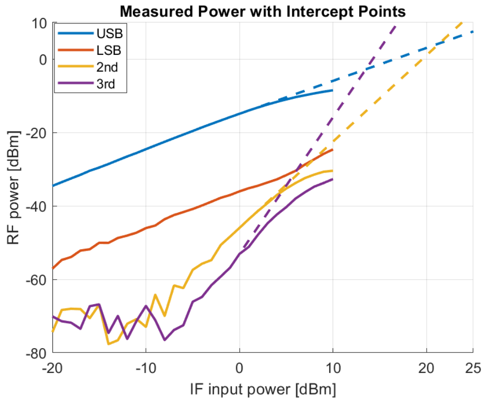

(d) 500MHz

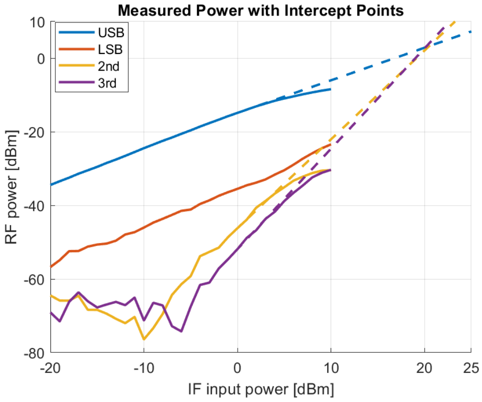

(e) 1GHz

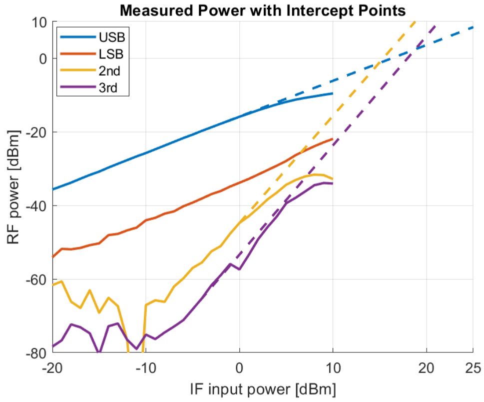

(f) 2GHz

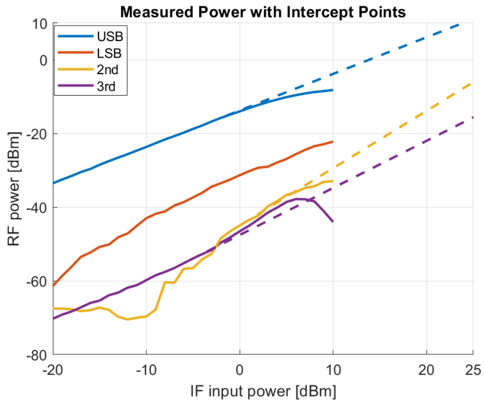

(g) 3GHz

Figure 3.6: Linearity of MUT measured at different IF frequencies

4

Reference Phase Channel Implementation for a Frequency Extender Based Setup

The phase acquisition required for the EVM characterization will be explained in this chapter. First, the phase of the RF channel is analysed. Second, a reference phase channel is proposed and explained . Then the setup is tested in ADS simulation software and implemented on a WR10 fundamental mixer. Finally, the proposed setup is implemented with the MUT using different reference sources, the phase stability is checked with both single tone signals and modulated signals.

4.1. Introduction

Consider the setup that was introduced in 2.2. Suppose the VNA_{src1} has a stable phase ϕ_{src1} at frequency f_{src1}. After the WR10 extender, the frequency will be multiplied by 6 to f_{LO} with a phase φ_{LO} equal to $6\varphi_{src1}$.

For the AWG output, consider the I^+ channel to have φ^i_{IF} at frequency f^i_{IF}. The superscript i means that the IF signal can have multiple tones. The other ports will be synchronized to the I^+ port with a fixed relation, and therefore will not effect the analysis.

Meanwhile, since the MUT is a sub-harmonic mixer, the RF frequency will be the double of LO input frequency. At the mixer output, the phase of the LO-RF leakage at f_{RF} will be $2\varphi_{LO}$. For the unconverted upper side band signal at $f^i_{USB} = 2f_{LO} + f^i_{IF}$, the phase will be $2\varphi_{LO} + \varphi^i_{IF}$, which can be written as $12\varphi_{src1} + \varphi^i_{IF}$. Similarly, the phase of the LSB tone at $f^i_{LSB} = f_{RF} - f^i_{IF}$ will be $12\varphi_{src1} + \varphi^i_{IF}$, as illustrated in Fig. 4.1.

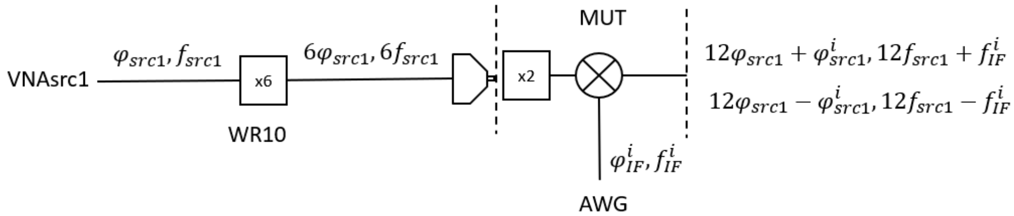

Figure 4.1: Illustration of the phase before and after the MUT

Meanwhile, the VNA^i_{src2} will generate a signal with phase φ^i_{src2}, to convert the signal at $f^i_{USB}$to the receiver frequency f_{rec} . Consider the case when $12f^i_{src2} > f_{RF} + f^i_{IF}$, then the down converted signal at b_{rec} will have a phase φ_b that is equal to $12\varphi^i_{src2} - \varphi^i_{USB}$. It can then be rewritten as $12\varphi^i_{src2} - 12\varphi_{src1} - \varphi^i_{IF}$, which is presented only by the direct phase out from either the VNA source of the AWG output. Fig. 4.2 shows the phase relation after the MUT RF output port.

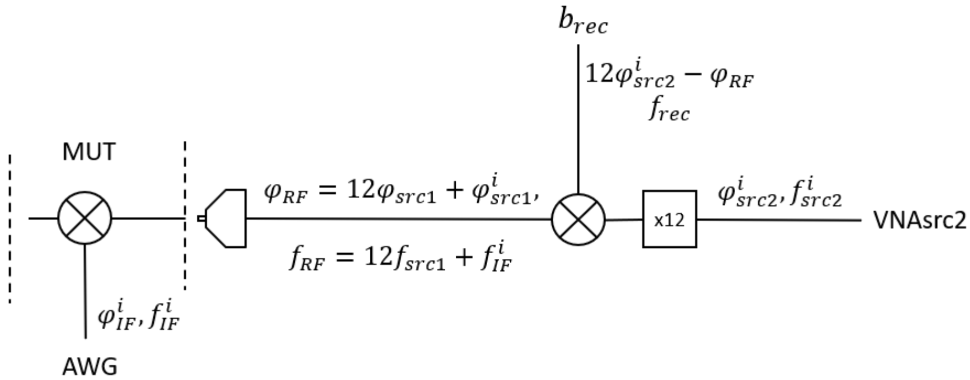

Figure 4.2: Illustration of the phase at the received port

For EVM measurements, repeated measurements of the spectrum are realized to obtain the constellation diagrams of the symbols transmitted. On each of measurements, the phase of φ_{src2} is swept across the spectrum grid. If the phase of VNA_{src2} is left unhandled, the readout of the phase is randomized when performing repeated measurements. From our measurements, we saw that when using the Keysight M8524B VNA which is equipped with the DDS synthesizer, the b_{rec} phase remains only stable when RF measurements were swept over $k \cdot 10$MHz frequency grid, with $k = 1, 2, 3....$ This poses a large limitation for the frequency resolution when performing demodulation measurements (e.g. EVM). To overcome this problem, we introduce an auxiliary channel that provides a reference phase. This way, despite an unstable b_2 phase when using fine grids, the relative phase can always be recovered from the auxiliary channel.

4.2. Proposed Reference Channel Setup

The reference channel carries the random VNA_{src2} phase information, which is read out by a second VNA receiver port c_{ref}. The goal is to generate a reference signal c_{ref} that has a coherent phase with b_{rec}. Since the VNA is a mixer-based receiver, which means the received signal will be mixed by an internal LO inside the VNA, as shown in Fig.4.3, it is essential that the reference channel output c_{ref}

has the same readout frequency f_{ref} as b_{rec}. Otherwise, the VNA will use different internal LO, which will still eliminate the phase coherency between the two channels. Thus, the reference channel will generate a multi (single) tone that matches the original multi (single) tone signal The b_{rec} phase can then be corrected by applying post-processing techniques.

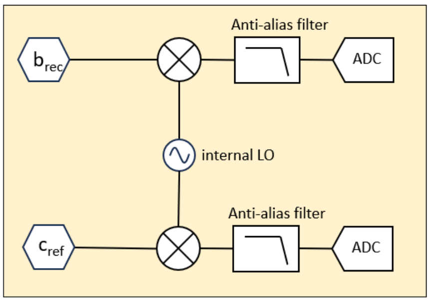

Figure 4.3: Simple illustration of the VNA receiver block diagram

Fig. 4.4 shows the proposed setup with reference channel similar to [15]. It uses two mixers, MXaux1 and MXaux2 operating <20GHz that will mix the source signals VNA_{src1} and VNA_{src2} from the VNA and a multitone signal from the AWG, AWG2. Under the scope of this project, we have explored the implementation of this AWG2 by an auxiliary AWG card, or the Sample Marker Out channel. This two cases will be explored in sections 4.4.

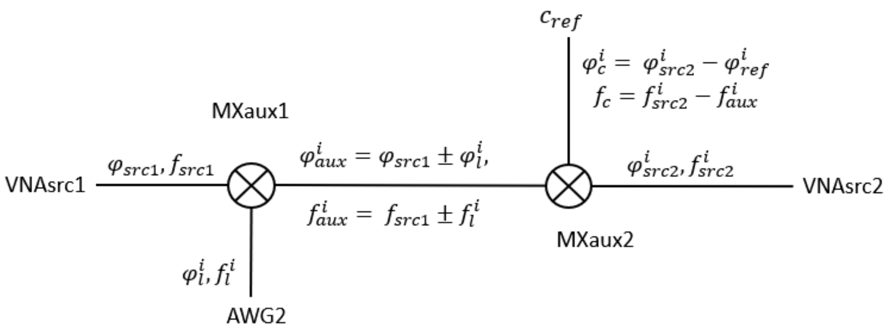

Figure 4.4: Proposed Auxiliary Channel

4.3. Validation of the Reference Channel Operation

Before implementing this concept a series of verification have been realized in order to tune and understand the concept. Subsection 4.3.1 validates the concept using ADS simulation software. Subsection 4.3.2 validates the concept on a waveguide based WR10 fundamental mixer.

4.3.1. Simulation verification in ADS

To verify the proposed setup, we first start to build a test simulation in ADS software. Fig. 4.5 illustrates the overview of the setup. Furthermore, instead of using the Wilkinson power divider, we separate the Duty Channel and Reference channel to reduce the simulation order, so that a shorter simulation time is required. A multiplication factor nRF and NLO is introduced at the source definition to simulate the frequency extender.

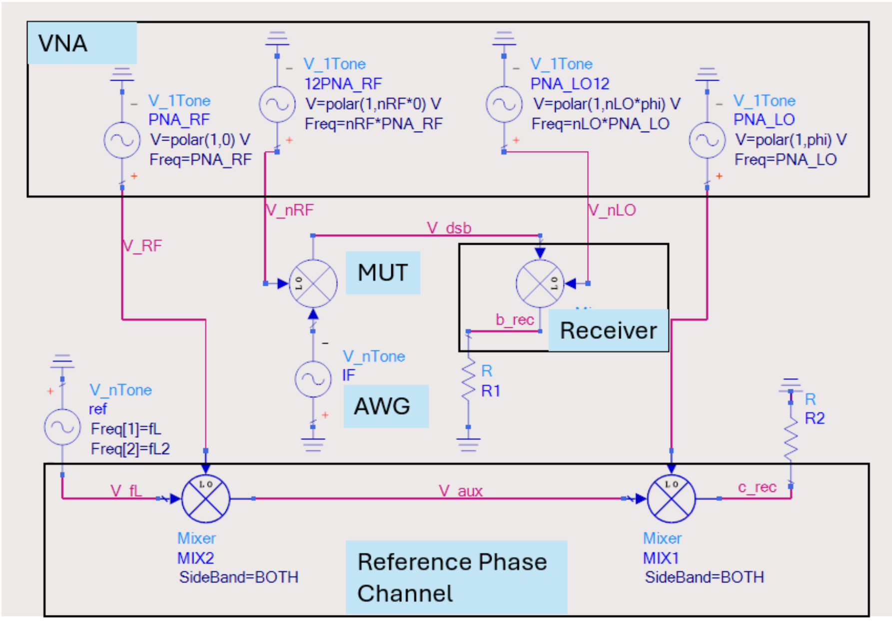

Figure 4.5: Schematic of simulation in ADS

We start with the multiplication factors nRF and nLO that are equal to 12. The IF is a two tone signal at 39MHz and 69MHz. The VNA_{src1} is at 12.5GHz. The readout frequency is at 279MHz. The VNA_{src2} is at 12.529GHz with a sweeping phase to represent the random phase of VNA, and it will down convert the IF at 69MHz signal to 279MHz. The reference channel source is set as shown in Fig. 4.13, with two tone signals at 308MHz and 305.5MHz

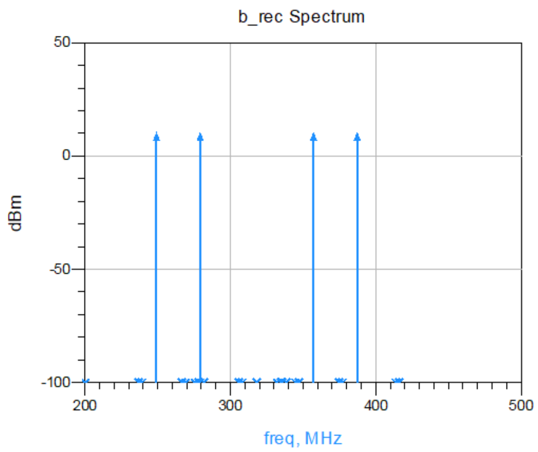

(a) b_{rec} port

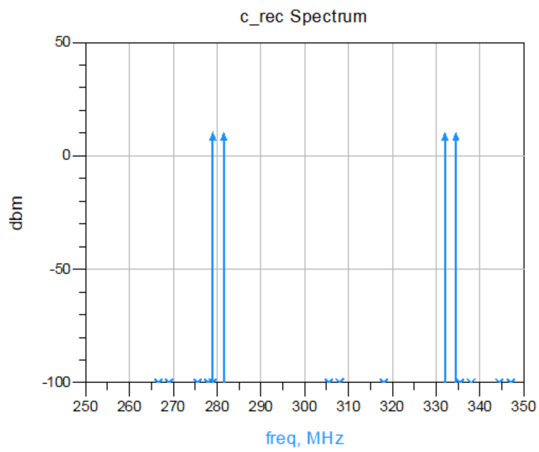

(b) c_{rec} port

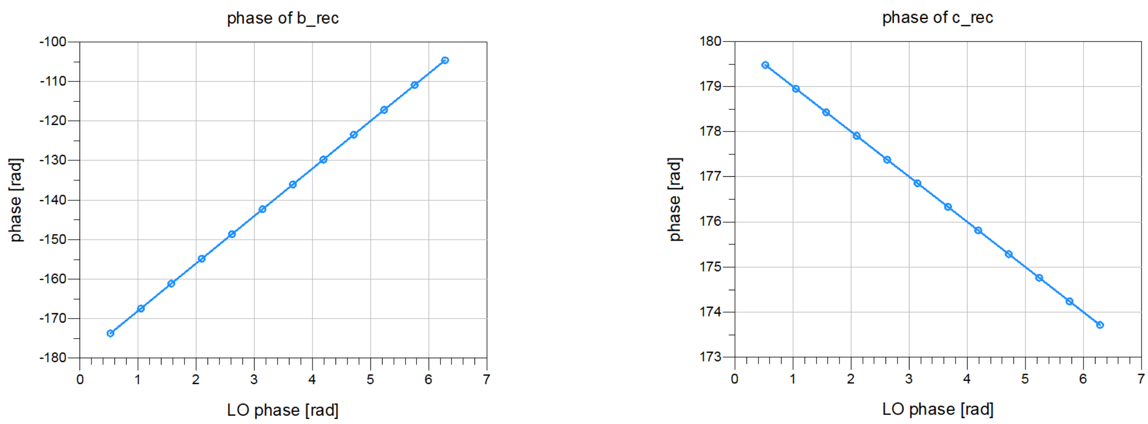

(c) b_{rec} port **(d)** c_{rec} port

Figure 4.6: Simulated Spectrum and Phase at receiver ports

Fig. 4.6a shows the simulated spectrum at b_{rec} channel. The image tones caused by the Mxau1 and MXaux2 lies on 380MHz, leaving no interference of the desired tone at 279MHz The phase at 279MHz is shown in Fig. 4.6c, and is swept according to the phase of VNA_{src2}. However, if we calculate the phase as $b_{rec} + 12c_{rec}$, then that phase will be stable, as shown in Fig. 4.7. This confirms the validity of the phase reference method to correct for random phase errors in b_{rec}.

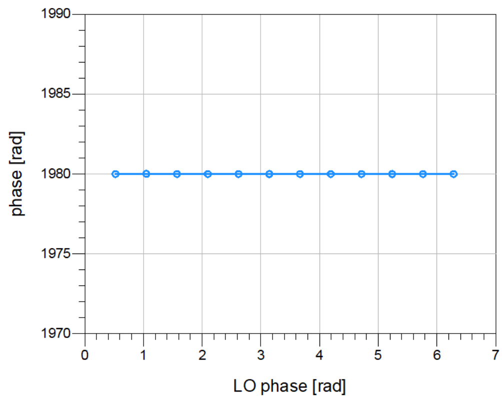

Figure 4.7: Simulation results of calculated phase

Then, the simulation is also tested with different multiplication factors. In this case, the LO is changed to 8 and 6. This changes the relationships between the b_{rec} and phase correction factors. The reference channel now requires a higher frequency input. Meanwhile, a different frequency setup as case 4 from section is used. The simulation results are shown in Fig. 4.8, where once again a stable phase can be obtained in this case.

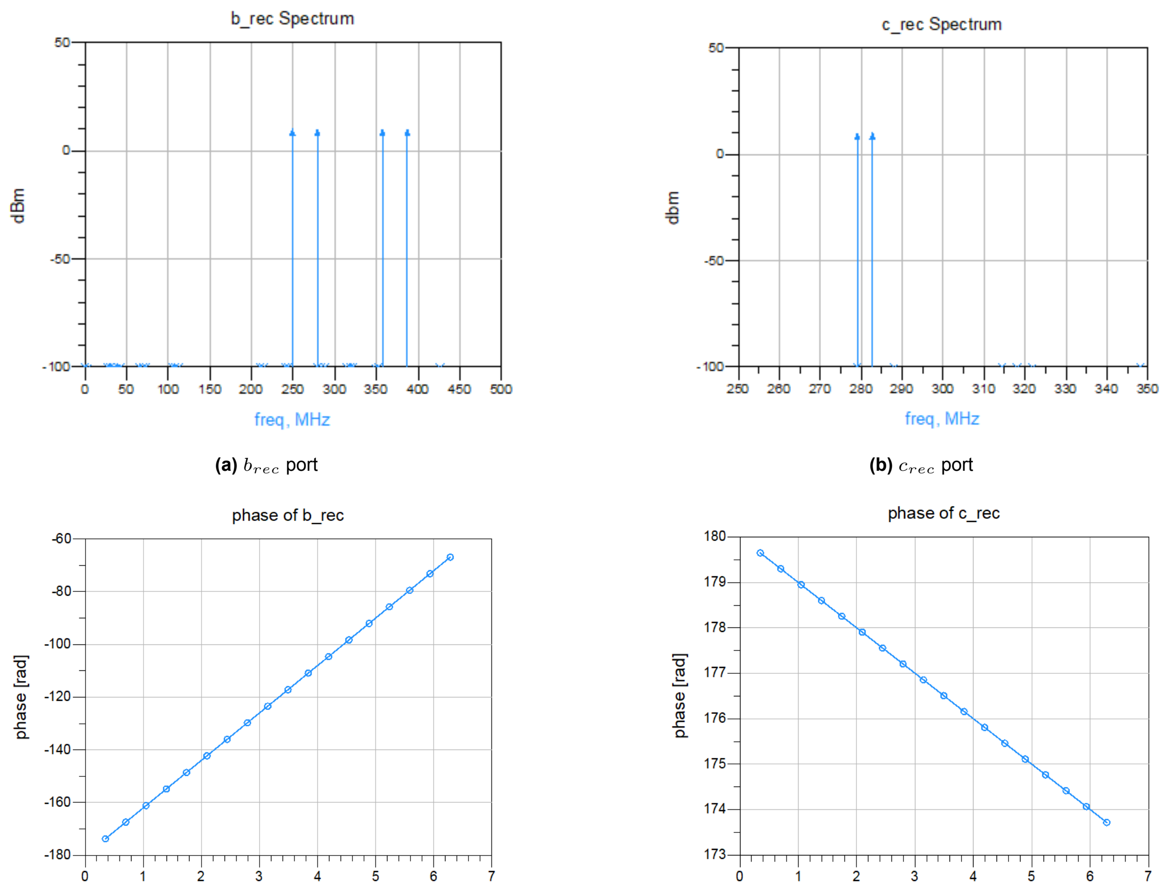

(a) b_{rec} port

(b) c_{rec} port

(c) b_rec port

(d) c_rec port

Figure 4.8: Simulated spectrum and phase at receiver ports

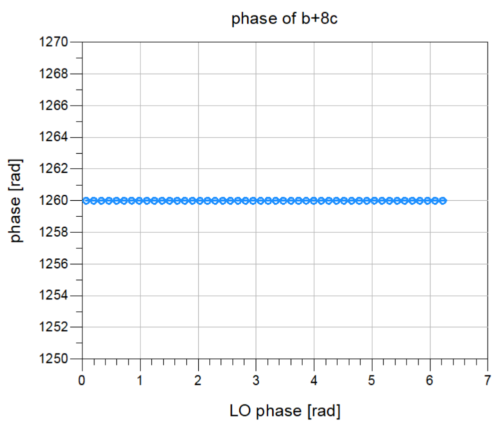

Figure 4.9: Calculated phase

4.3.2. Measurement verification using a fundamental mixer at WR10

After obtaining a validation from the simulation, before actually performing the measurements at D-Band with the RF probes, we tested the methods on a fundamental mixer at WR10. The setup is shown in Fig.

4.10. The waveguide mixer has a CL around 10dB from 70-90GHz. However, the WR10 frequency extender has a multiplication factor of 6 for RF path and 8 for the LO path. This requires a higher IF frequency output from AWG card reference channel As listed in Appendix C. Therefore, to reduce the IF frequency, we switched to WR6.5 which has same multiplication factor 12, operating at a bandwidth from 110-170GHz. In this case, the mixer is expected to still be working, but with a higher conversion loss. The reference channel mixer, MXaux 1 and MXaux2 are MiTEQ IRM0226MC1Q mixers, which support IQ signals input with an IF bandwidth of DC-500MHz. However, in this case only I port is feed with the power, and the Q power is terminated by a short. The splitter are the Marki PD0126 power dividers.

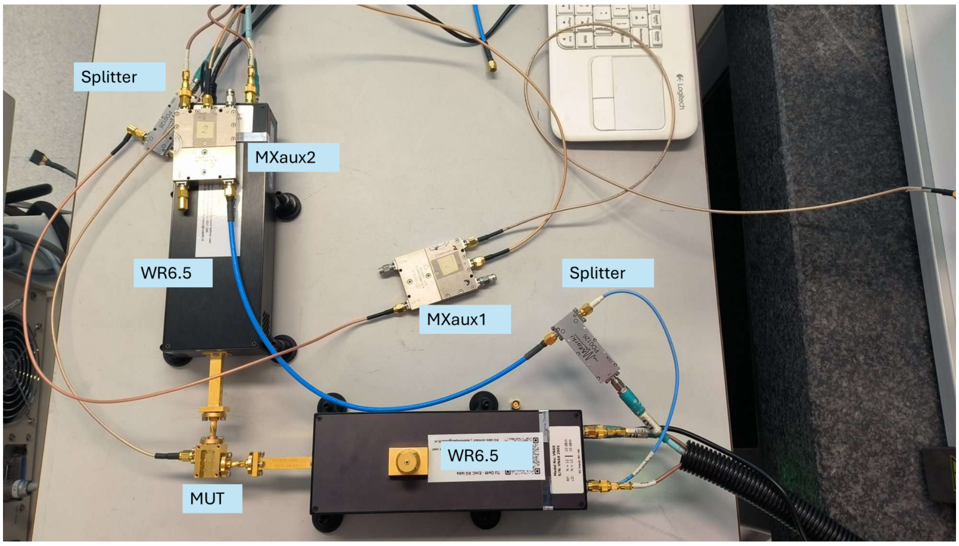

Figure 4.10: Measure Setup in Lab

Similar to the simulation, we start generating a two tone signal and verify it on the receiver. The IF frequency tone is 39MHz and 69MHz, and the auxiliary source tone are 305.5MHz and 308MHz. The VNA_{src1} is set to 12.5GHz and the VNA_{src2} is set to 12.529GHz. Therefore, the IF frequency at 69MHz will be readout at b_{rec} and auxiliary source at 308MHz will be read out at 279MHz. The calculated phase results are listed in Fig 4.11.

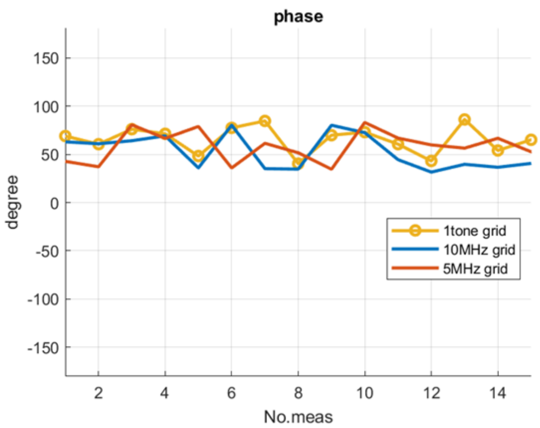

(a) Calculated phase using different sweeping grids

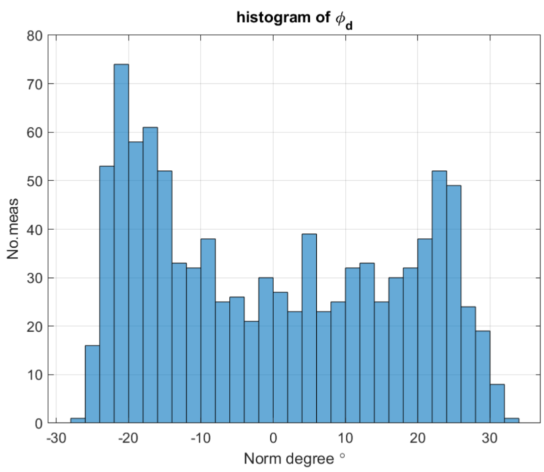

(b) d_{cal} port

Figure 4.11: Calculated phase with measurement results

At first glance, the phase still looks somewhat random. Therefore, we change the frequency grid setup, and measure the results again using a single tone setup, as shown in Fig. 4.11. In this case, single tone grid measurements is carried out to prevent the random LO fluctuation. As it turns out, even for the single tone grid setup, the corrected phase looks stable yet has a very high noise. One possible reason is due to the raw noise from c_{ref}, since any smaller noise will destroy the system after multiplication by 12.

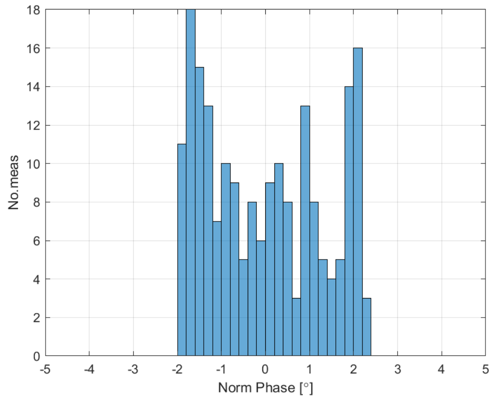

(a) f_{IF} = 305MHz

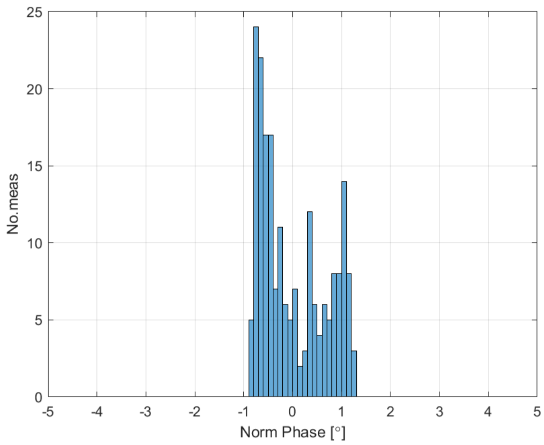

(b) f_{IF} = 150MHz

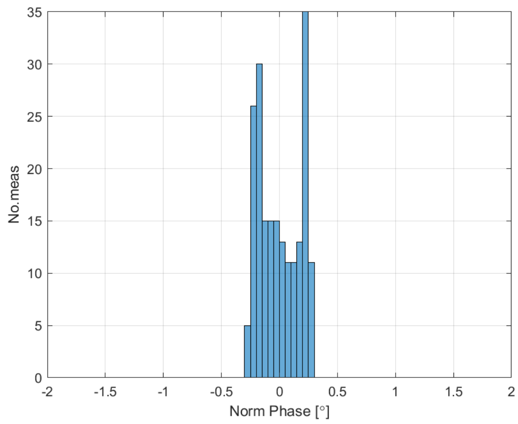

(c) f_{IF} = 50MHz

Figure 4.12: Measured AWG phase at receiver ports

To assess the problem, we start to de-embedded the reference phase channel. The raw performance of AWG is characterized by directly connecting the AWG channel to the VNA receiver port. The phase stability is shown in Fig. 4.12. Comparing the distribution of the measured phase of AWG output and the calculated phase, it is clear that the 12 times of noise completely dominant the fluctuation of the φ_d, resulting a fluctuation over $\pm 30 \circ$.

The AWG card we use is the Keysight N6030A, which has a frequency bandwidth of 500MHz and a sample rate of 1.25GSa/s. The frequency we used is around 300MHz, and is close to its Nyquist Sampling frequency limits. The phase stability is also measured at lower frequency such as 50MHz and 150MHz. As illustrate in Fig. 4.12, the lower frequency will have a better phase stability. The low sample rate of the N6030A can be solved by switching to the M8190A cards, which have 12GSa/s. For the actual implementation we switch to use the broadband M8190A AWG with 5GHz bandwidth. In the next section, the operation and phase stability will be studied.

4.4. Implementation of the Reference Channel

This section explores the implementation of the AWG signal for the reference channel $AWG2$. As mentioned in 4.2, in the scope of this project we have tested the generation of the multitone signal can be generated using a separate channel of the AWG card, and using the Sample Marker Out channel. Its trade offs and operability will be explained in the following subsections. A broadband AWG, Keysight M8190A with DC-5GHz bandwidth has been considered for these test.

4.4.1. Auxiliary AWG channel

In this subsection, the $AWG2$ signal has been implemented using an auxiliary AWG card. We will only consider how the signal can be readout from frequency at f_{rec}, which is expected to be a number that is less than 1GHz in order to avoid the use of expensive wideband AWG cards.

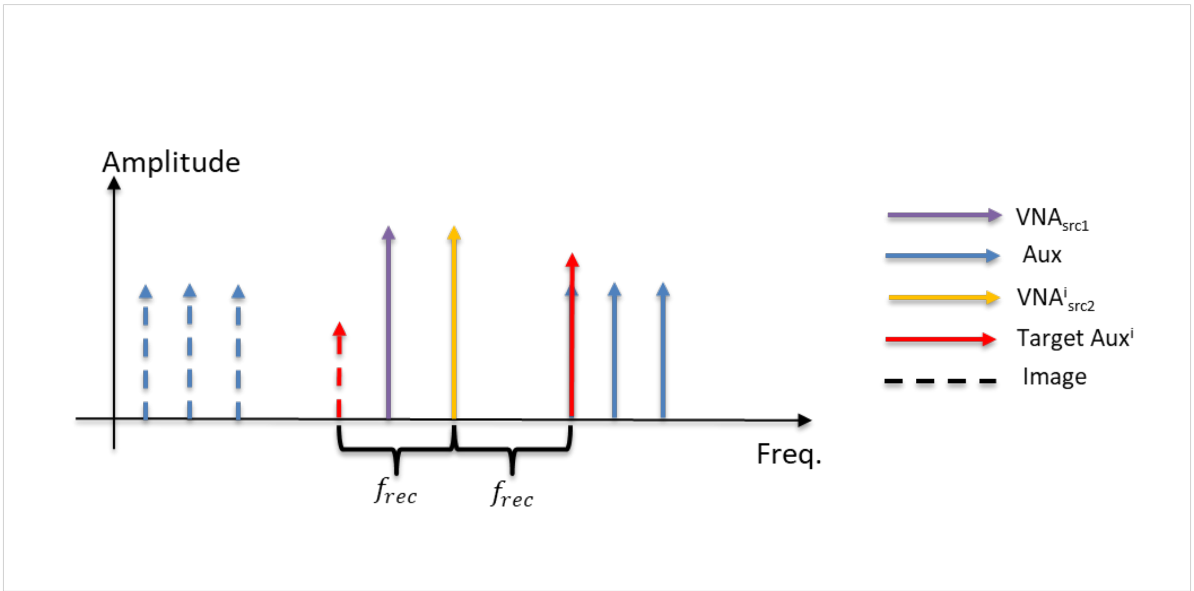

Figure 4.13: Illustration of the auxiliary channel spectrum

Table 4.1: Measurement Grid Setup

LO	IF	RF	b_{rec}	VNA_{src1}	VNA_{src2}	AWG2
f_{LO}	f_{IF}	f_{RF}	f_{rec}	$f_{LO}/6$	$(f_{RF} + f_{IF} + f_{rec})/12$	$(f_{IF} + 13f_{rec})/12$

Fig. 4.13 shows the example spectrum at auxiliary channel and how the auxiliary spectrum is down converted by the VNA_{src2}. The purple line represents the VNA_{src1}, and the blue lines represent the signals f_l that are upconverted by VNA_{src1}. The solid blue lines represent the upconverted signals f_l from that will be used as the reference tones. The sweeping VNA^{i}_{src2} signal is illustrated in the yellow line, and only refers to the i^{th} tone used in frequency sweeping. The solid red line, target tone will be down converted to the frequency f_{ref}. To allow the VNA to receive the current LO phase information at c_{ref}, the f^{i}_{aux} should be the sum of f^{i}_{src2} and f_{ref}. Note that f_{ref} is equal to f_{rec}, therefore it is replaced in Fig .4.13 . Since the f_{src2} is related to the IF frequency injected to the MUT, as described in Chapter 2, we find that the auxiliary channel source f^{i}_{l} is equal to $1/M \times f^{i}_{IF} + (M+1)/M \times f_{rec}$. Where M is the multiplication factor of the frequency extender.The frequency setup is listed in Table .4.1.

However, since the mixers MXaux1 and MXaux2 are not applying image rejection, the image frequency which appears at $f^i_{src2} - f_{rec}$ will also be down converted to the target frequency. The image tones from the MXaux1 are illustrated as dashed blue lines in Fig.4.13, while the image tones from the MXaux2 is illustrated by the dashed read lines. Since that VNA_{src2} is always greater than VNA_{src1}, therefore the LSB signal will never cause interference. However, the LO leakage could coincide with the image frequency. To avoid this interference, the frequency of VNA_{src1} must not equal to $f^i_{src2} - f_{rec}$ for any i. Meanwhile, when the modulated signal IF BW is wide, the sweeping LO tones will also occupy a larger bandwidth. When the LO overlaps with the USB signals, it is possible that the one of the USB tones will be the interference of another. Therefore, either the IF BW of the MUT channel is greater than $2Mf_{rec}$, or the multiple integer frequency grid $i \times \Delta f$ is never equal to $2M \times f_{rec}$, so the image frequency will never coincide with a existing tone.

4.4.2. Sample Marker Out from AWG

The previous proposed implementation requires an auxiliary AWG card for the reference channel. However, the M8190A AWG card has a special out put port Sample Marker Out (SMO). The Sample Marker Out can generate a user-defined on-off signal. In this case, we will define a simple periodic square wave, which results a discrete sinc function in the frequency domain. In this section, the implementation of the reference phase channel with such a signal is discussed.

Fig. 4.14 shows an example square wave in time domain and frequency domain. This signal has a period of 40ns and a duty cycle of 10%. This results in a sinc shape spectrum in frequency domain, with a grid of 25MHz and the first null at 250MHz. In practical, a denser frequency grid will needed, and the duty cycle may be reduced to 0.33%, and we expect the auxiliary AWG will perform better than the Sample Marker Out channel.

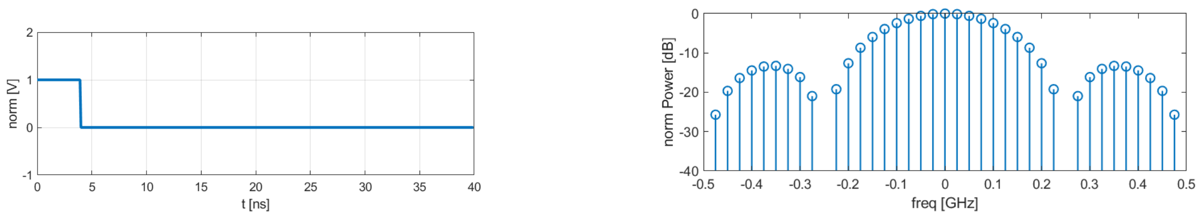

Figure 4.14: Ideal periodic square wave

The previous implementation only discussed how the single side band signals are served as phase references. In this case, we will discuss the special case where the DSB can also be used as the reference signal. The spectrum example is shown in Fig. 4.15

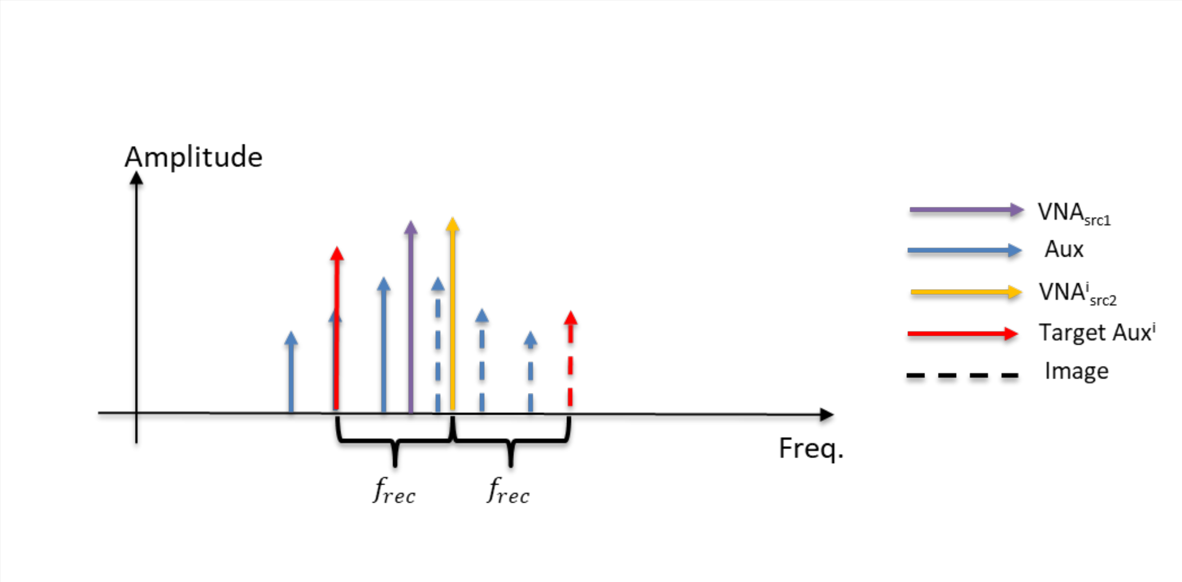

Figure 4.15: Illustration of the auxiliary channel spectrum

Table 4.2: Measurement Grid Setup with Sample Marker Out

LO	IF	RF	b_{rec}	VNA_{src1}	VNA_{src2}	reference source
f_{LO}	f_{IF}	f_{RF}	f_{rec}	$f_{LO}/6$	$(f_{RF}+f_{IF}+f_{rec})/12$	$(f_{IF}-11f_{rec})/12$

In this case, instead of separating the USB and LSB signals, we will consider a general case for the frequency tones from the source f_l^i which can be negative to represent the negative frequency at the auxiliary channel source output. Clearly, the phase of f_l is odd symmetric while the amplitudes are even symmetric. Then unconverted signal after MXaux1 f_{aux}^i will then be $f_{src1}+f_l^i$, as illustrate in Fig .4.15. To use all the DSB tones as reference signals, the auxiliary channel source tones f_l^i has to be $1/M \times f_{IF}^i - (M-1)/Mf_{rec}$. Furthermore, since the LO leakage of the MXaux1 at f_{src1} overlaps with the DC tone from the square wave, it will also serve as one part of the reference phase sources. The frequency setup is listed in Table .4.2.

Similarly, to avoid the interference from the image frequencies, $i \times \Delta f$ cannot equal to $2Mf_{rec}$.

4.4.3. Phase stability measurement of the AWG outputs

The phase stability for both implementations has been measured directly at the output of the AWG, to estimate their performance. To remove the synchronization fluctuations between the AWG and VNA, the first AWG Channel output is directly connected to the VNA port B, while the auxiliary AWG channel output is connected to VNA port A. Both AWGs are set to generate a single tone signal at 200MHz, with 0dBm power. The VNA is set to measure continuously at 200MHz. The phase is obtained by calculating the angle of B/A, removing any drifting error between the AWG and VNA. Fig. 4.16a and Fig. 4.16b show the phase stability when comparing the VNA IF BW of 300Hz and 5KHz.

Similar tests are performed with the AWG sample marker out. In this case, the signal length is specified as 960 Samples, resulting a sinc signal at sample marker out with 12.5MHz frequency grid and a frequency tone with about -20dBm at 200MHz.

Fig. 4.16 shows the measurement results with the different AWG outputs. For the auxiliary AWG channel, it is obvious that by calculating the phase of B/A, the variation is reduced. This proves that the noise and drifting errors between different AWG channels only contributes to a phase fluctuation that is less than $\pm 0.1°$. For the sample marker out, however, the fluctuation cannot be cancelled when the VNA IF BW is set to 5kHz. This could be due to the limited power range since 200MHz tone is close to the first null of the sinc spectrum, as shown in Fig. 4.14. What's more, when measured phased will be multiplied by 12 when

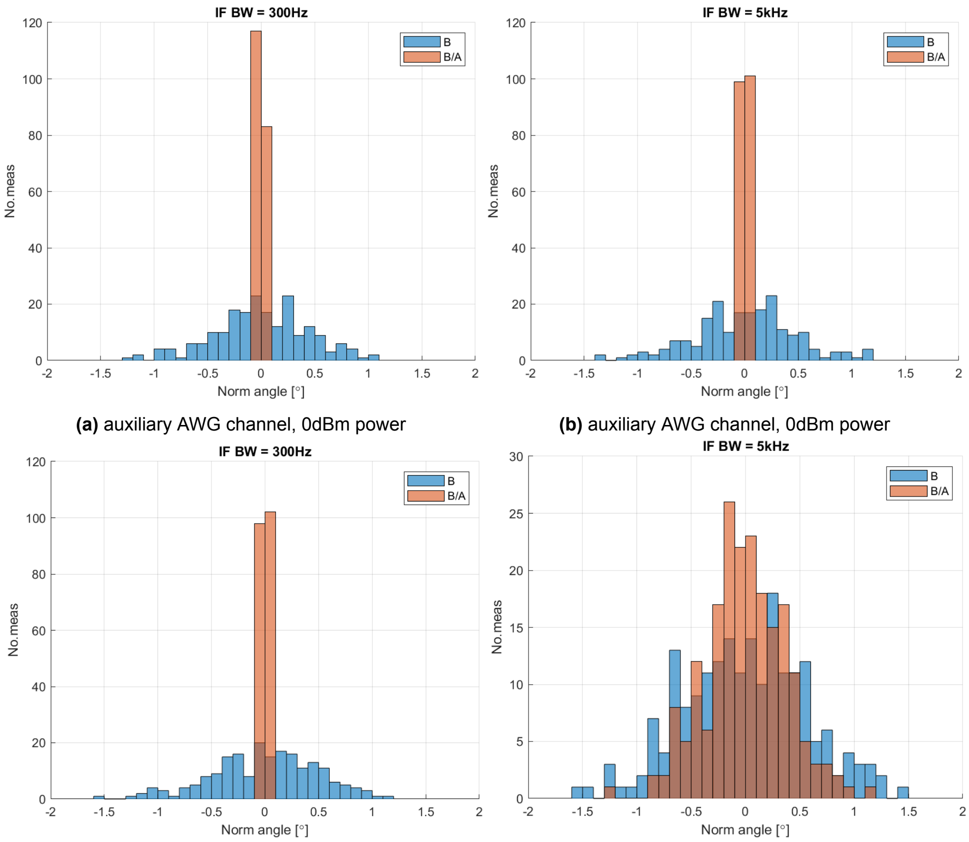

(a) auxiliary AWG channel, 0dBm power

(b) auxiliary AWG channel, 0dBm power

(c) Sample Marker Out, -20dBm power

(d) Sample Marker Out, -20dBm power

Figure 4.16: Phase Stability directly measured at the output of the auxiliary AWG channel and SMO of the AWG

4.5. Phase Stability Measurements of the Proposed Measurement Setup

The completed measurement setup is built, and the down-converted phase from the MUT RF output is studied to assess the stability of the phase a stable that can be achieved for EVM measurements. Fig. 4.17 and Fig. 4.18 show the complete schematic layout of proposed measurement setup and the implementation in the lab. Both the auxiliary AWG channel and the sample marker out will be used as the reference phase channel. When using two cards, the synchronization between them is achieved using the Keysight M8192A synchronization module. In this section the measurements shown have been realized with the Keysight N5224B VNA. With this specific model which has a DDS synthesizer, a stable phase can be achieved with a special measurement frequency grid of 10MHz. Additional phase stability measurements using an older Agilent N5242A VNA are shown in the Appendix B.

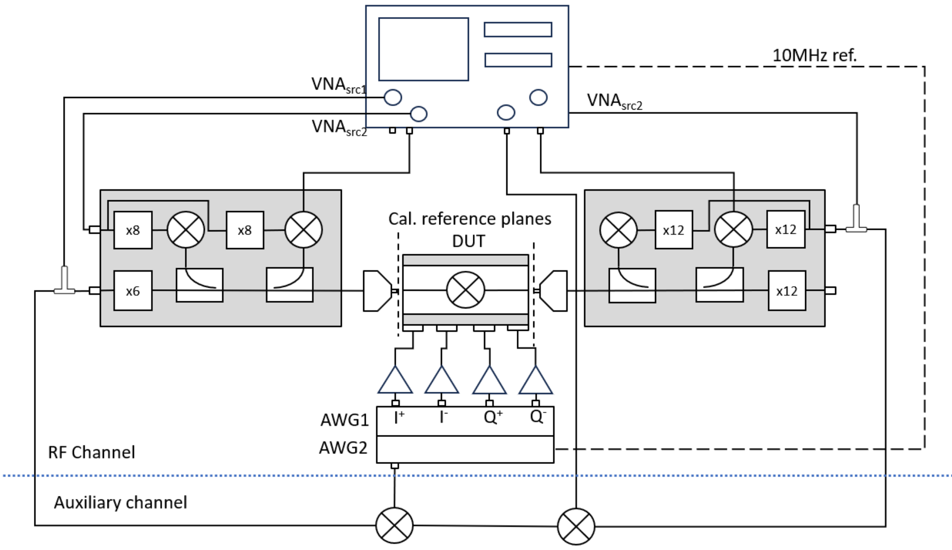

Figure 4.17: Schematic layout of the Proposed Setup

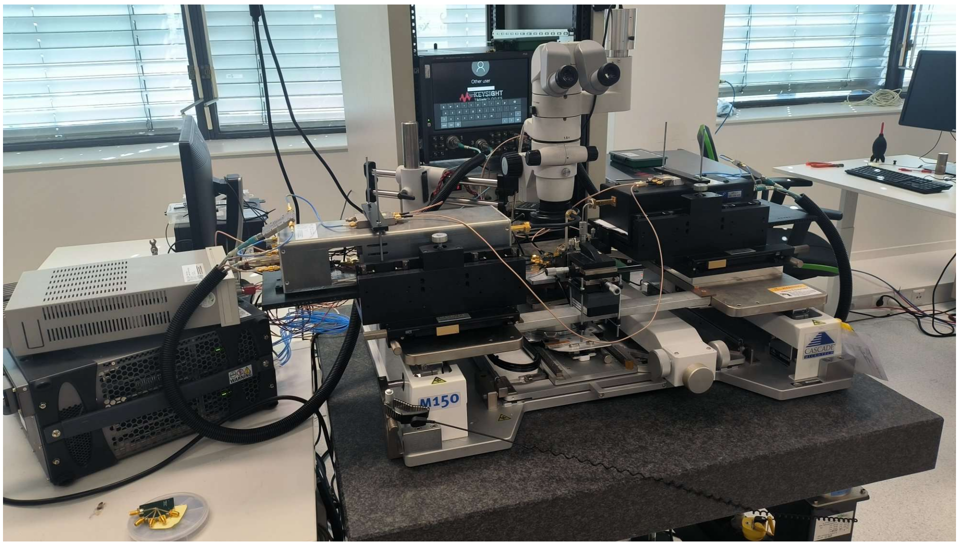

Figure 4.18: Photograph of the Proposed Setup in the Laboratory

4.5.1. Single-tone signal measurements

The phase stability of single-tone signals have been realized using the proposed setup using the AWG signal implemented using the auxiliary AWG channel and the Sample Marker Out. Table .4.3 lists the frequency setups foe different measurements.

Table 4.3: Single tone frequency Setups

reference source	f_{LO}	f_{IF}	f_{RF}	f_{rec}	f_{src1}	f_{src2}	f_l
Sample Marker Out	80GHz	250MHz	160GHz	63.63MHz	13.33GHz	13.3595GHz	15MHz
auxiliary AWG	80GHz	250MHz	160GHz	65.1MHz	13.33GHz	13.3596GHz	320.525MHz
auxiliary AWG	80GHz	250MHz	160GHz	279.1MHz	13.33GHz	13.3774GHz	552.3583MHz

The setup for the Square wave auxiliary source uses the same parameter as the one used in the previous section with an offset frequency f_{rec} of 63.6363MHz. Fig. 4.19 shows the results for the the phase stability, indicating a stability within 20 degrees.

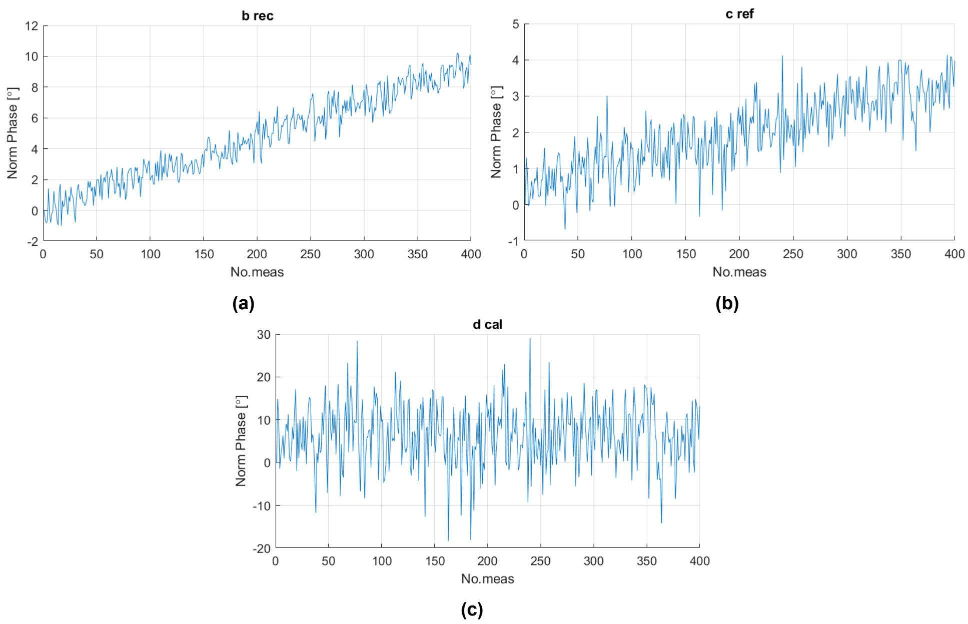

Figure 4.19: Phase Stability directly measured with Sample Marker at offset 63.6363MHz

The measurements of the auxiliary AWG channel are also tested with two different offset frequencies f_{rec}. One is 65.1MHz, close to the offset frequencies used with the Sample Marker Out. However, this frequency is far away from the recommended frequency (279MHz), therefore, similar measurement are also performed with f_{rec} set to 279.1MHz. The measurement results are listed in Fig. 4.20 (65.1MHz) and Fig. 4.21 (279.1MHz)

In addition, a drifting can be observed from the port c_{ref} and port b_{rec} when the offset frequency is low. Also the noise of phase d_{cal} is dominated by the 12 times multiplication of the noise from c_{ref}.

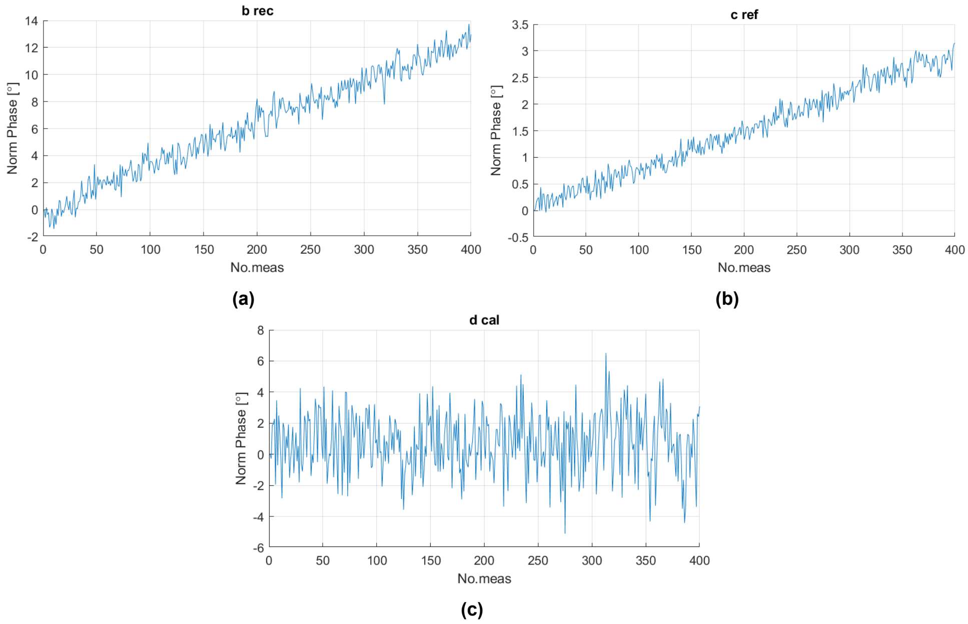

Figure 4.20: Phase Stability directly measured with auxiliary AWG channel at offset 65.1M

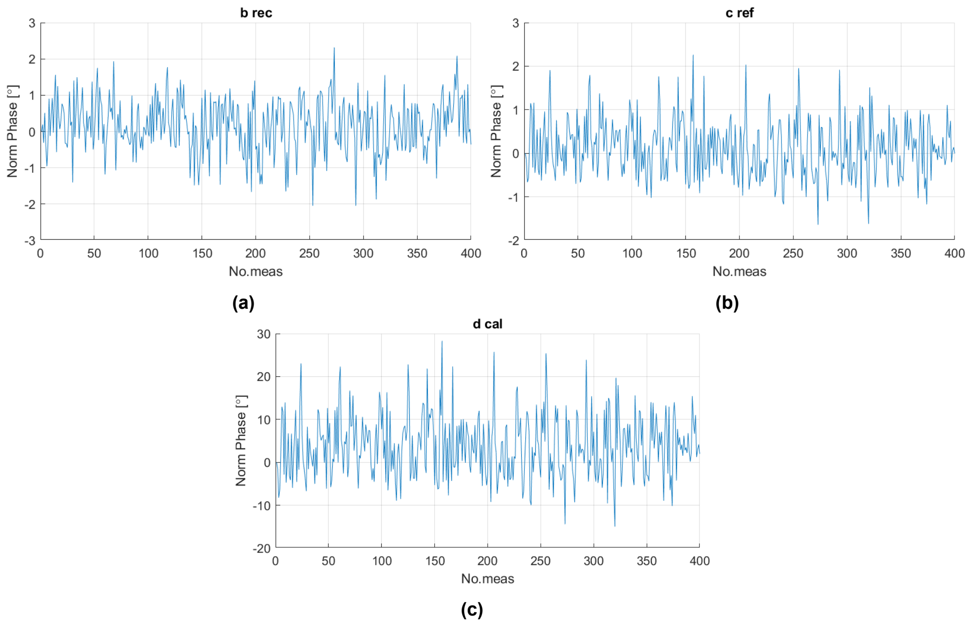

Figure 4.21: Phase Stability directly measured with auxiliary AWG channel at offset 279.1MHz

4.5.2. Modulated signal measurements .

The Phase stability is now tested with modulated signals using a multi-tone sweeping setup. Note that for this specific VNA, the phase source remains coherent through the repeated measurements if the VNA_{src2} is swept on a 10MHz grid, due to the nature of the DDS synthesizer employed. In this case, the LO phase shows a random 30° jumping, resulting in a relatively stable phase at b_{rec} port, since

$30° \times 12$ presents an integer number of 2π phase jumps.

A 100ns period, 300MHz BW QPSK signal that occupies a BW from 100MHz to 400MHz is generated. A 10MHz grid measurement setup is applied to measure the total 31 tones that represent the USB spectrum of the modulated signals. To check the phase stability of the measurement results, only one of the 31 tones is analysed, which is the frequency tone at 250MHz. The LO signal is set to 80GHz, therefore, the signal lies on 160.25GHz will be used to check the phase stability. Therefore, the frequency grid setup is same as Table .4.3 used for singel tone phase measurements.

Fig. 4.22 shows the measured raw phase results at b_{rec}, c_{ref} and the calculated phase d_{cal} with the Sample Marker Out. A phase stability of $\pm$15 degrees was obtained using the Sample marker out.

The same QPSK signal is also measured using the auxiliary AWG channel, setting the offset frequency at 65.1MHz and 279.1MHz, as shown in Fig. 4.23 and Fig. 4.24. A phase stability of $\pm$20 degrees is obtained when the offset frequency is 279.1MHz, while the other setup achieved a phase stability of $\pm$6 degrees. The resulting EVM will be discussed in chapter 5.

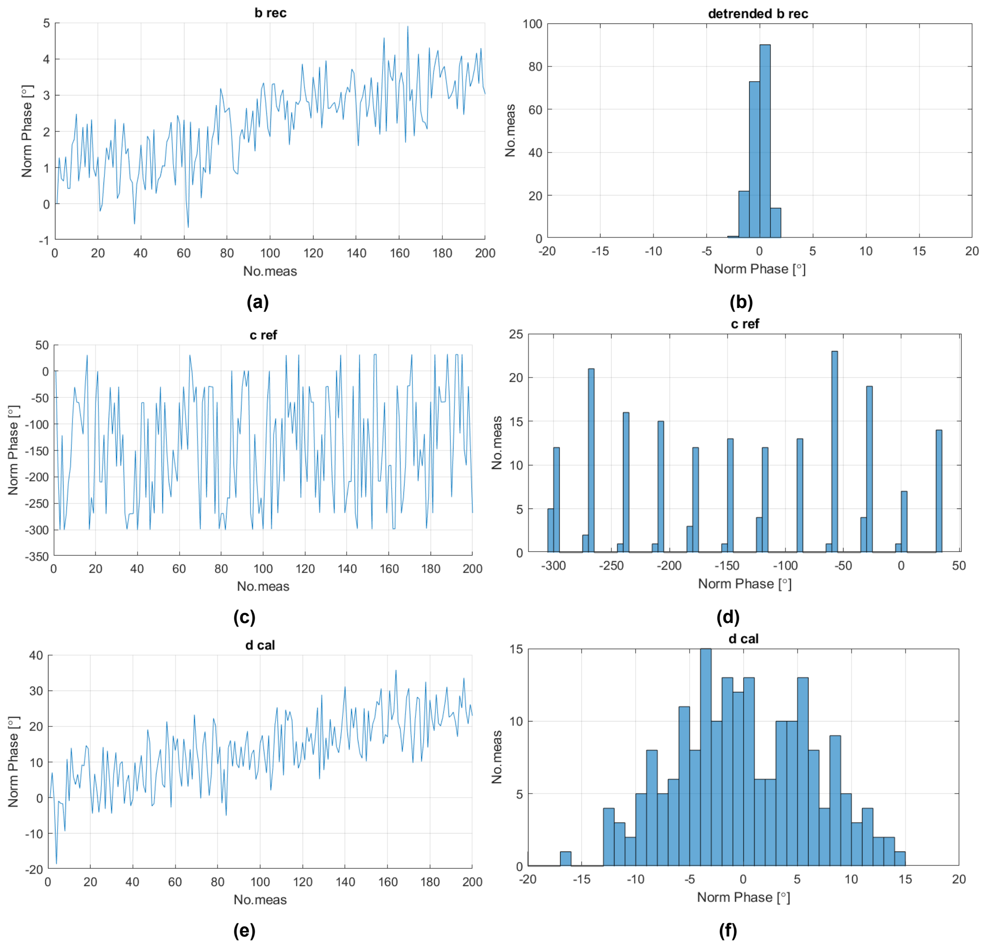

Figure 4.22: QPSK phase stability measured with Sample Marker Out at 63.6363MHz

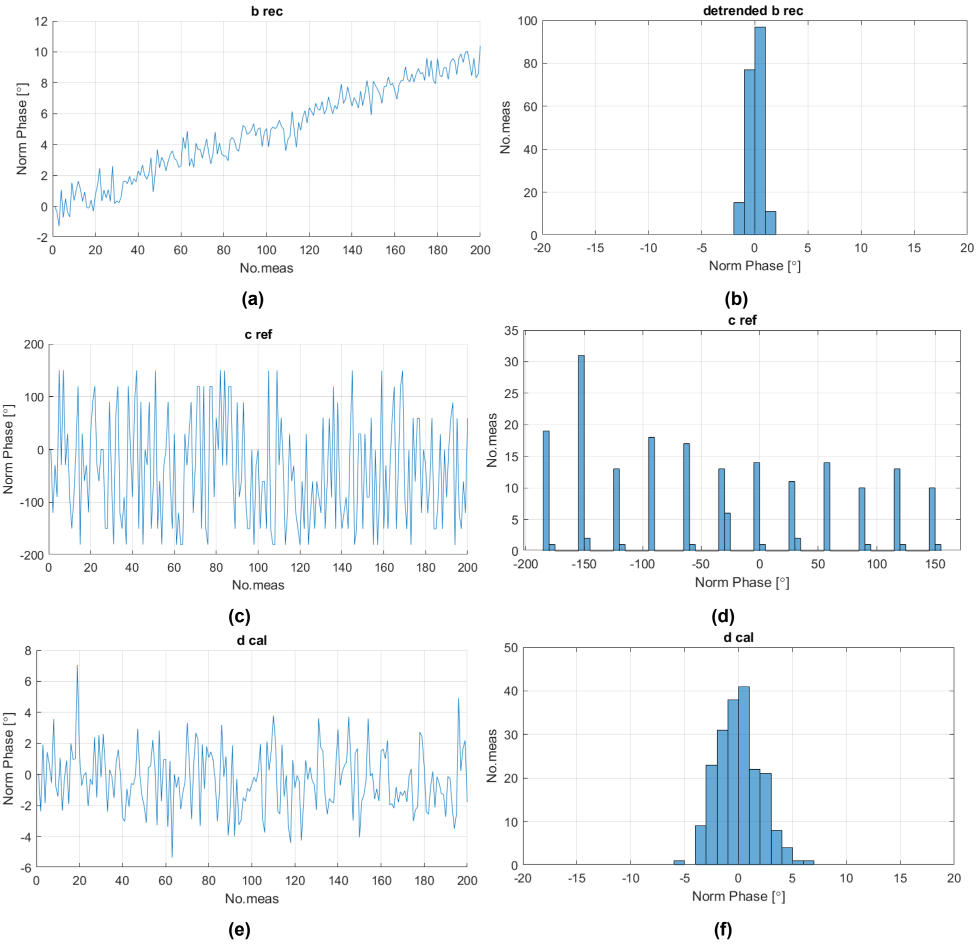

Figure 4.23: QPSK phase stability measured with the auxiliary AWG channel at 65.1MHz

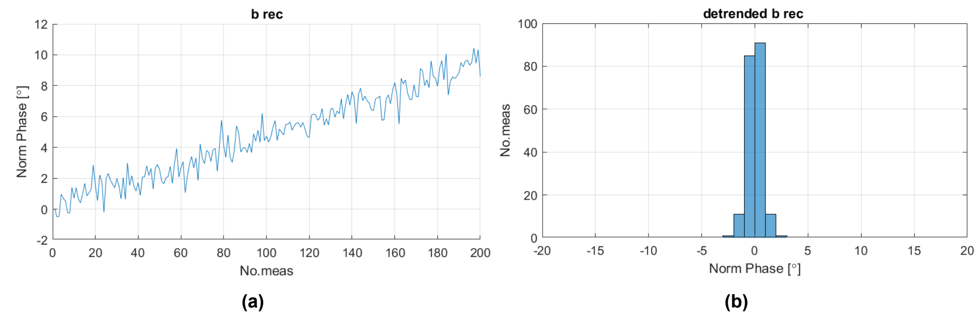

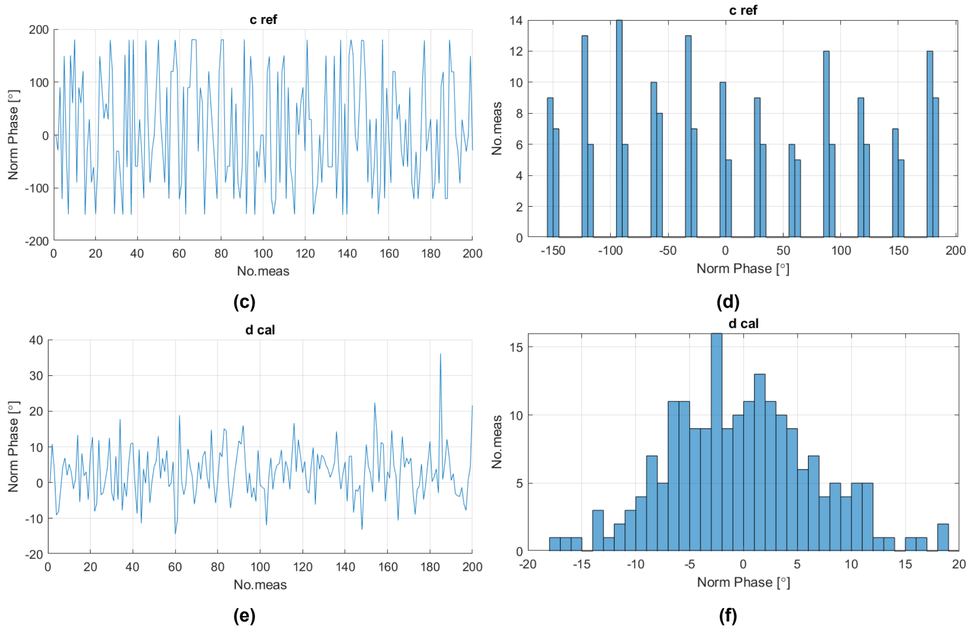

Figure 4.24: QPSK phase stability measured with the auxiliary AWG channel at 279MHz

To find out the reason that cause the different in the measured phase stability, we start to check the raw measurements data at port c_{ref}. Fig. 4.25 shows the measured raw amplitude and there corresponding auxiliary frequency tone. Note that in this case, the power is not calibrated, and the amplitude only represents the final read out combining all the possible losses in the auxiliary channel.

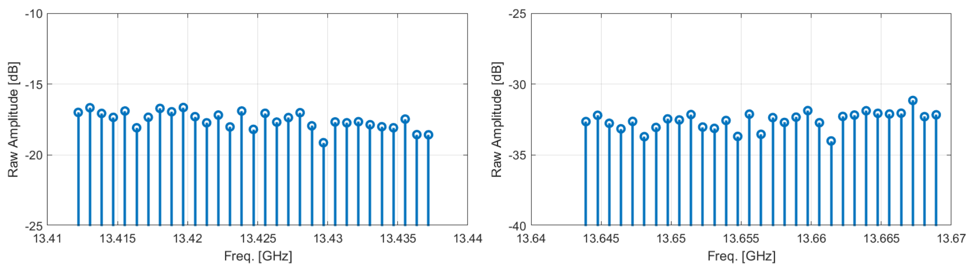

(a) results with the auxiliary AWG channel at 65.1MHz **(b)** results with the auxiliary AWG channel at 279.1MHz

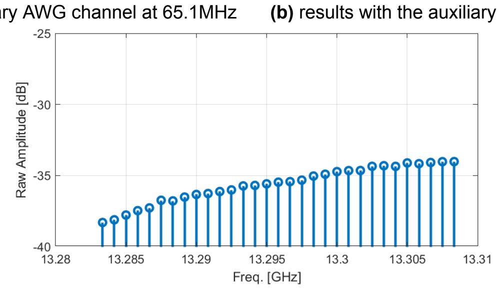

(c) results with the Sample Marker Out at 63.63MHz

Figure 4.25: Raw Measure Amplitude at port c_{ref}

While the readout using the second DAC at 65.1MHz has an amplitude around -17dBm, for the other two setups, the amplitude is less than 30dBm. Therefore, the phase stability is limited by the SNR from the auxiliary channel readout. For the square wave channel, the SNR is mainly limited by the output power at AWG cards. For the second AWG with offset at 279.1MHz, the limitation could be the IF bandwidth of the auxiliary mixers used in the setup. In this case, both the mixers work on an IF frequency around 300MHz, however, when the offset frequency is set to 65.1MHz, the mixers work on an IF frequency around 70MHz. The difference in the conversion loss could limit the final out put power and reduce the phase stability.

Then the phase is tested with 2MHz grid signal, using the auxiliary AWG channel. The results are listed in Fig .4.26. In this, stable phase results can not be obtained from the port b_{rec}. However, the calculated phase d_{cal} still remains a stability of ± 5 degrees for f_{rec} at 65.1MHz.

In conclusion the AWG direct out channel can still provide sufficient power and obtain same stability comparing to the 10MHz grid setup, the Sample marker start to lose the stability, due to the lower power per tone and the extremely small duty cycle (0.067%). For this reason, the auxiliary AWG channel is preferred for EVM measurements where phase stability in the setup is essential, but does come at the cost of requiring an extra AWG card.

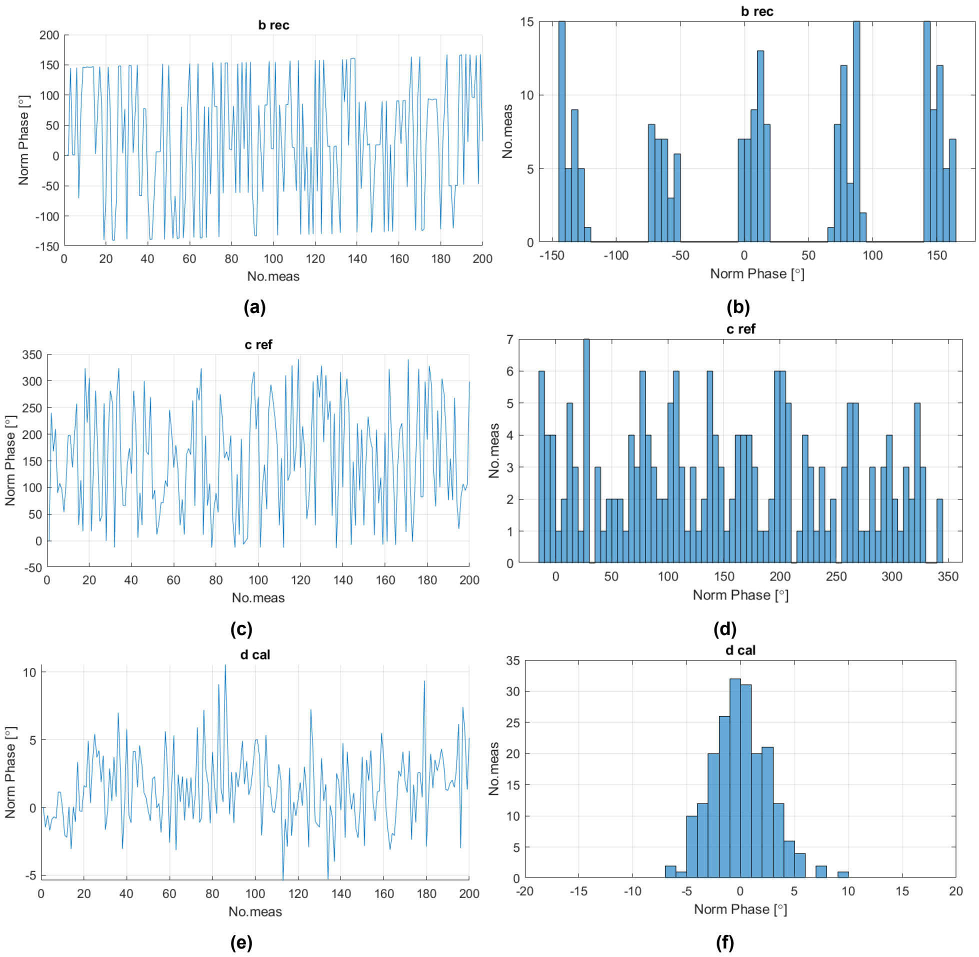

Figure 4.26: EVM phase stability measured with the auxiliary AWG channel at 65.1MHz

5
EVM Measurement

With the reference phase channel validated and implemented, the stable phase measurements can now be achieved with the combined VNA and extender setups. The EVM at baseband generated by the AWG card is directly measured using the Keysight UXA signal analyzer. After that, the EVM is measured with different modulation schemes over various bandwidths, and an EVM bathtub curve is derived by measuring the EVM over sweeping IF input powers. Finally, the results are compared with traditional EVM measurements performed by a wideband oscilloscope.

5.1. EVM Floor Measurements at Baseband

In order to assess the EVM measurement at D-band, we first measure the EVM that is obtained directly from the AWG channels. Thus, the modulated signal generated by the M8190A AWG are measured using a Keysight UXA signal analyser, to check the EVM floor at baseband. Unfortunately, the measurement is not performed with the N6030A AWG card due to the instrument availability. The modulated QPSK signals are generated with -6dBm at single channel, and the signal is demodulated and analysed by Keysight VSA software. The signal period is 100ns. However, due to the internal hardware setup of the UXA signal analyzer, only signals that have a BW less than 1.5GHz can be measured. Table5.1 lists the EVM for different modulated signals. While the QPSK signal has similar EVM with the 8PSK signal, the EVM of a 16QAM is always smaller. A EVM up to -30.5dB can be observed when the signals occupy a bandwidth from 100MHz to 400MHz without equalization, indicating a distortion within the channel. However, since the equalized filter will also be used in the proposed setup, only the equalized EVM will be used as the reference. Comparing the results of QPSK signals, the equalized EVM increase about 6dB as the bandwidth is increased from 300MHz to 1.2GHz. This can be explained by the increased thermal noise that contributes to the EVM as $-20log10(kTB)$.

Table 5.1: EVM floor measured with signal analyzer

Data Rate (bps)	Modulation	Symbol Rate (baud)	IF(GHz)	BW(GHz)	EVM (dB)	equalized EVM (dB)
500M	QPSK	250M	0.25	0.3	-30.4	-39.2
750M	8PSK	250M	0.25	0.3	-29.8	-39.2
1G	16QAM	1250M	0.25	0.3	-30.4	-41
500M	QPSK	250M	0.75	0.3	-38.8	-41.4
750M	8PSK	250M	0.75	0.3	-38.1	-41.4
1G	16QAM	250M	0.75	0.3	-40	-43
2G	QPSK	1G	0.7	1.2	-29.9	-33.2
3G	8PSK	1G	0.7	1.2	-30.2	-33.5
4G	16QAM	1G	0.7	1.2	-32.4	-35

5.2. EVM Measurements without Reference Phase Channel

As discussed in Chapter .4, by setting up a specific measurement frequency grid, with the Keysight M5224B VNA which has the DDS synthesizer, a stable phase results can also be achieved. Therefore, firstly the modulated signals with 100ns periods is measured without the reference phase channel. The EVM measurement based on such setup can be used to compare with the EVM obtained with the reference phase channel.

5.2.1. Narrowband EVM measurements

Firstly, the measurement is performed with the national instrument N6030A AWG cards, which has a sampling frequency up to 1.25GSa/s. In this case, a QPSK signal that has a symbol rate of 250M baud, with 25 symbols is generated. A root-raised cosine with a roll-off factor of 0.2 is used, and the central IF frequency is 230MHz. Therefore, the signal occupies a bandwidth from 80-380MHz, and the expected RF output is at 165.08-165.38GHz. Fig. 5.1 shows the signal in time domain and frequency domain at I^+ channel.

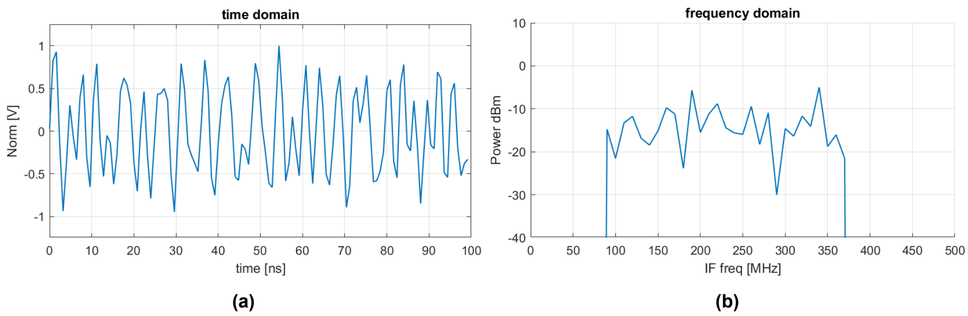

Figure 5.1: time domain and frequency domain of the QPSK modulated signals

Fig .5.2b shows the measured RF spectrum at the MUT output. The IF input power is 8.11dBm, which was derived from the previously characterized AWG power. And the offset frequency is set at 279MHz, with a VNA IF BW of 1kHz. It is clear to observe the USB signals from 165.08 to 165.38GHz, the LSB signals from 164.72-164.02GHz and the LO leakage. Compared to the reference signal spectrum, the setup successfully obtains the required RF spectrum.

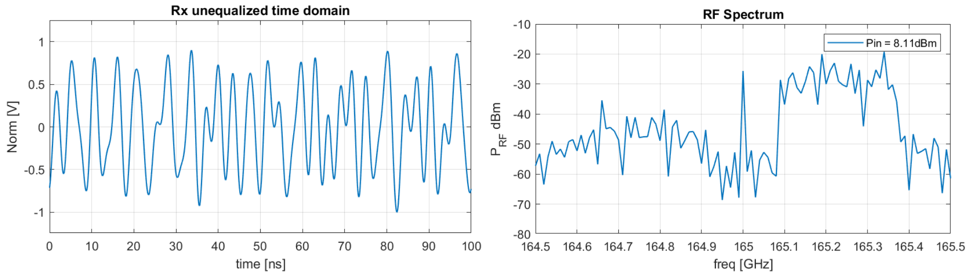

(a) **(b)**

Figure 5.2: time domain and frequency domain of the Rx QPSK modulated signals

To reconstruct the time domain signal and calculate EVM, only the frequency grid that covers the USB signals are measured to reconstruct the time domain signal. For example, to measure the EVM of the 300MHz BW QPSK signals , only the frequency tones from 160.08 to 161.38GHz with a frequency grid of 10MHz is needed.200 measurements are recorded for the EVM procedure.

To calculate EVM, the USB spectrum from the calculated data is then digitally down-converted to the same bandwidth as the reference signals, as shown in Fig. 5.2a. At the first glance, the signal is not similar to the transmitted signal. On one hand, the MUT channel response will cause a distortion. On the other hand, there is a constant time delay τ between the AWG card and the PNA receiver. This time shift is then related to a phase shift according to $\varphi_{delay} = 2\pi f_{IF}\tau$. Therefore A equalization filter is implement to compensate the channel response though the MUT and rotate the phase of each tone. Fig.5.3 shows the gain and phase rotation factor for each measured frequency tone.

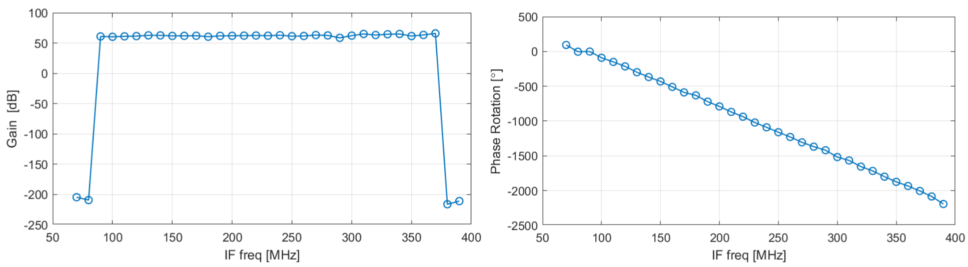

(a) Gain **(b)** Phase Rotation

Figure 5.3: Gain and Phase rotation of the equalization filter

After phase correction, the recovered signals is now similar to the reference one, as shown in Fig. 5.4a. Then we can apply demodulation and get the Rx symbols, The constellation diagram is shown in Fig. 5.4b, with an EVM of -32.2dB. In this case, the white noise could be the main errors source for the EVM.

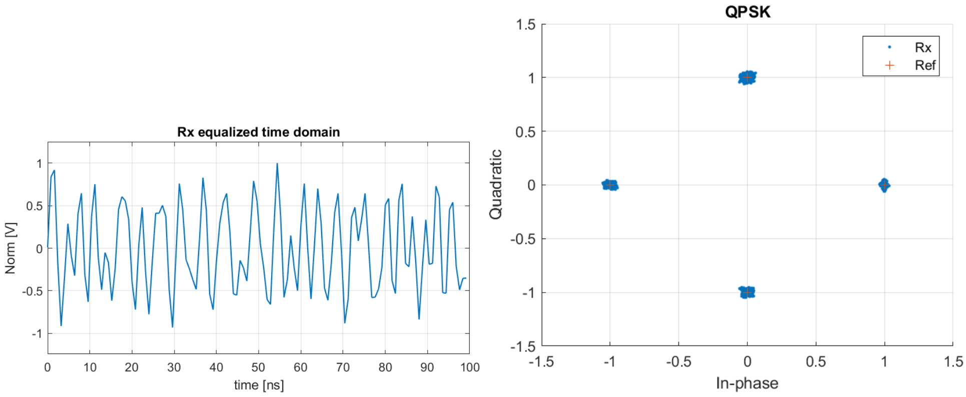

(a) equalized QPSK signal **(b)** Constellation

Figure 5.4: Equalized RX signal and Constellation diagram

Finally, the EVM is measured with a sweeping IF input power. Fig .5.5 shows the resulting EVM curve. The proposed setup obtains a EVM floor of -32dB. The thermal noise starts to dominant the error when the IF power is below -10dBm. However, the system fails to see the error due to the MUT linearity.On one hand, the higher-order harmonics mainly contribute to a coherent interference, which will be cancelled by the equalization filter. On the other hand, the relative low VNA IF BW might prevent us reconstructing the real behavior of the RF signals.

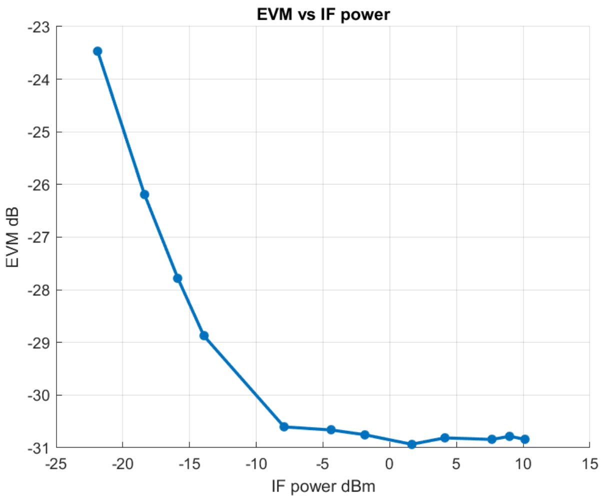

Figure 5.5: EVM vs. IF input power

5.2.2. Wideband EVM measurements

Similar measurements is continued with the M8190A AWG cards, which has a sample frequency up to 12GSa/s. Thus, the modulated signal bandwidth can be pushed to 3.6GHz as listed in Table .5.2. In this case, they are still on 10MHz frequency grid, and we can still relies on the phase results without the implementation of auxiliary channel. A root-raised cosine filter with a roll-off factor of 0.2 is implemented, as the one used before.

Fig. 5.6 shows the modulated signal in time domain and frequencies domain at the MUT I^+ channel, with a total input power of 0dBm. The absolute input spectrum can be estimated from the previous

Table 5.2: QPSK modulated signal parameters

Data Rate (bps)	Symbol Rate (baud)	IF	BW(GHz)	frequency grid (MHz)
500M	250M	0.25	0.3	10
2G	1G	0.7	1.2	10
4G	2G	1.3	2.4	10
6G	3G	1.9	3.6	10

calibrated AWG output power in Chapter 2. It is clear as the symbol rate increases, the time domain signals become more dense. Also, as the frequencies tones increases, the power will be shared by more tones.

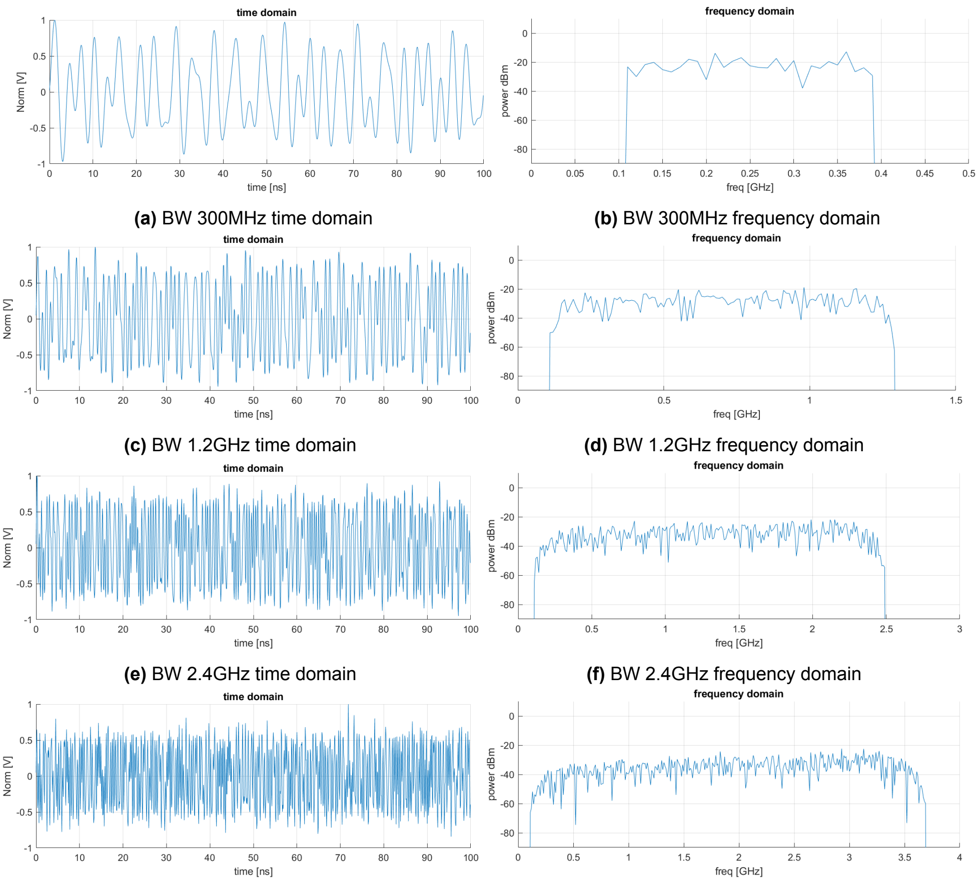

(a) BW 300MHz time domain **(b)** BW 300MHz frequency domain

(c) BW 1.2GHz time domain **(d)** BW 1.2GHz frequency domain

(e) BW 2.4GHz time domain **(f)** BW 2.4GHz frequency domain

(g) BW 2.4GHz time domain **(h)** BW 2.4GHz frequency domain

Figure 5.6: time domain and frequency domain of the QPSK modulated signals

The modulated signals are sent to the MUT with different IF input powers. The LO frequency is 80GHz with 15dBm power, therefore the RF frequency is 160GHz. As described in Chapter 4, the EVM can be measured at different offset frequencies, since any amplitude offset will be cancelled by the equalization filter used during post-processing technique. However, the absolute power can only be measured at the calibrated offset frequency, 279.09MHz, since only there was the absolute power calibration applied. Fig. 5.7 shows the measured RF spectrum. It is obvious to see how the non-linearity affects the out-of-band noise floor as the MUT starts to saturate. The out of band rejection ratio is about 20dB when the input power is 10dBm and 40dB for a input power of 0dBm. Also, as the IF power decrease, the high order harmonics and even the LSB signals reaches the VNA noise floor, resulting in a increased

SNR. Comparing to the EVM measured in based band, the EVM for 1.2GHz signal is also around 6dB higher than t

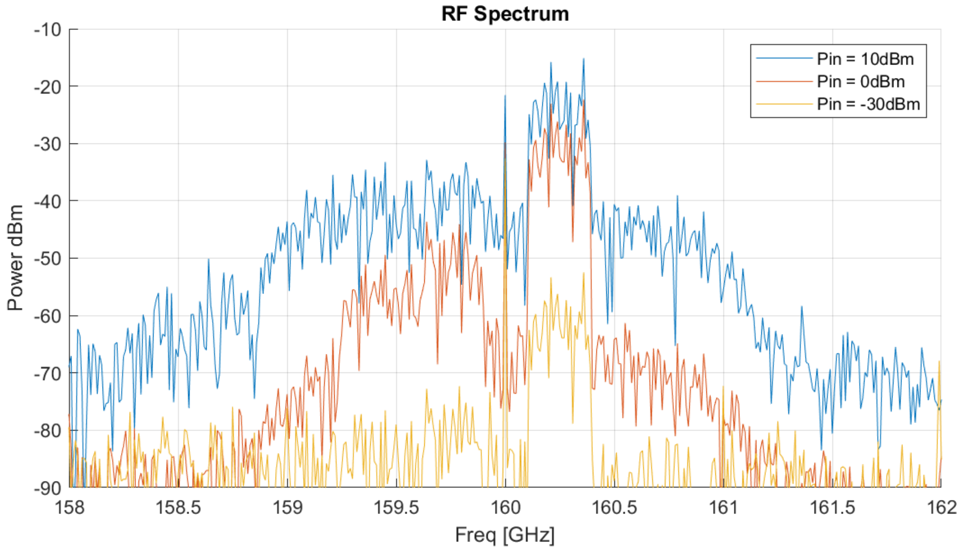

Figure 5.7: BW 300MHz

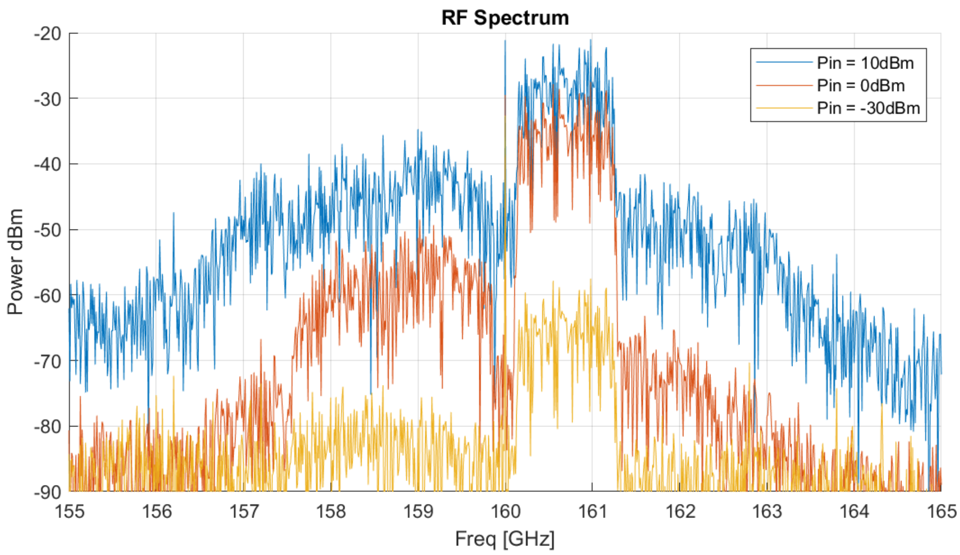

Figure 5.8: BW 1.2GHz

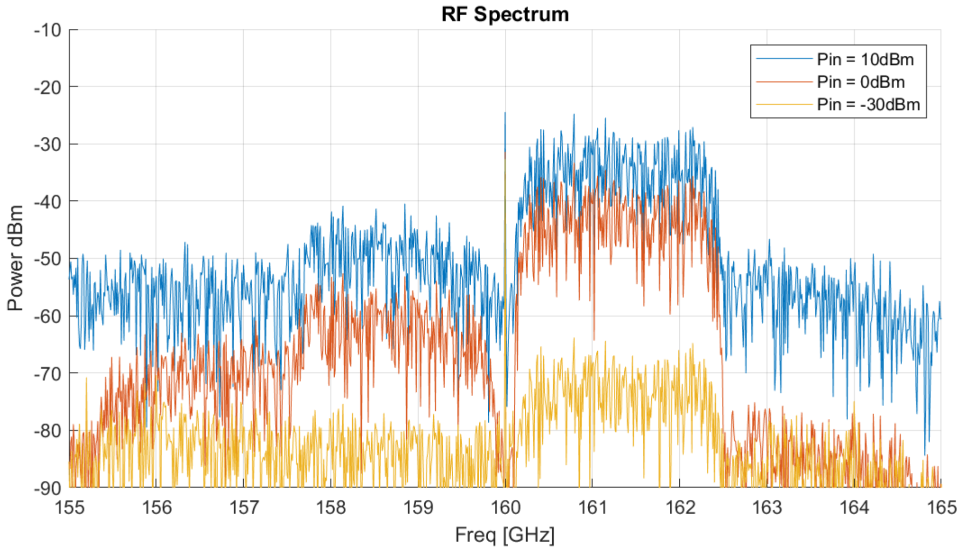

Figure 5.9: BW 2.4GHz

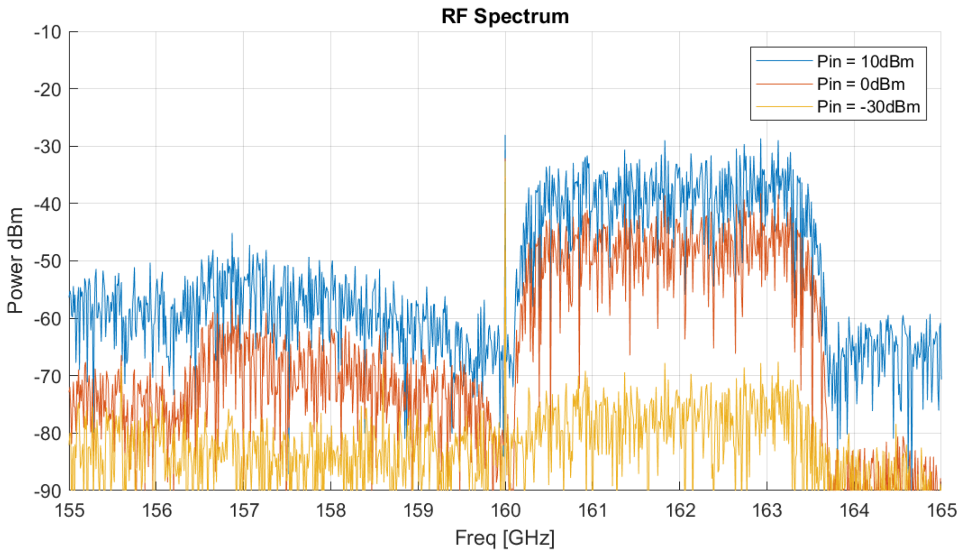

Figure 5.10: BW 3.6GHz

After checking the RF spectrum out of the MUT, the EVM from the modulated signal are measured. In this case, the offset frequency f_rec is set to 65.1MHz and 279.1MHz for EVM, and there fore will have the similar value used when the different reference phase channel setups are implemented.

Fig. 5.11 shows the measured EVM constellation diagram fro different bandwidths with a lower offset frequency (65.1MHz), with an IF input power of 0dBm. The VNA IF BW is set to 1kHz. In this case, the setup achieves the same EVM floor as the results measured directly at the baseband.

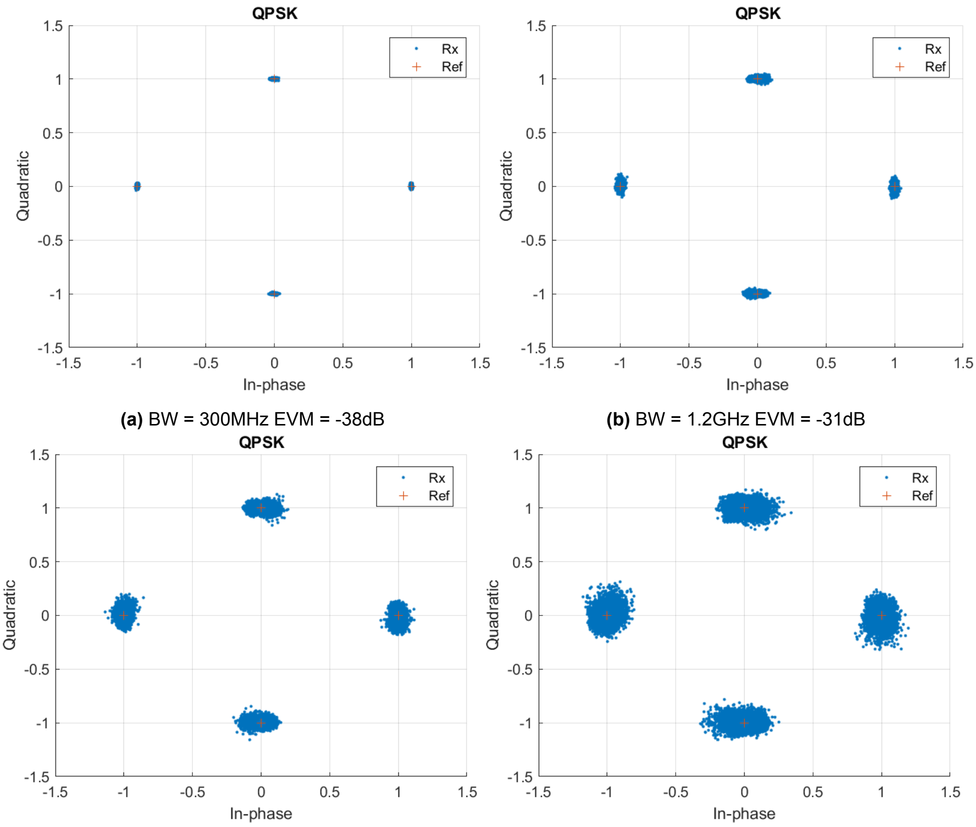

(a) BW = 300MHz EVM = -38dB

(b) BW = 1.2GHz EVM = -31dB

(c) BW = 2.4GHz EVM = -25.4dB

(d) BW = 3.6GHz EVM = -23.12dB

Figure 5.11: EVM measured without reference phase channel, and f_{rec} equal to 65.1MHz

Then the EVM is measured at different IF input power levels, as shown in Fig .5.12. The EVM floor can be obtained with an IF power equal to -10dbm. As the IF power goes to a lower level, the thermal oise starts to dominant the EVM error. However, in this case, the EVM error due to NUT non-linearity remains invisible. It can be notice that as the EVM floor increase about 3dB as the signal bandwidth doubles.

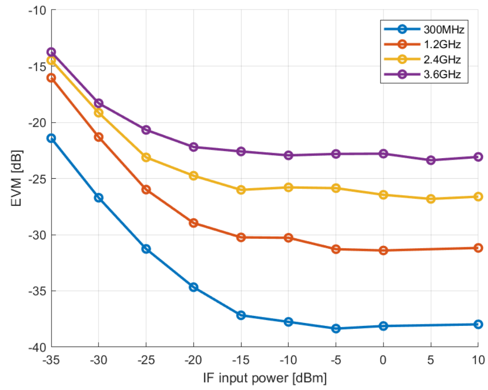

Figure 5.12: EVM curve measured without reference phase channel, and f_rec equal to 65.1MHz

The same procedure is carried out with a higher offset frequency at 279.1MHz. Fig .5.13 shows the measured constellation diagram when the IF power is 0dbm. The EVM curve is illustrate in Fig .5.14. The higher offset frequency does not provide a lower EVM floor, but it does provide a wider EVM floor range, since the WR5 extender is optimized around 279MHz, which has a lower conversion loss, resulting in a higher SNR of the VNA receiver port. However, the error due to MUT non-linearity still does not appear.

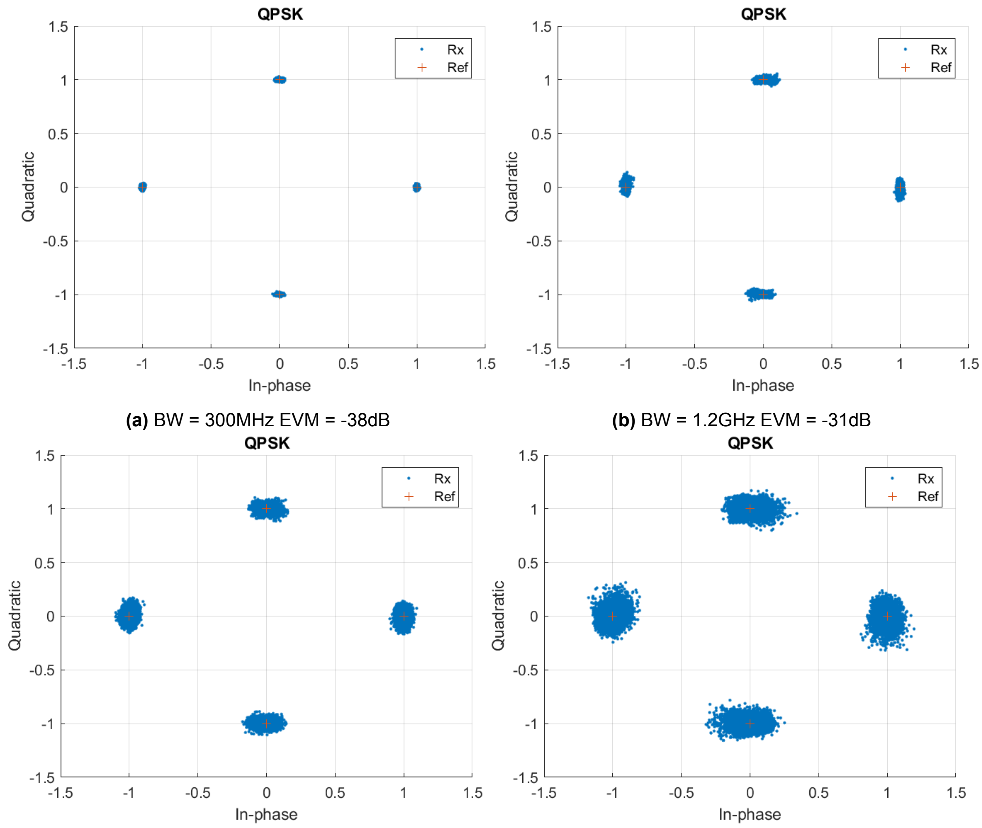

(a) BW = 300MHz EVM = -38dB

(b) BW = 1.2GHz EVM = -31dB

(c) BW = 2.4GHz EVM = -26.8dB

(d) BW = 3.6GHz EVM = -23.12dB

Figure 5.13: EVM measured without reference phase channel, and f_{rec} equal to 279.1MHz

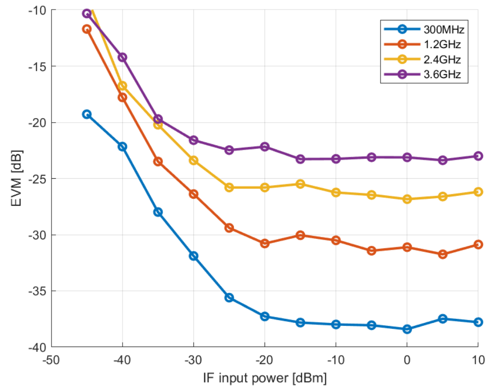

Figure 5.14: EVM curve measured without reference phase channel, and f_rec equal to 279.1MHz

5.3. EVM Measurements with Oscilloscope

To validate the proposed setups, and find out the reason why the nlinearity-limited error is not observed, the EVM is measured using an oscilloscope. For conventional EVM measurements using an oscilloscope, instead of deriving the RF spectrum, the whole bandwidth is now converted to the IF bandwidth. To minimize the change of measurement setups, the oscilloscope is directly connected to the WR5 extender output, as illustrated in Fig.5.15. However, due to the instrument availability, only the narrow band EVM measurement are compared, with the N6030A AWG cards. The same QPSK signal is used, with the same RF frequency at 165GHz. However, in this case, instead of a sweeping grid, the VNA_{src2} is set to a CW tone at 13.72GHz, so that it will down convert the signal to 440-740MHz. The oscilloscope is the Rhodes & Schwartz RTO1000 oscilloscope, with a normal sample frequency up to 10GSa/s

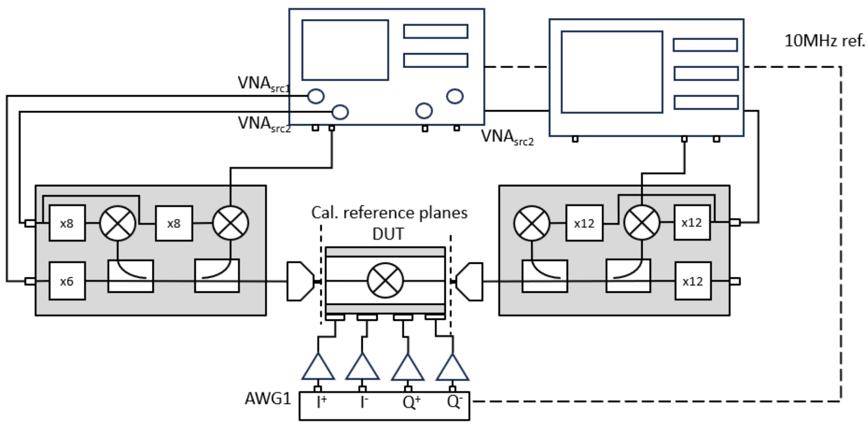

Figure 5.15: Measurement Layout with the oscilloscope

The measured raw signal is shown in Fig. 5.16, where the signal now is converted to 440-740MHz. In time domain, the signal voltage is reaching the limits of oscilloscope sensitivity (1.5mV). In frequency domain, the noise floor is about 20dB lower than the modulated signals. Also, a drop of power can be notice at frequencies around 700MHz, due to the increased conversion loss from the WR5 extender.

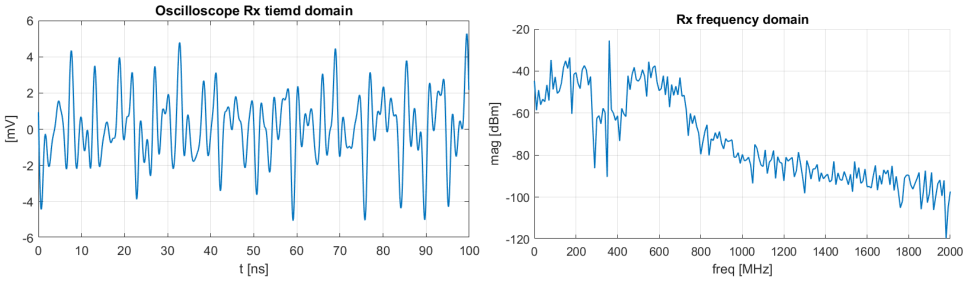

(a) timed domain **(b)** frequency domain

Figure 5.16: measurement raw data from the oscilloscope

To keep the same conditions as the proposed setups, the measured signals are filtered so that they only keep the same frequency tones as the PNA measurements results. Then it is also digitally down-converted to the same frequency as the reference signals. The same post equalization filter is used to compensate for the distortion before the demodulation of the recovered signals. 200 Measurements are recorded, and the resulting EVM is -13.4dB due to the relative high SNR. The constellation diagram is shown in Fig. 5.17a.

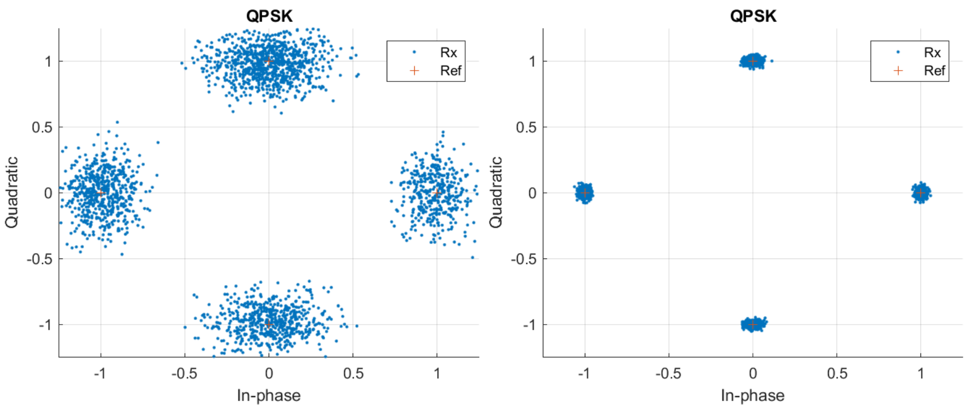

(a) raw constellation diagram **(b)** averaged constellation diagram

Figure 5.17: constellation diagram form oscilloscope measurement results

To compare the EVM results of the two measurement setups, we have to make sure that the received signals from these two setups have the same SNR so that they will have the same EVM behaviours. Coherent averaging is applied to the oscilloscope measurement results to increase the SNR to the same . After choosing an average factor of 45, the two measurements share a similar SNR, and we can compare the EVM results. However, now it takes about 10 minutes time recording, while the measurements with VNA only take about 2 minutes. The average constellation diagram is shown in Fig. 5.17b, with a EVM of -29.5dB.

The EVM versus different IF power is also tested, and the results is listed in Fig.5.18. By coherent averaging, the EVM floor measured with the oscilloscope is equal to the EVM floor measured by VNA. The error due to the system non-linearity can be observed when the IF power is above 6dBm.However, the high noise floor causes the thermal noise to dominant the error with a higher IF input power.

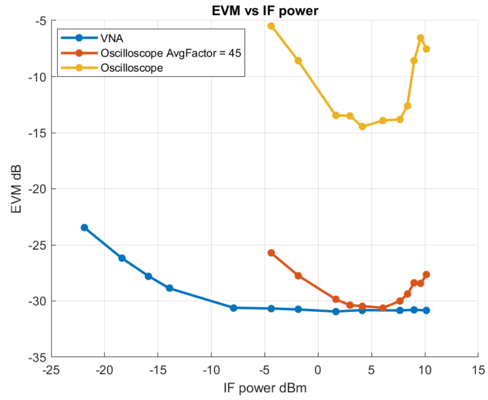

Figure 5.18: measured EVM curve using oscilloscope

5.4. EVM Measurements with Reference Phase Channel

To compare with the measurements wihtout using the reference phase channel, we start the same QPSK signals used in wide band signal measurement, keeping the frequency grid to 10MHz. However, different reference phase channel are realized to obtain the stable phase measurements.

Firstly, the auxiliary AWG channel is used as the reference phase source, the offset frequency is set to 65.1MHz. Fig .5.19 shows the meassure constellation diagram with an IF input power of 0dBm. Similarly, the EVM curve is illustrate in Fig .5.20.

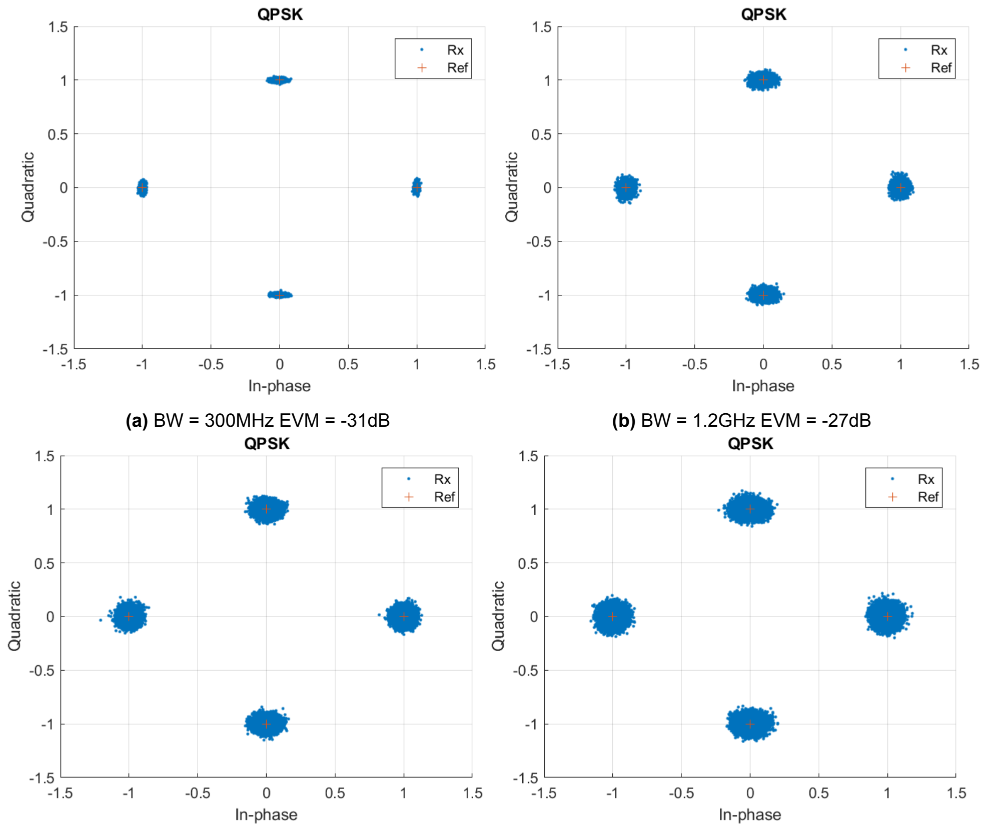

(a) BW = 300MHz EVM = -31dB
(b) BW = 1.2GHz EVM = -27dB
(c) BW = 2.4GHz EVM = -25dB
(d) BW = 3.6GHz EVM = -23.5dB

Figure 5.19: EVM measured with auxiliary AWG channel, and f_{rec} equal to 65.1MHz

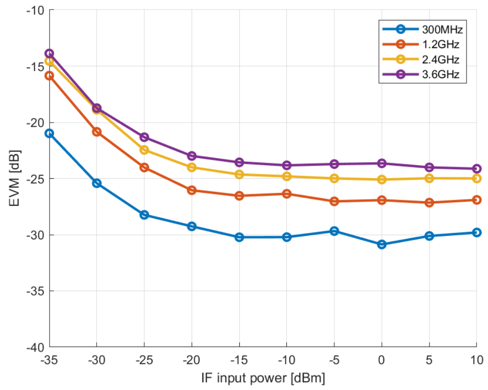

Figure 5.20: EVM curve measured with auxiliary AWG channel, and f_{rec} equal to 65.1MHz

The offset frequency is changed to 279.1MHz, which is close to the optimized frequency for WR5 extender. Fig.5.21 and Fig.5.22 shows the resulting constellation diagram and EVM curve. Comparing to the EVM results with an offset frequency at 65.1MHz, the EVM floor increase to -20dB for 300MHz BW QPSK signal, due to the reduced SNR from the reference phase channel, as discussed in Chapter 4. Meanwhile, the constellation also illustrate the phase noise, especially when the signal BW is smaller than 1.2GHz. The error due to the thermal noise from the MUT channel is hidden until the IF input power drop below -30dBm. On one hand, the high phase noise dominants the EVM errors. On the other hand, now the WR5 is working with a lower conversion, and a higher SNR would be expected from the MUT channel receiver b_{rec}.

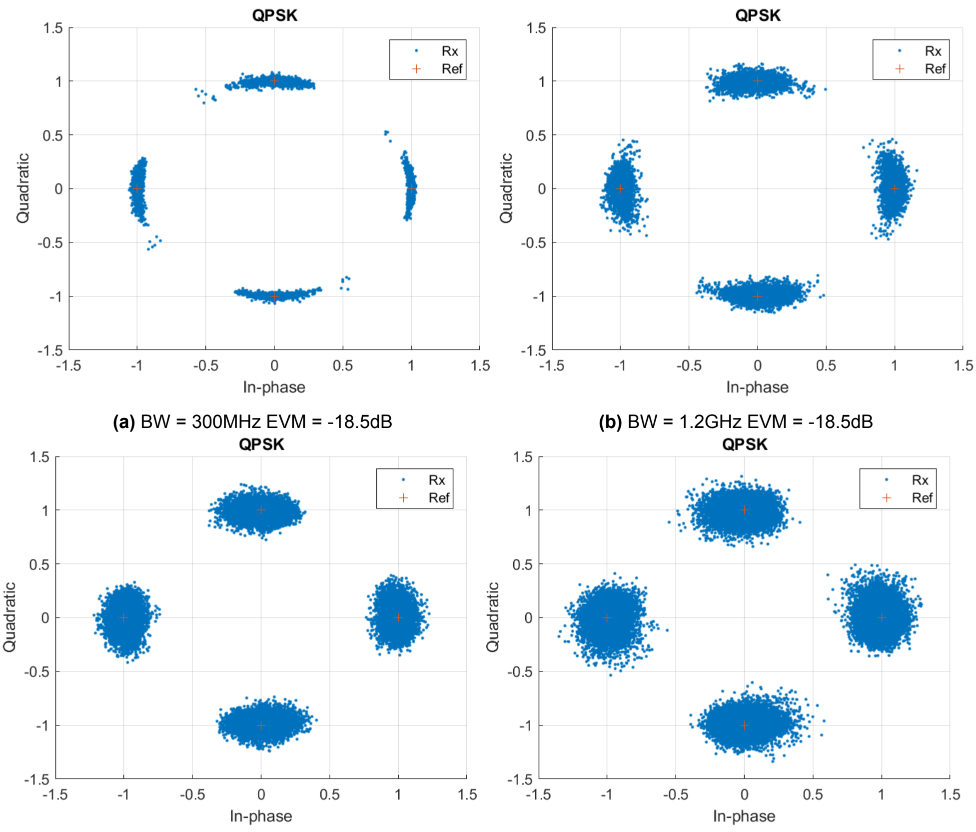

(a) BW = 300MHz EVM = -18.5dB

(b) BW = 1.2GHz EVM = -18.5dB

(c) BW = 2.4GHz EVM = -18.5dB

(d) BW = 3.6GHz EVM = -17.6dB

Figure 5.21: EVM measured with 2nd DAC channel and f_{rec} equal to 279.1MHz

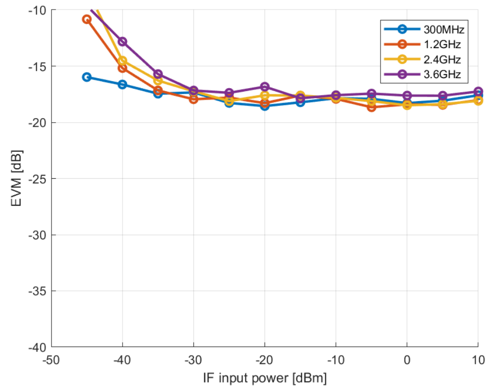

Figure 5.22: EVM curve measured with auxiliary AWG channel, and f_{rec} equal to 279.1MHz

Then the reference source is switch to the Sample Marker Out. In this case, the offset frequency is set to 63.6363MHz, since the frequency grid of a sinc function is fixed. Fig.5.23 and Fig.5.24 shows the resulting constellation diagram and EVM curve. The EVM floor is now increased to -20dB due to the increased variation from the reference channel. An averaging factor of 10 can reduce the EVM floor to -28dB, which is close to the EVM results using the additonal AWG channel with an offset frequency of 65.1MHz. Due to the high EVM floor, the error from thermal is hidden until the IF power is reduce to -25dBm. Meanwhile, only the QPSK signal that has a BW of 300MHz or 1.2GHz are measured, due to the limited power from the square wave references source. Due to the same reason, the sample is not used when the offset frequency is set close to 279MHz.

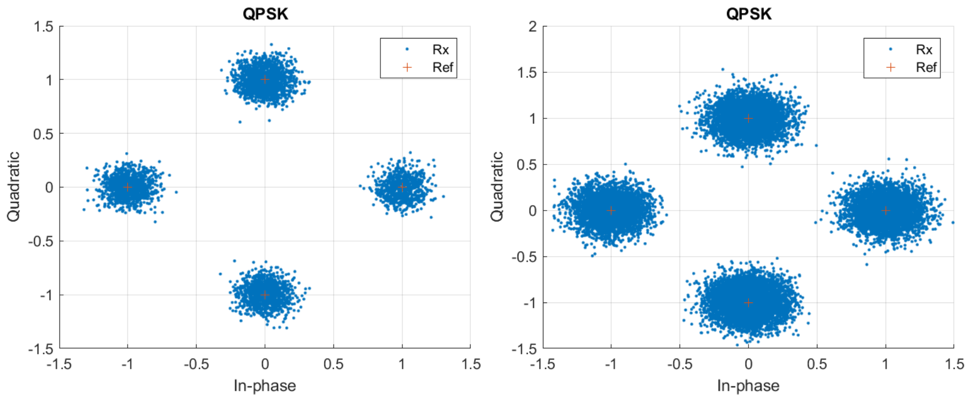

(a) BW = 300MHz EVM = -19.97dB **(b)** BW = 1.2GHz EVM = -19.0dB

Figure 5.23: EVM measured with Sample Marker Out and f_{rec} equal to 63.6363MHz

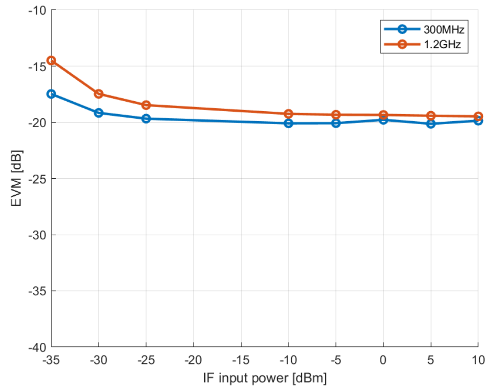

Figure 5.24: EVM curve measured with Sample Marker Out, and f_{rec} equal to 63.6363MHz

5.4.1. EVM measurement with 2MHz grid

Finally, a QPSK signal with 500ns period is measure. The signal still occupies a BW from 100MHz to 400MHz, with a symbol rate of 250M baud. The difference is that now it requires a measurement frequency grid of 2MHz. Fig. 5.25 shows the QPSK signal in time domain and frequency domain. Comparing to the QPSK signal with 100ns period that has 300MHz BW, the new QPSK spectrum is slightly lower, since the same power is share by 5time more frequency tones.

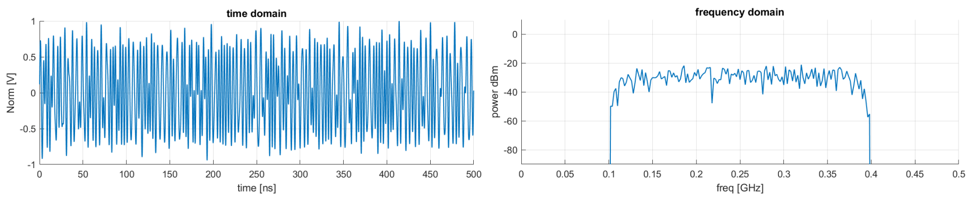

(a) RF spectrum **(b)** Constellation diagram EVM = -26.9dB

Figure 5.25: 500ns QPSK signal in time domain and frequency domain

As mentioned in Chapter .4.5.2, in this case, the measure cannot rely only on the phase from receiver b_{rec}. In this case, the second DAC channel is used as the reference source, with an offset frequency at 65.1MHz, to provide a better phase stability. Fig. 5.26 shows the measured RF spectrum and the constellation diagram at 0dBm. The measured EVM is -26.8dB.

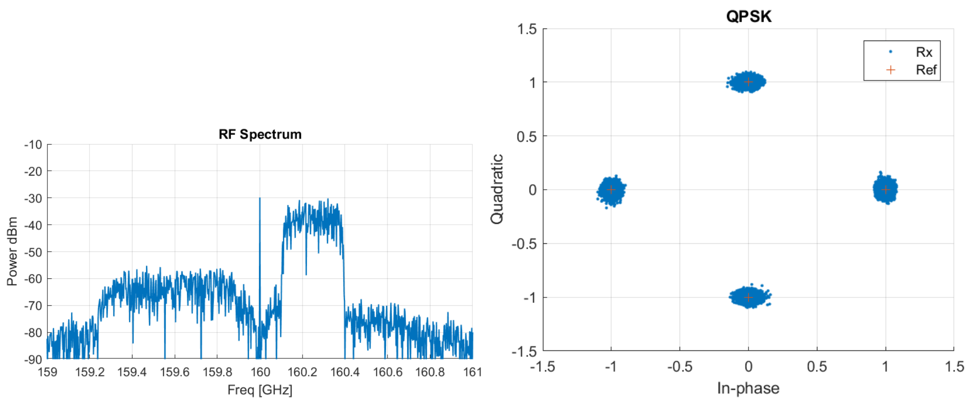

(a) RF spectrum **(b)** Constellation diagram EVM = -26.9dB

Figure 5.26: measured RF spectrum and EVM constellation

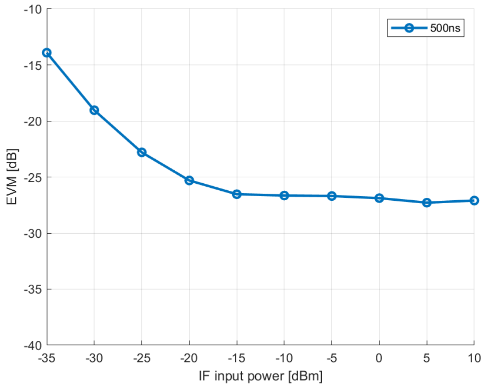

H

Figure 5.27: Measured EVM vs. IF power

Then the EVM vs.IF power curve is measure, as shown in Fig. 5.27. Comparing to the measurements result with 100ns QPSK signal, the EVM floor is about 4dB higher, due to the reduced power per tone from both the RF MUT channel and the auxiliary channel. The thermal noise starts to dominant the error when the power is below -15dBm, which is same to the previous EVM measurement. Again, the error due to the MUT non-linearity cannot be observed.

5.5. Discussion

In this chapter, various of measurement setups are applied for the EVM measurements. When the Keysight M5224B VNA is used, the auxiliary channel is not needed by measuring on a specific frequency grid. By fixing the measured signal period, this setup provides the best accuracy and less system complexity. On the other hand, the proposed auxiliary channel can support any VNA model and any signal period. The Sample Marker Out of the M8190A AWG can be served as the auxiliary channel source, saving one AWG card. However, due to the limited power, a phase stability of $\pm$15 degrees is achieved with a 10MHz RF grid.

When a denser grid is required, an auxiliary AWG channel can be used as the auxiliary channel source. And there is a trade-off between the dynamic range and phase stability. When the offset frequency is set at around 279MHz, the extender is optimized to provide a lower conversion loss. However, a phase stability of $\pm$15 degrees is observed, since the auxiliary mixer is not optimized at this frequency. When the offset frequency is set around 65MHz, the system achieves a phase stability of $\pm$5 degrees, due to the reduce conversion loss of the auxiliary mixer. Yet the EVM limited by the thermal noise appears earlier, due to the increased CL from the WR5 extender.

Comparing to the measurements with the oscilloscope, all the proposed setups has lower EVM, due to the narrow band measurement performed by the VNA. The EVM caused by thermal noise is also pushed away to a lower IF operating power due to the same reason. The proposed setups requires less measurement time to achieve the same EVM level. However, all the measurements failed to observe the increased EVM due to the MUT non-linearity. On one hand, the higher-order harmonics mainly contribute to a coherent interference, which will be cancelled by the equalization filter. On the other hand, the relative low VNA IF BW might prevent us reconstructing the real behavior of the RF signals.

6 Conclusion and Future Work

6.1. Conclusion

This work aims to build a measurement test bench for wideband mixer EVM characterization at sub-terahertz frequencies. The convention measurement setup with an oscilloscope provides a high EVM floor due to the limited dynamic range.The state of the art setup with VNA achieves a lower EVM floor, but the time domain signal is not recovered. The main challenge is to achieve an accurate phase and amplitude measurements for modulated signals on the at sub-THz frequencies.

To this end, a VNA based setups with two frequency extenders are implemented. While one of the VNA sources can be used as the LO input, the other source will be swept over a frequency grid so that the RF output of the mixer under test will be down converted and read out tone by tone. The narrow band receiver of VNA allows the system to measure the signal at RF output with a high dynamic range. A two-tier calibration method is used to extract the absolute power from the target RF channel. The test-bench has been used to characterize the mixer's conversion loss, image rejection ratio and linearity. Moreover, by implementing a reference phase channel, a stable phase is achieved to characterize the mixer's EVM.

The MUT key performance of the mixer under test, such as conversion loss, image rejection ratio and linearity is measured over a IF bandwidth up to 4GHz. The conversion loss is between 14-15dB over the characterized IF bandwidth with a RF frequency of 160GHz. The IRR is above 20dB for a IF frequency up to 3GHz, but gradually decreases to 13dB as the IF frequency increase to 4GHz. As for the linearity, the MUT also shows a P1dB of -10dBm, a OIP2 of 5dBm and a OIP3 of 0dBm. While the IRR agrees with provide data sheet from the manufacture, the CL is about 3dB higher. The increased CL also leads to the decrease of P1dB. The difference in CL may due to the wire bonding losses at IF ports and the calibration errors.

Next, an auxiliary phase channel setup is proposed, which is able to carry the unhandled phase information from one of the VNA source, thus providing a stable phase results for EVM measurements. The different options for the auxiliary channel sources are tested and compared. Firstly, an additional AWG card is used as the auxiliary sources, which is able to provide a phase stability of ± 5 degrees for for each tone. Then, the M8190A Sample Marker Out is implemented, which can generate a sinc function in frequency domain for reference source. In this case, the resulting phase stability is ± 15 degrees. On one hand, the square wave signal are expected to be less stable comparing to multitone signals from the AWG card. On the other hand, the available power per tone for AWG card is also much higher, providing enough SNR for the auxiliary channel readout. When the power of the 2nd AWG cards is set to the same level as the Sample Marker Out, similar phase stability performance can be observed. It is clear that the phase stability is now limited by the SNR from the reference phase channel.

Finally, EVM characterization is performed using the proposed setups. QPSK signal with different bandwidths are measured with different IF input power. The measurement results are compared with the EVM obtained by oscilloscope. A lower EVM floor is achieved, due to the narrow band receiver of the VNA. The EVM error due to the thermal noise is reduced for the same reason

6.2. Future Work

This project demonstrate that the EVM characterization is possible using VNA based setups at sub-THz frequencies. However, there are still some improvements can be conducted.

As explained in Chapter .4, both the WR5 extender output and the auxiliary mixer out put are set to the same frequency. However, while the WR5 is optimized at 279MHz, the auxiliary mixer used in this case is not. This results in a trade-off between the phase stability and the dynamic range of the MUT channel. Therefore, the system can be improved by optimizing the auxiliary mixer .

When the test signal require a more dense grid, the available power per tone RF, due to the increased number of frequency tones. This will limits the system dynamic range. Meanwhile, the power per tone in the auxiliary channel will reduce, resulting a worse phase stability and a higher EVM floor. To provide sufficient power per tone, firstly, the concept of compact test signal in [12] can be applied to reduce the number of tones needed. Second, for the auxiliary channel, it is interesting to the frequency tones in the reference phase channel can be minimized, thus increasing the SNR and phase stability.

References

[1] Alberto Maria Angelotti et al. “Broadband Measurement of Error Vector Magnitude for Microwave Vector Signal Generators Using a Vector Network Analyzer”. In: *IEEE Transactions on Instrumentation and Measurement* 71 (2022), pp. 1–11. DOI: 10.1109/TIM.2022.3181904.

[2] Dustin Brown and Yahya Rahmat–Samii. “Compact Antenna Test Range EVM Measurements of a Millimeter-Wave Phased Array using a VNA”. In: *2022 IEEE International Symposium on Phased Array Systems & Technology (PAST)*. 2022, pp. 01–05. DOI: 10.1109/PAST49659.2022.9975019.

[3] Steven Callender et al. “A Fully Integrated 160-Gb/s D-Band Transmitter Achieving 1.1-pJ/b Efficiency in 22-nm FinFET”. In: *IEEE Journal of Solid-State Circuits* 57.12 (2022), pp. 3582–3598. DOI: 10.1109/JSSC.2022.3208510.

[4] Liang Chen et al. “A Compact 140-GHz CMOS Power Amplifier With 10.5-dBm Output Power and 27.6-dB Power Gain Supporting up to 128-QAM Modulation”. In: *IEEE Solid-State Circuits Letters* 5 (2022), pp. 214–217. DOI: 10.1109/LSSC.2022.3201091.

[5] Joel Dunsmore and Jean-Pierre Teyssier. “Improvements in 6G (D-band) Amplifier EVM Measurements using Clock-Locked Sources”. In: *2023 100th ARFTG Microwave Measurement Conference (ARFTG)*. 2023, pp. 1–4. DOI: 10.1109/ARFTG56062.2023.10148888.

[6] Ali A. Farid et al. “A Fully Packaged 135-GHz Multiuser MIMO Transmitter Array Tile for Wireless Communications”. In: *IEEE Transactions on Microwave Theory and Techniques* 70.7 (2022), pp. 3396–3405. DOI: 10.1109/TMTT.2022.3161972.

[7] *gMDR0035 A D-band IQ-subharmonic mixer MMIC 140-170 GHz*. Accessed: 2024-08-05. 2017. URL: https://www.gotmic.se/documents/gMDR0035A_Rev%20A01-17.pdf.

[8] Abdelaziz Hamani et al. “A D-Band Multichannel TX System-in-Package Achieving 84.48 Gb/s With 64-QAM Based on 45-nm CMOS and Low-Cost PCB Technology”. In: *IEEE Transactions on Microwave Theory and Techniques* 70.7 (2022), pp. 3385–3395. DOI: 10.1109/TMTT.2022.3162296.

[9] B. Razavi. *RF Microelectronics*. 2nd ed. Paul Boger, 2011.

[10] Justin Romstadt et al. “A D-Band Vector Network Analyzer Extension Module Based on a SiGe Reflectometer MMIC”. In: *2023 IEEE/MTT-S International Microwave Symposium - IMS 2023*. 2023, pp. 927–930. DOI: 10.1109/IMS37964.2023.10188062.

[11] Jan Verspecht et al. “Characterizing Amplifier Modulation Distortion Using a Vector Network Analyzer”. In: *2019 93rd ARFTG Microwave Measurement Conference (ARFTG)*. 2019, pp. 1–4. DOI: 10.1109/ARFTG.2019.8739226.

[12] Jan Verspecht et al. “The Vector Component Analyzer: A New Way to Characterize Distortions of Modulated Signals in High-Frequency Active Devices”. In: *IEEE Microwave Magazine* 23.12 (2022), pp. 86–96. DOI: 10.1109/MMM.2022.3203939.

[13] *Verttigo Technology mmW-Studio*. Accessed: 2024-08-06. URL: `https://vertigo-tech.com/services/mmwave-studio/`.

[14] Yichi Zhang et al. “Evaluation of EVM Performance of Antenna System under Digitally Modulated OTA Scenarios”. In: *2022 International Conference on Microwave and Millimeter Wave Technology (ICMMT)*. 2022, pp. 1–3. DOI: `10.1109/ICMMT55580.2022.10023289`.

[15] Yichi Zhang et al. “Repeatable Phase Spectrum Measurements of 75–110-GHz Modulated Signals Using a VNA-Based LO Phase Cancellation Technique”. In: *IEEE Transactions on Instrumentation and Measurement* 70 (2021), pp. 1–11. DOI: `10.1109/TIM.2021.3049557`.

A

Signal Modulation and Demodulation Process

A.1. Schematic layout of modulation process

Fig. A.1 shows the schematic layout of the IQ signals modulation process. First, a serial-to-parallel(S/P) converter collects the randomly generated bits and map them into symbols according to the modulation schemes. For a m-order PSK or QAM signal, let us assume a symbol rate of Rs. Therefore, the data rate of the random bits is $Rs \times log2(m)$. Each symbol can be represented by two separate bit sequences, and all the two bit sequences will be transformed into two digital levels. These two digital levels then are used to generate the corresponding waveforms and upconverted to the IF frequency by two separate carrier waves. Since the two carrier waves are of the same IF frequency but are out of phase by 90, these two waveforms and their corresponding digital levels can be recognized as In-Phase and Quadrature parts. The In-phase digital level can be plotted on the x-axis, and the Quadrature digital level can be plotted on the y-axis, which is known as the Constellation plot. Finally, the modulated signal is phase-shifted by 90, 180 and 270 degrees to generate 4-channel differential IQ signals. It is worth mentioning that the In-phase and Quadrature parts do not relate to these IQ channels of the MUT. The differential IQ channels describe the phase requirements of the inputs of the MUT, while the

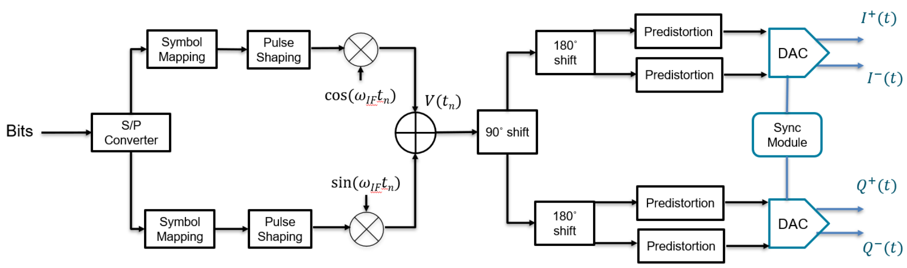

Figure A.1: Modulation process of PSK/QAM signals

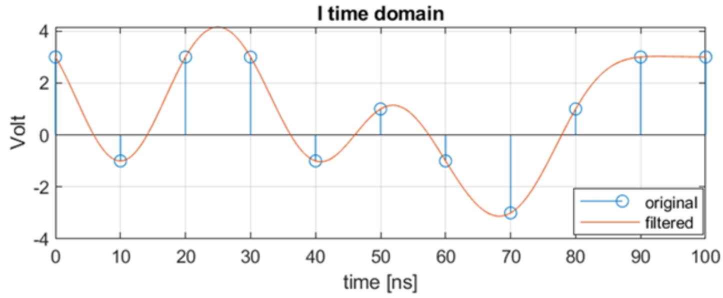

Figure A.2: Original digital levels and generated waveform by raised cosine filter

In-phase and Quadrature describe the carrier phase of the modulated signals. To distinguish them, we use A and B to describe the two digital levels of the modulated signals.

A.2. Pulse shaping filter

The process that generates waveforms based on the digital levels is called pulse-shaping. It aims to minimize the inter symbol interference while reducing the bandwidth of the modulated signals. In the practical communication systems, a raised cosine filter is frequently used for this function. The frequency response of a raised-cosine filter can be expressed as :

$$H_{rc}(f) = \begin{cases} 1, |f| < \frac{1-\alpha}{2T} \\ \frac{1+\cos\left(\frac{\pi T}{\alpha}\left(|f|-\frac{1-\alpha}{2T}\right)\right)}{2}, \frac{1-\alpha}{2T} < |f| < \frac{1+\alpha}{2T} \\ 0, \frac{1+\alpha}{2T} < |f| \end{cases} \tag{A.1}$$

Where T is the reciprocal of symbol rate Rs, and α is the roll-off factor that defines the property of the filter. For any given digital sequence, the output amplitude of the generated waveform at specified sampling points will be exactly the same as the amplitude of the digital sequence. The figure 3 shows the example of a bit sequence derived from a period of QPSK signal. Specified sampling points will be exactly the same as the amplitude of the digital sequence. Fig. A.2 shows an example of a bit sequence derived from a period of QPSK signal.

However, in practical communication systems, a matched filter is need at the receiver side to reduce the white noise. Therefore the raised cosine filter is split into two identical parts, and each is the square root of the raised cosine filter.

$$H_{rc}(f) = \sqrt{H_{rrc}(f)} \times \sqrt{H_{rrc}(f)} \tag{A.2}$$

The root raised cosine filter will be implemented at both the transmitter and receiver side, one will be used for pulse-shaping, and the other will serve as the matched filter at receiver side. Meanwhile, the 2 root raised cosine filter forms a raised cosine filter of within the signal channels, the ISI is still minimized. The figure shows the frequency response and of a root-raised cosine filter with different roll-off factor.

A.3. Demodulation of the signal

Fig .A.4 shows the schematic layout to demodulate the received signals. Since the two carrier waves are 90 degree out of phase, by applying the same waveform, the two separate baseband waveforms can be recovered. The root raised cosine filter is used as matched filter. Together with the same root

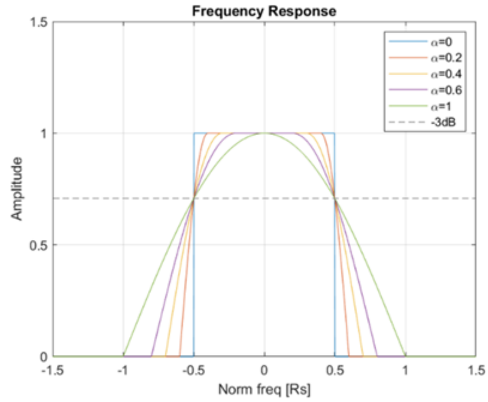

Figure A.3: Frequency domain of the root raised cosine filter

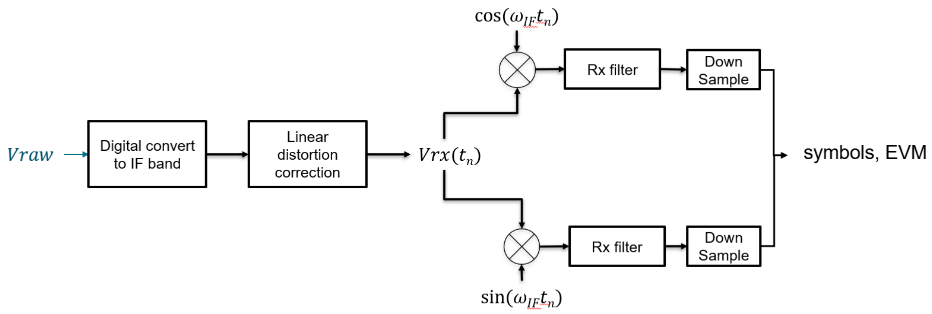

Figure A.4: Schematic layout of the demodulation process

raised cosine filter and transmit side, the ISI is minimized. Also, the root raised cosine filter serve as a lower pass filter to block the high frequency components. By sampling at specific time, the digital levels of transmitted symbols can be recovered as well. The data can then be used to recover the constellation diagram, and calculate EVM of the system

B

Phase Stability of measurement with Agilent N5242A VNA

This Appendix describes the preliminary phase stability measurements using the Agilent N5242A VNA, as an extension part of the measurement in Chapter .4. Only the Sample Marker Out is used as the reference channel source. Meanwhile, different offset frequencies f_b are set to measure the phase at different IF bandwidths.

As an example, a single IF tone f_{IF} at 2500MHz is sent to the MUT channel, while the offset frequency is set to 279.0909MHz. The signal length is 14400 samples, therefore, the frequency grid for the sample marker out is 0.833MHz. In the frequency domain, the sinc tone at -50MHz will serve as the reference signal source f_l.

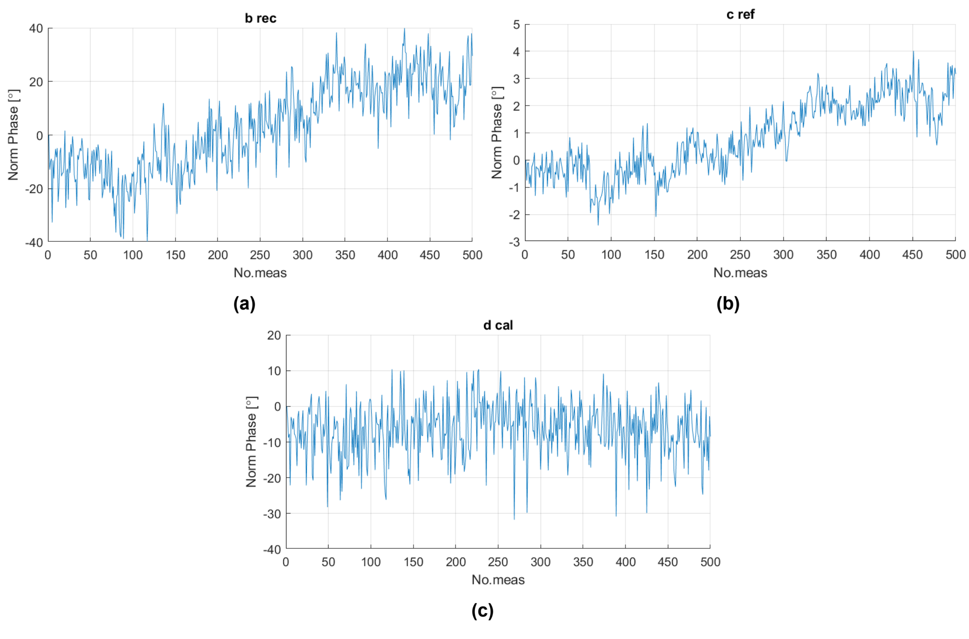

Figure B.1: Phase Stability measured at 279.0909MHz

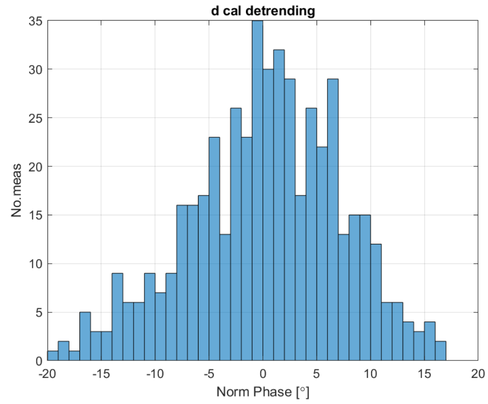

Figure B.2: Histogram of Phase at d cal

Fig .B.1 shows the measured phase information for different ports. The histogram of calculated phase φ_d is illustrated in Fig. B.2, with a variation of $\pm$20 degrees. However, it can be noticed that even in such a single frequency grid measurement setup, the phase directly measured from port b_{ref} has a drifting of 40 degrees.

The different internal synchronization hardware used could leads to such drifting errors. Therefore, we expect that the EVM measurement without reference phase channel cannot be performed with this VNA. To have a better reference results, the VNA is switch to the Keysight 5224B VNA for measurements, as described in Chapter .4.

C

Reference Phase Channel Implementation with WR10

This appendix discuss the special setup for the reference phase channel in Chapter 4, when when the frequency LO factor M is not equal to the RF factor N. The spectrum example is shown in Fig. C.1, where the M is bigger than N. In this case, since the frequency of VNA^i_{src2} is smaller than that of the VNA_{src1}, the target down converted tone is now become to $f^i_{src2} + f_b$. And the LSB auxiliary tone is used, the frequency f^i_l must be equal to $(M - N)/M \times f_{src1} - f_{rec}/M - f^i_{IF}/M$

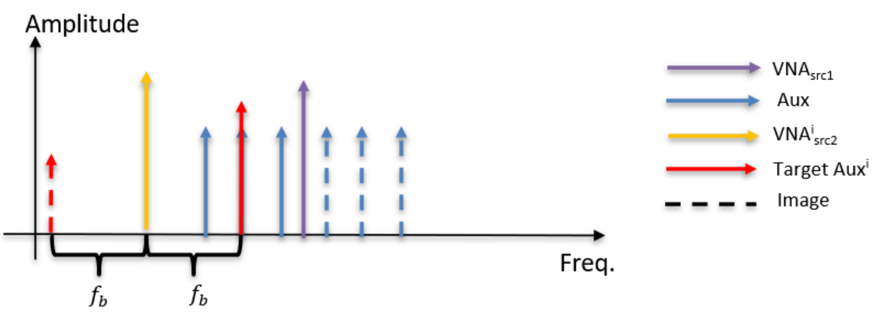

Figure C.1: Illustration of the auxiliary channel spectrum

Table C.1: Measurement Grid Setup with WR10

LO	IF	RF	b_{rec}	VNA_{src1}	VNA_{src2}	AWG2
f_{LO}	f_{IF}	f_{RF}	f_{rec}	$f_{LO}/6$	$(f_{RF} + f_{IF} + f_{rec})/8$	$f_{src1}/4 - f_{rec}/8 - f_{IF}/8$

Table C.1 illustrates the grid setup for WR10 extenders, where M is 8 and N is 6. Typically, once the f_{RF} and f_{IF} are determined, the f_{src1} becomes a fix frequency. Therefore, the trade-off is only the frequency at f_{rec} and f_l. A lower offset frequency f_{rec} will provide low conversion loss from the RF channel, however, this requires auxiliary channel source to provide a higher frequency tone.